EXTENSION IN HIGH-GRADE TERRANES OF THE SOUTHERN OMINECA BELT: EVIDENCE FROM PALEOMAGNETISM

by

Michael T.D. Wingate
B.Sc., Carleton University, 1990

A Thesis Submitted in Partial Fulfillment of the
Requirements for the Degree of

MASTER OF SCIENCE

in the School of Earth and Ocean Science

We accept this thesis as conforming
to the required standard

[redacted]
Dr. E. Irving, Supervisor (School of Earth and Ocean Science)

[redacted]
Dr. E. Van der Flier-Keller, Departmental Member (School of Earth & Ocean Science)

[redacted]
Dr. G. Spence, Departmental Member (School of Earth and Ocean Science)

[redacted]
Dr. T. Höy, Outside Member (British Columbia Geological Survey Branch)

[redacted]
Dr. J.T. Fyles, External Examiner (Retired)

University of Victoria

Supervisor: Dr. E. Irving

ABSTRACT

Previous paleomagnetic studies have shown that significant tilts have occurred in plutonic and high-grade metamorphic terranes within the zone of Eocene extension in the southern Omineca Belt (Bardoux and Irving 1989; Marquis and Irving 1990). The previous extent of sampling in the area (34 sites) has been augmented, during the current study, by an additional 78 sites, and the data used to produce a map of paleomagnetically-observed structural tilts across the extended region. The data are now of sufficient density that it is possible to test specific ideas and hypotheses regarding the kinematics of Eocene extension in the region. The following are the main conclusions of the present study:

1) A previously undiscovered, major west-dipping Eocene extensional fault, named here the Arrow Lake Fault (AF), has been defined paleomagnetically. Eastward apparent tilts are observed in the hanging wall of the east-dipping Kettle River Fault (KF), in the opposite sense to that expected in the hanging wall of the fault. These are juxtaposed, to the east, against westward apparent tilts north of Arrow Lake, and against apparently untilted syenites in the eastern parts of the 52 Ma Coryell Pluton. The AF is inferred to extend along the eastern limit of the eastward tilts, and to bisect the Coryell Pluton.

2) Apparent tilt data, combined with correlation of the polarities of the sampled rocks with the geomagnetic time scale, are employed to constrain the timing and duration of extensional events. The eastern parts of the study area were apparently tilted about 35° down-to-the-west, commencing at approximately 53 Ma, as a result of displacement on the east-dipping KF and Slocan Lake (SLF) Faults. The absence of apparent tilt in the eastern parts of the Coryell Pluton confirms that displacement on the SLF ended before cooling and magnetization of the Coryell Pluton at about 52 Ma. Normal displacement on the west-dipping AF and Granby Faults produced down-to-the-east apparent tilts averaging 38° in the hanging walls of these faults, but left the eastern parts of the Coryell Pluton untilted. Cooling of the Coryell Pluton is inferred to have occurred very rapidly, and therefore motion on the AF may have commenced very soon after 52 Ma.

3) Apparent tilt data allow inferences to be made regarding the subsurface geometry of the major Eocene extensional faults. The similarity of apparent tilt in the hanging wall and footwall of the SLF suggests it is a planar rotational fault. Conversely, the absence of apparent tilt in the footwall of the AF suggests the fault is listric at depth.

4) Re-evaluation of older structures is possible after they are restored to their pre-extensional attitudes by removing the effects of Eocene deformation. Restoration of about 40° degrees of westward apparent tilt observed in the footwall of the SLF indicates that, during the Early Eocene, the Valkyr Shear Zone (VSZ) dipped about 40° to the east, and is indeed an east-rooting extensional fault, thus making unlikely the possibility (raised by Carr and others 1987) that the VSZ is a west-rooting thrust fault. Similarly, eastward apparent tilts observed in syenites of the Granby Pluton confirm the interpretation of Carr and Parkinson (1989) that the Jones Fault, which presently is flat-lying, dipped originally to the west. The Mount Verde normal fault, and the Waneta, Tillicum Creek, and other thrust faults, all of Jurassic age, are believed to have been overturned to the west (Höy and Andrew 1990; Einarson 1991); the paleomagnetic data provides independent confirmation of these interpretations.

Examiners:

[redacted]

Dr. E. Irving, Supervisor (School of Earth and Ocean Science)

[redacted]

Dr. E. Van der Flier-Keller, Departmental Member (School of Earth & Ocean Science)

[redacted]

Dr. G. Spence, Departmental Member (School of Earth and Ocean Science)

[redacted]

Dr. T. Höy, Outside Member (British Columbia Geological Survey Branch)

[redacted]

Dr. J.T. Fyles, External Examiner (Retired)

TABLE OF CONTENTS

TABLE OF CONTENTS, continued

LIST OF TABLES

LIST OF ILLUSTRATIONS

Page

LIST OF ILLUSTRATIONS, continued

Page

LIST OF ABBREVIATIONS

AF	alternating field
ALF	Arrow Lake Fault
AM	Absaroka Mountains
BM	Bearpaw Mountains
CLF	Champion Lakes Fault
CRF	Columbia River Fault
CRM	chemical remanent magnetization
D	declination
FL	Flores Volcanics
GAD	geocentric axial dipole
GF	Granby Fault
GWF	Greenwood Fault
h	heave
H,Hc,Hs	magnetic field, coercive force, saturation field
HM	Highwood Mountains
I	inclination
IRM	Isothermal remanent magnetization
J, Js, Jr	induced, saturation, residual magnetization (IRM)
JF	Jones Fault
k, K	Fisher's precision parameter
KCx	Kettle River - Grand Forks Metamorphic Complex
KA	Kamloops Volcanics
KE	Kelowna Volcanics
KF	Kettle River Fault
λ_p	paleolatitude
M	NRM intensity
Ma	million years
MCx	Monashee Complex
MD	Monashee Décollement (*also* multi-domain)
MDF	median destructive force
MDT	median destructive temperature
M_R	removed magnetization vector
MVF	Mt. Verde Fault
n, N	number of sites, poles
NRM	natural remanent magnetization
OVF	Okanagan Valley Fault
PEF	present Earth's field
P	probability
PSV	paleosecular variation
PTF	Purcell Trench Fault
R	resultant vector
SD	single domain
SLF	Slocan Lake Fault
SS	Summit Stock
τ	magnetization relaxation time
T, Td	magnitude, direction of apparent tilt
Tc,Tb, Tub	Curie, blocking, unblocking temperature
TCF	Tillicum Creek Fault
TRM	thermoremanent magnetization
V_b	blocking volume
VCx	Valhalla Metamorphic Complex
VRM	viscous remanent magnetization
VSZ	Valkyr Shear Zone
WF	Waneta Fault

ACKNOWLEDGMENTS

I wish to thank Dr. Ted Irving, who suggested and supervised this project, for his wise and patient guidance and his attentive support, while allowing me the freedom to learn, in part, through my own mistakes. I am grateful for field visits and insightful discussions with Ted, and with Drs. Doug Archibald, Jim Fyles, and Trygve Höy. Sincere thanks to the staff at the Pacific Geoscience Centre, in particular to Drs. Tark Hamilton, Roy Hyndman, Trevor Lewis, Carmel Lowe, Tom Vandall, and Chris Yorath. Special thanks to Jane Wynne and Judith Baker, who introduced me to the paleomagnetic laboratory, and who were a constant source of advice and suggestions. I am indebted to Chris Ash and Drs. Sharon Carr, Jim Monger, Randy Parrish, and others, whose interest and constructive comments are gratefully appreciated. Dr. Phil Simony provided advice and copies of unpublished geological maps which helped greatly in my understanding of the field area. This thesis benefitted from editorial review by Drs. Ted Irving, Jim Fyles, Trygve Höy, George Spence, and Eileen Van der Flier-Keller.

This thesis is dedicated to my wife, Janien, to whom I would like to express my sincere thanks for her continuing enthusiasm, understanding, and unfailing moral support, and for many long hours she worked as my assistant in the field.

Funding for this research was provided, in part, by graduate teaching assistantships and Fellowships from the University of Victoria, and by a Post-graduate Scholarship from the Natural Sciences and Engineering Research Council of Canada. Additional support came from an NSERC Operating Grant to Dr. Irving.

CHAPTER 1

INTRODUCTION

1.1 INTRODUCTION

Paleomagnetism provides a means of observing late-stage tilting in high-grade metamorphic or plutonic bodies, which lack visible indicators of the paleohorizontal plane immediately prior to tilting. The principle is as follows. Mid-crustal rocks become magnetized in the direction of the geomagnetic field at the time of uplift and cooling. Such magnetizations can be measured in oriented rock specimens, and their directions compared to those previously observed in undisturbed rocks. If the directions do not agree, then the aberrancies, under certain conditions, can be interpreted as apparent tilts of the extended terrane.

In extensional terranes, such as the study area, knowledge of the degree of tilting which accompanied extension provides vitally important constraints in understanding the nature of the extension process. Without such information, for example, one cannot draw structural cross-sections, determine whether normal faults have planar or listric geometry at depth, or make accurate estimates of the magnitude of extension. Furthermore, it is only when the effects of the latest deformation are adequately understood, that palinspastic restoration of the extended terrane can be made, and the effects of previous episodes of deformation studied.

Previous work (reviewed below) in the study area and elsewhere has shown that the method is viable, and that very substantial tilts, not otherwise suspected, have occurred. The objective of the present study was to undertake a very extensive sampling and measurement programme in order to provide what

can reasonably be described as the first adequate tilt map of a high-grade extensional terrane. It is "adequate" in the sense that the density of data now is such that the map may be compared with maps of upper crust extensional terranes where bedding attitudes and tilts can be obtained by standard geological procedures, thus allowing some of the questions raised above to be addressed.

The technique has been employed to measure apparent tilts across part of the southern Omineca Belt, a region which consists mainly of plutonic rocks and high-grade metamorphic rocks of the middle crust, in which few visible indicators of the paleohorizontal plane immediately prior to extension exist. The age of extension and rapid uplift of this area during the Eocene is well constrained by radiometric dating, and propitiously occurs during a time when previous studies have shown that, irrespective of sign, the mean geomagnetic field remained essentially constant over the sampling area.

1.2 PREVIOUS WORK

Recent studies have demonstrated the feasibility of this method of observation in the zone of Eocene extension in the southern Omineca Belt. From an analysis of specimens collected from meta-igneous rocks of the Valhalla Complex and an unmetamorphosed Eocene syenite stock, Bardoux and Irving (1989) suggested westward apparent tilts of the order of 35° antithetic to the east-dipping Slocan Lake extensional fault. The studies of Marquis (1988) and Marquis and Irving (1990) expanded upon this earlier work, and reported results from additional sites which suggested that such apparent tilts are widespread and antithetic to the major normal faults across the extended region. Irving and

Archibald (1990) combined paleomagnetic data with bathozonal information obtained from contact metamorphic assemblages to infer 25° of post-Cretaceous westward tilt of the Summit Stock at the eastern margin of the study area (see Figure 5.6), presumably, they argued, the result of Eocene extension.

Several studies have proposed tilt as a viable explanation for aberrant paleodirections observed in pre-Eocene rocks of the Cordillera. Symons (1971, 1972) proposed that aberrant paleodirections observed in the Triassic Guichon Batholith are best explained by 30 to 50° of clockwise rotation of a large crustal block in southern British Columbia. However, LeCouteur and Agar (1972) argued that these data could equally well be explained by invoking westward tilting of about 20°, and that gravity data, from which the shape of the batholith could be inferred, favoured tilting.

Aberrant paleodirections observed in mid-Cretaceous plutons of the southern Coast Belt have been interpreted to indicate that parts of this region have undergone a combination of large-scale northerly latitudinal displacement and clockwise rotation during Late Cretaceous - Early Tertiary time (Beck and others 1981; Irving and others 1985; and others). On the other hand, Butler and others (1989) argued that geological and geochronological evidence exists to support the alternative hypothesis that the aberrant paleodirections were caused by regional-scale tilting of approximately 30° about north-northwest-trending horizontal axes. Irving and others (1992) sampled one of these plutons, the Porteau Pluton, in greater detail and argued that the aberrant magnetizations can best be explained by a combination of tilt and latitudinal displacement. They observed an elongate distribution of paleodirections which they interpreted as

the result of tilting during magnetization, in the manner described by Beck (1992).

Beck (1992) summarized some of the thermal and paleomagnetic consequences of tilting a batholith. He showed that, because of the large amount of structural relief involved, tilting of a very large igneous body may commence before magnetization is fully acquired at lower levels, and hence tilting of the body need not produce equal deflection of its paleodirections. The paleodirections acquired during tilting will, on a stereographic plot, define a smeared or streaked, rather than circular, distribution, which can be used to constrain the kinematics of the tilting process. Beck (1992) also investigated the effects of starting depths, uplift rates, and tectonic denudation on the minimum times required to cool igneous bodies through the range of typical magnetic blocking temperatures.

There are several other examples of the use of paleomagnetic methods to observe structural tilts in unbedded igneous or metamorphic rocks. An early example was given by Hood (1961), who demonstrated that the NRM directions measured in norites of the south and north ranges of the Sudbury Basin differed in direction by approximately 40°. He hypothesized that the disparity could be explained by assuming 40° of relative tilting about a horizontal east-west axis through the middle of the basin. More recently, Shaver and McWilliams (1988) inferred up to 70° tilt of the plutonic rocks of the Upper Cretaceous Hall Molybdenum Deposit in Nevada. Their analysis combined detailed structural mapping with a comparison of the magnetization directions of core samples and a cratonic reference direction.

Halls and Shaw (1987) showed that paleomagnetic and structural data from 2.6 Ga Matachewan dyke swarms on the east shore of Lake Superior could provide a means for observing crustal tilts caused by Proterozoic rifting, in an area where stratified rocks of pre-tilting age are scarce. They compared the paleodirections of dykes with those observed in dykes inferred to have been undisturbed since their emplacement. Halls and Shaw (1987) measured apparent tilts of the order of 60° to the west, in agreement with dips measured in isolated outcrops of stratiform rocks. They also attempted to use the data to define the location and geometry of a major fault hypothesized to exist along the transition between tilted and untilted crust.

1.3 GENERAL PLAN

As already noted, the primary objective of this thesis is to produce a map of paleomagnetically-observed structural tilts across part of the zone of Eocene extension in southeastern British Columbia, in which little visible evidence of the attitude of the pre-extensional horizontal plane exists.

This information will then be employed to assist in clarifying the extensional history of this part of the southern Omineca Belt. The distribution of apparent tilts of similar sense and magnitude will be used to make inferences about the subsurface geometry of the major extensional faults, and to reveal the existence of previously unmapped structures. Correlation of the paleomagnetic information with the geomagnetic time scale will be combined with existing geological and radiometric data to constrain the timing and duration of extensional events. Older structures will be re-assessed after they have been restored to their pre-extensional attitudes by removing the effects of Eocene tilting.

CHAPTER 2

GEOLOGICAL AND TECTONIC SETTING

2.1 THE CORDILLERAN OROGEN

Although the evolution of the Cordilleran Orogen of western Canada spans an interval of about 1.7 Ga, its main characteristics are primarily the result of Mesozoic to Recent tectonism, during which time two large composite allochthonous superterranes are thought to have collided with each other and with the western ancestral margin of North America (Monger and others 1982; Gabrielse and Yorath 1989). The Omineca and Coast Belts are uplifted zones ("regional tectonic welts") of concentrated deformation, metamorphism, and magmatism, which separate three other belts of less metamorphosed rocks (Figure 2.1). The Intermontane and Insular Belts consist mainly of volcanic-arc and oceanic rocks accreted during mid-Jurassic to Early Cretaceous time and mid-Cretaceous to Paleocene time, respectively. The Foreland Belt consists of an imbricated and folded wedge of miogeoclinal and platformal carbonates, craton-derived clastics, and overlying Cordillera-derived foreland basin deposits, which has been horizontally compressed and displaced northeastward up to 200 km onto the craton during the collisional episodes (Price and Mountjoy 1970; Gabrielse and Yorath 1989).

2.2 OMINECA BELT

The Omineca Belt forms the eastern metamorphic core zone of the Cordilleran orogen, and links the western ancestral (Early Jurassic) margin of

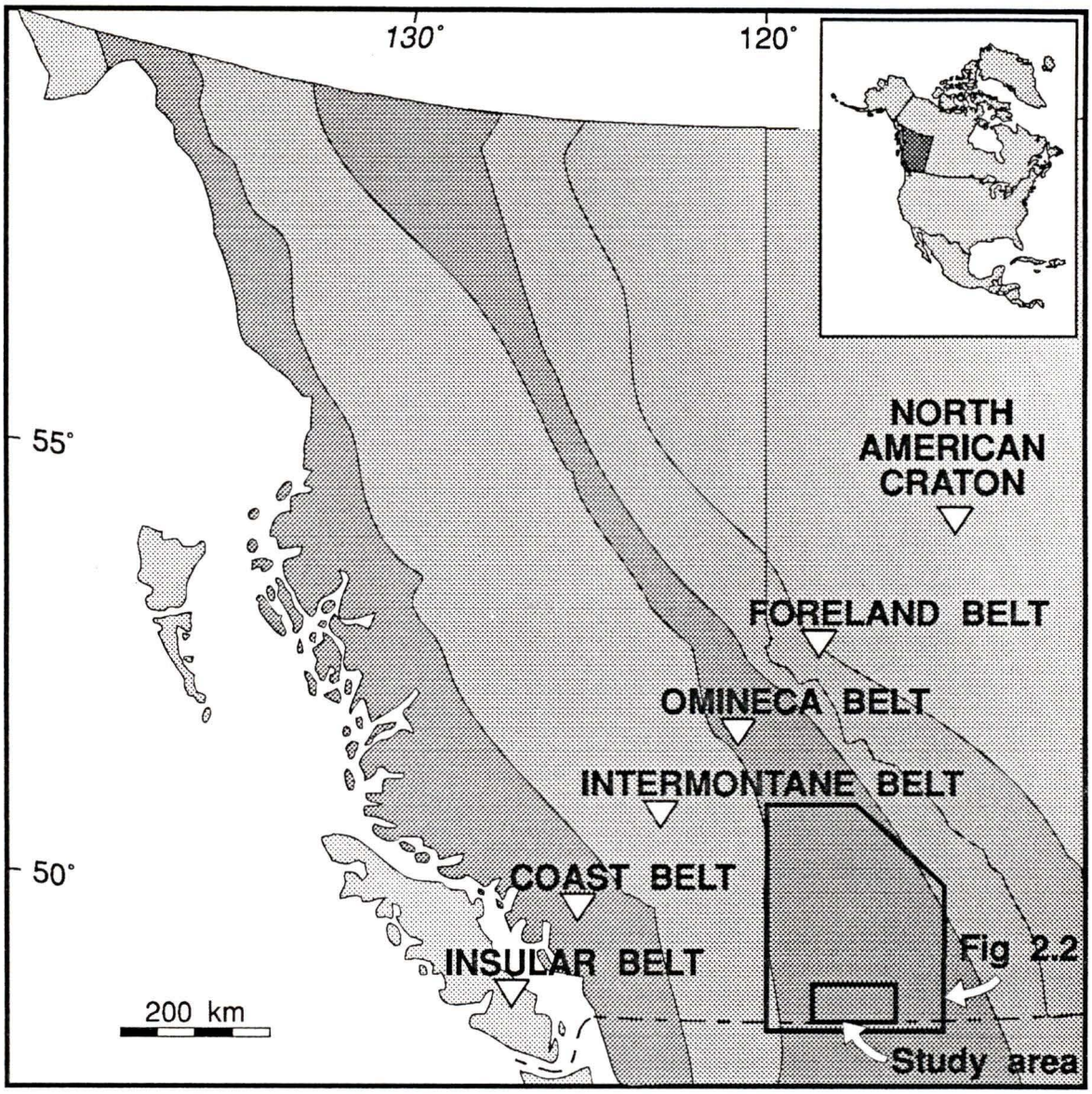

Figure 2.1: Location map showing the outline of the southern Omineca Belt (Figure 2.2) and the area sampled for paleomagnetic study (Figure 5.6, in back pocket) with respect to the major tectonic belts of the Canadian Cordillera.

the North American craton with accreted Paleozoic oceanic and Mesozoic volcanic arc rocks now located mainly in the Intermontane Belt (Monger and others 1982). The latter were tectonically overlapped onto what is interpreted to be the continental margin, and occur as erosional remnants at high structural levels within the Omineca Belt (Figure 2.4 and section 2.3). The present study is located in the southern part of the Omineca Belt, which consists mainly of a series of north-trending structural culminations and depressions, abundantly intruded by Paleozoic to Paleogene granitoid rocks. The fault-bounded antiformal culminations are typical *metamorphic core complexes* (Coney 1980), and expose penetratively deformed and highly metamorphosed mid-Proterozoic to mid-Paleozoic rocks of the North American miogeocline, locally enclosing late Precambrian basement gneiss. These culminations, or core complexes, are structurally overlain, in the depressions, by lower-grade and less penetratively deformed allochthonous upper plate rocks (Gabrielse and others 1991).

There has been much debate on the origin and tectonic significance of metamorphic core complexes of the North American Cordillera (Crittenden and others 1978, 1980). In the Basin-and-Range Province of the southwestern U.S., where Oligocene to Miocene extension has been readily documented in well-preserved bedded sequences, researchers have considered core complexes to be mainly the result of regional uplift and extension (references in Crittenden and others 1980). North of the Snake River Plain, in the northwestern U.S.A. and southeastern British Columbia, extension is Eocene in age, and deep erosion has removed much of the stratified rocks of the upper crust. Most early workers in the north did not recognize the evidence for significant extension, and interpreted what are now recognized as core complexes to have formed primarily

as the result of east-directed thrust uplift during Mesozoic compression (Monger and others 1982; Brown and Read 1983; Journeay 1983, 1986).

The present interpretation of the architecture of the southern Omineca Belt is that it results from the superposition of widespread Eocene crustal extension on a crust previously thickened during Mesozoic to Paleocene compression (Parrish and others 1988). During the culmination of compressional deformation in the Late Cretaceous and Paleocene, it is inferred that the southern Omineca Belt was the locus of crustal-scale imbrication and duplexing which balanced the thin-skinned shortening of miogeoclinal rocks of the Foreland Belt (Brown and others 1986). A thick, composite sheet of internally-deforming middle and upper crustal rocks, the Selkirk Allochthon (Read and Brown 1981), was thrust eastward and ramped onto basement of the North American craton (Brown and others 1986). Gneisses of the Monashee Complex (Figure 2.2), the deepest structural level now exposed in the southern Omineca Belt, were uplifted as much as 25 km along the Monashee Décollement (Journeay 1983, 1986; Brown and Journeay 1987). By the end of compressional deformation in the late Paleocene, the southern Omineca Belt is inferred to have formed an elevated crustal welt at least 60 km thick (Coney and Harms 1984; Brown and Journeay 1987).

Recent work has indicated that although the deep crustal rocks of the core complexes may have been uplifted to middle crustal levels during compression, they were not ultimately exposed until the Eocene, when they were exhumed by displacement along a series of regionally extensive normal fault systems (Brown and Journeay 1987; Parrish and others 1988). During the Eocene, commencing

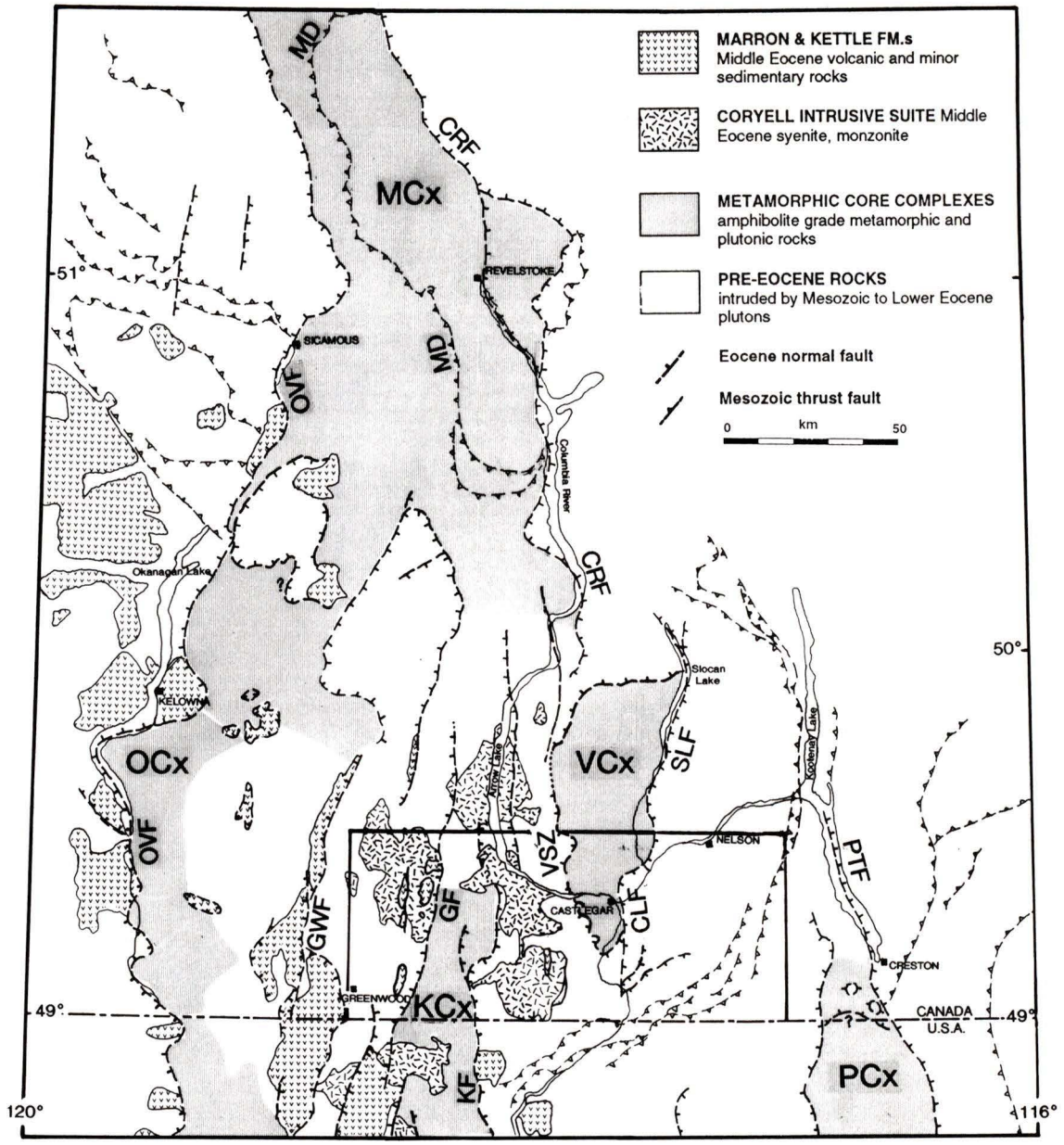

Figure 2.2: Simplified tectonic map of the southern Omineca Belt, showing the distribution of metamorphic core complexes, their bounding faults, and mid-Eocene igneous rocks (after Carr and others 1987; Parrish and others 1988). Outlined is the sampling area of the present study (Figure 5.6). Ornamentation indicates hanging wall of faults. MCx: Monashee Complex; VCx: Valhalla Complex; OCx: Okanagan Complex; KCx: Kettle Complex; PCx: Priest River Complex; MD: Monashee Décollement; CRF: Columbia River Fault; OVF: Okanagan Valley Fault; PTF: Purcell Trench Fault; SLF: Slocan Lake Fault; CLF: Champion Lakes Fault; VSZ: Valkyr Shear Zone; KF: Kettle River Fault; GF: Granby Fault; GWF: Greenwood Fault.

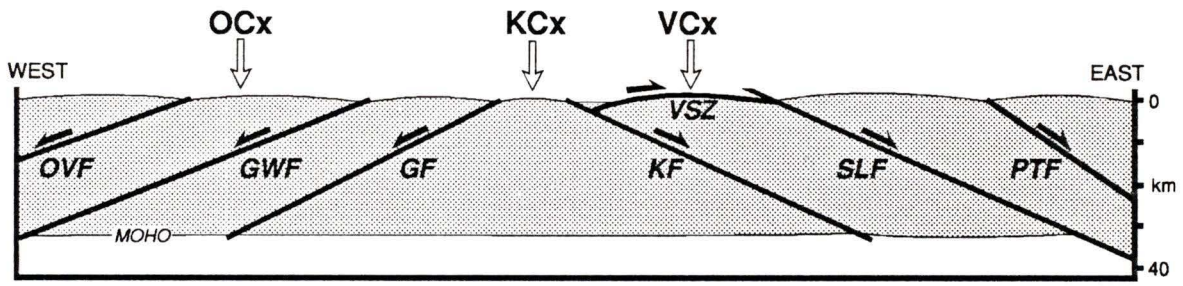

Figure 2.3: Schematic east-west cross-section through the southern Omineca Belt, at the latitude of the Valhalla Complex, showing the spatial relationship between major Eocene normal faults and metamorphic core complexes as inferred by Parrish and others (1988). Abbreviations as in Figure 2.2.

within 3 Ma of the cessation of compressional deformation, the southern Omineca Belt was rapidly uplifted a further 10 to 20 km and tectonically denuded via normal displacements on a series of north-south trending, outward-dipping, brittle-ductile faults and shear zones (Figures 2.2 and 2.3), which have been interpreted to be fundamental crustal breaks (Parrish and others 1988; Brown and Carr 1990). Displacement on these low- and moderate-angle faults brought to the surface large high-grade metamorphic and plutonic bodies of the middle and lower crust - the metamorphic core complexes (Brown and Journeay 1987; Parrish and others, 1988).

2.3 PRE-EOCENE GEOLOGY OF THE STUDY AREA

Upper Proterozoic to Ordovician metasedimentary rocks, inferred to belong to the North American miogeocline, are exposed in the southeast corner of the study area (Figure 2.4). These are overlain, along an arcuate belt of Middle Jurassic thrust faults, by allochthonous Paleozoic oceanic and Mesozoic volcanic arc rocks (Höy and others 1992). In the eastern part of the area, Pennsylvanian to Permian(?) oceanic crust is composed mainly of siltstone, chert, argillite, and carbonate, with minor volcanic, intrusive, and ultramafic rocks (Drysdale 1915; Little 1982; Ash and others 1992). The Lower Jurassic Rossland Group, which unconformably overlies the Paleozoic rocks, consists of mainly fine-grained clastic rocks of the basal Archibald Formation, overlain by augite-porphyritic volcanic and epiclastic rocks of the Elise Formation, which in turn are overlain by fine- to coarse-grained clastic rocks of the Hall Formation (Höy and Andrew 1989; Höy and others 1992). In the western part of the study

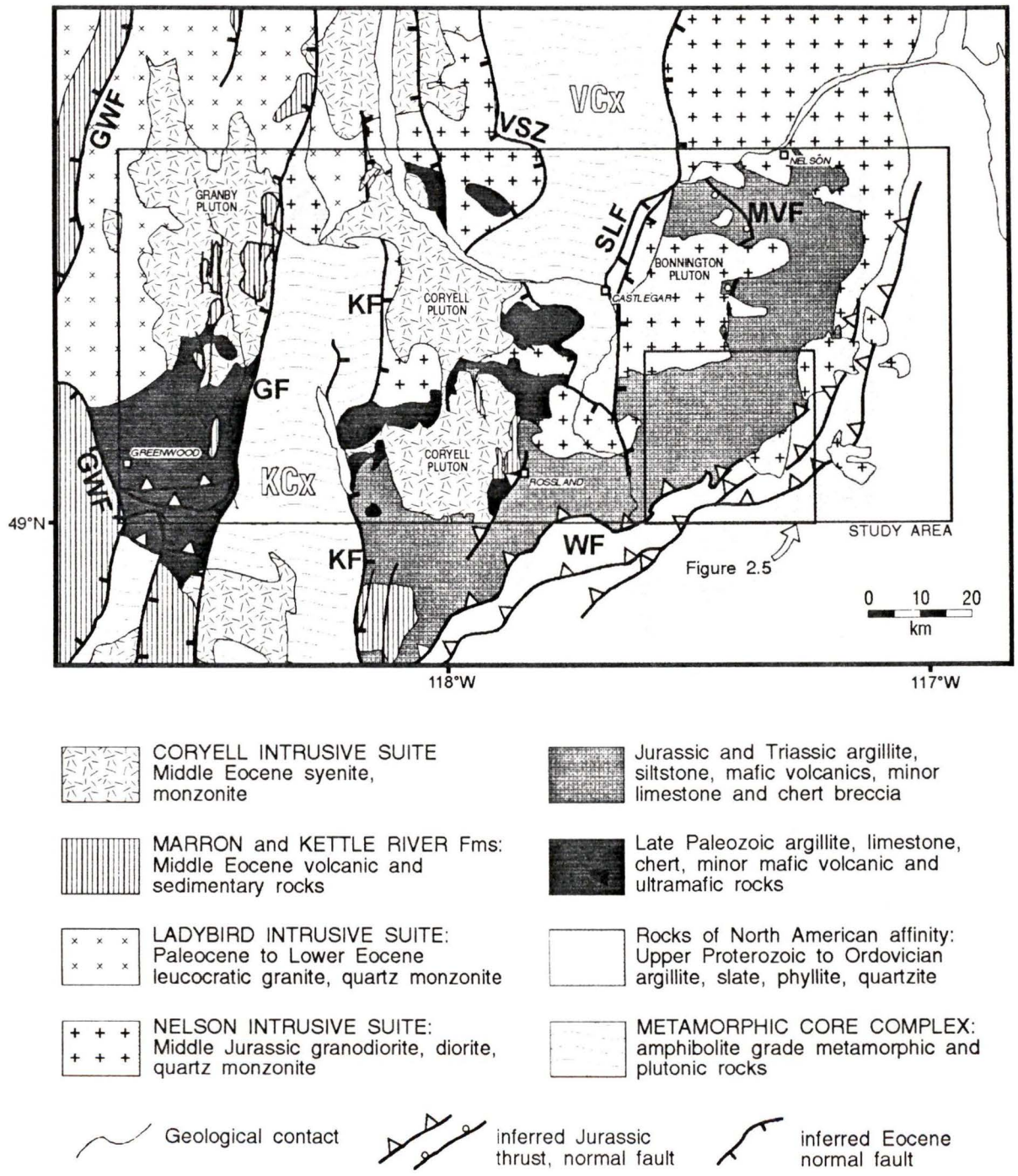

Figure 2.4: Simplified geology of the study area and surrounding region. WF: Waneta Fault, MVF: Mt. Verde Fault, other abbreviations as in Figure 2.2. Ornamentation on fault traces indicates inferred upper plate (see text). (Compiled from Little 1957, 1960, 1982; Carr and others 1987; Parrish and others 1988; Fyles 1990; Stoffel 1990; Andrew and others 1991; Höy and Andrew 1991.)

area, the Late Paleozoic sequence consists of an ophiolitic suite of greenstone, chert, and ultramafic rocks, and another suite of argillite and limestone; these are overlain unconformably by Lower Triassic chert breccia, argillite, limestone, and greenstone (Fyles 1990). Mid-Jurassic imbrication locally has resulted in Paleozoic rocks tectonically overlying Mesozoic rocks.

The allochthonous rocks have been intruded and variably metamorphosed, locally to amphibolite grade, by abundant Jurassic to Tertiary intrusions (Figure 2.4) (Thorpe and Little 1973; Little 1982; Carr and others 1987). Monzonitic and dioritic intrusions of Early Jurassic age in the Rossland and Nelson areas may be comagmatic with Mesozoic volcanics of the Rossland Group (Fyles 1984; Höy and others 1992). These are older than the large bodies of Middle Jurassic granodiorite, diorite, and quartz monzonite of the Nelson Intrusive Suite (Daly 1912; Little 1960, 1982; Simony 1979; Carr and others 1987). Leucocratic granite and monzonite of Paleocene to Early Eocene age, named the Valhalla or Ladybird Intrusions, intrudes granitoid rocks of the Nelson suite and the Early Eocene Valkyr Shear Zone (described below) (Little 1957, 1960, 1982; Carr and others 1987; Parrish and others 1988). Mid-Eocene extension was accompanied by emplacement of large plutons of predominately coarse-grained syenite and monzonite (the ca. 52 Ma Coryell Intrusive Suite) and related mafic dykes, and by widespread resetting of isotopic systems to Eocene ages (particularly in footwall rocks) throughout the southern Omineca Belt (Parrish and others 1988, and references therein). Limited outcrop of andesitic volcanics of the Marron Formation are interpreted to be coeval with the Coryell intrusions (Monger 1968; Little 1982; Holder and Holder 1988).

At least four main phases of pre-Eocene deformation have been recognized. Firstly, block faulting during Early Jurassic extensional tectonics is believed to have produced a tectonic high in the Rossland area, and the basal Archibald Formation of the Rossland Group records deposition in a structural basin to the east (Höy and Andrew 1991; Höy and others 1992). The western and northern margins of the tectonic high may have controlled the location and orientation of later thrusts and normal faults in the Rossland area (Fyles 1984; Höy and Andrew 1991; Höy and others 1992).

Secondly, mid-Jurassic compression produced an arcuate belt of thrust faults in the eastern part of the study area, and a series of north-dipping thrust sheets in the southwestern corner of the area. In the east, within volcanic arc rocks of the Rossland Group, the intensity of folding and shearing increases towards the Waneta and Tillicum Creek Faults (WF in Figure 2.4) (Höy and Andrew 1989, 1990). Thirdly, in the eastern part of the study area, continued compression is recorded by a second generation of east-directed thrust faults and north-trending, upright to east-verging folds (Figure 2.5) (Höy and Andrew 1990; Andrew and Höy 1991). Segments of the Waneta and Tillicum Creek Faults, as well as several of the slightly younger thrusts, have been observed to dip steeply to the east or southeast, and have been interpreted as west-verging structures along which accreted terranes were driven into and beneath miogeoclinal rocks of the craton (Archibald and others 1983, and references therein). More recently, an alternate possibility has been presented (Höy and Andrew 1990; Einarson 1991), based on interpretation of the results of detailed mapping and of paleomagnetic studies (Marquis 1988; Bardoux and Irving

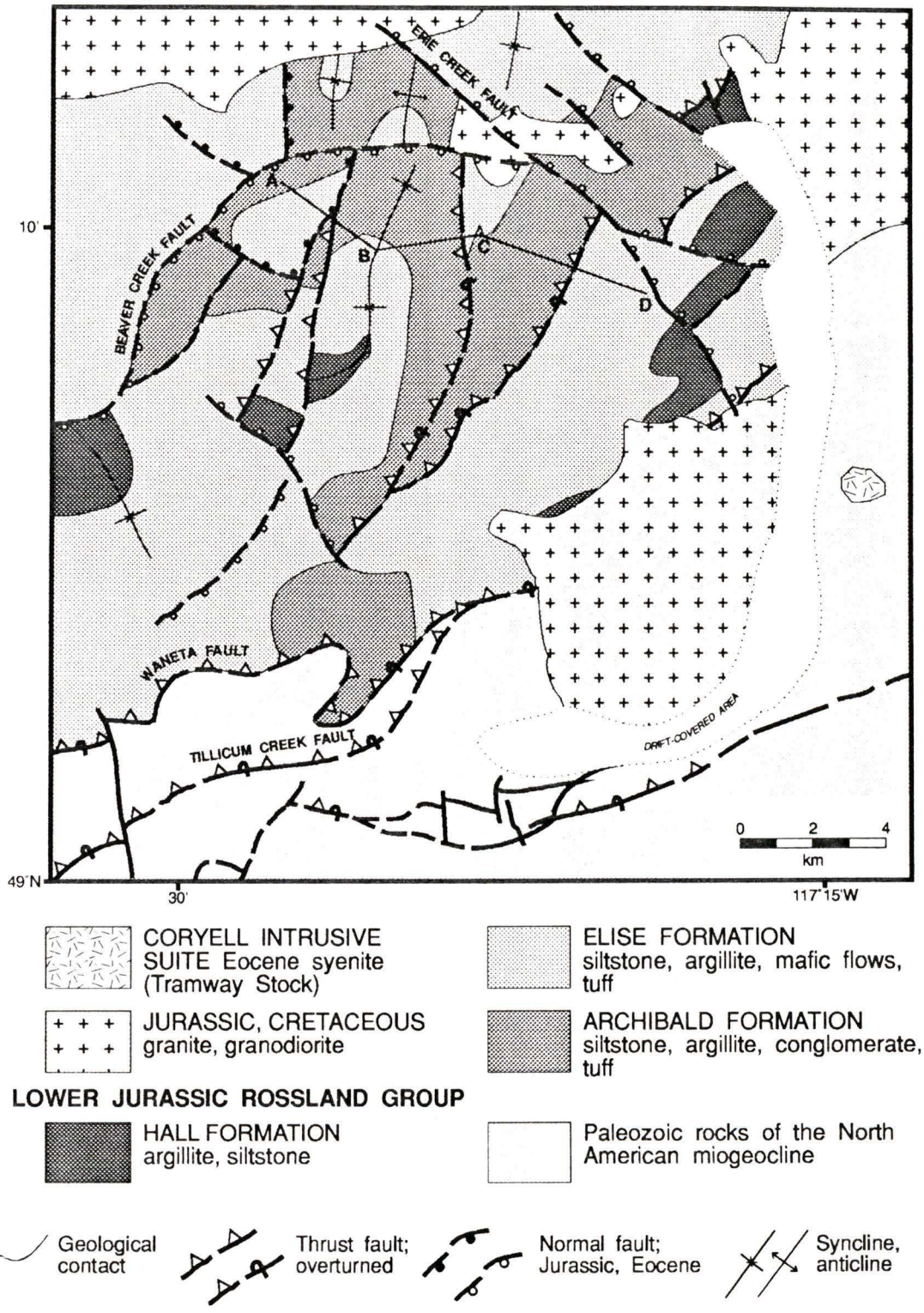

Figure 2.5: Geology of the Mt. Kelly - Hellroaring Creek area (location shown in Figure 2.4), illustrating the different generations of faulting. Cross-section ABCD appears in Figure 6.6. Simplified from Hoy and Andrew (1990) and Andrew and others (1991).

1989), in which these faults are interpreted as east- or southeast-verging thrusts which have been overturned at the surface, possibly due to regional tilting during Eocene extension.

Fourthly, a number of north-trending normal faults in the east half of the study area offset folds and thrust faults in the Rossland Group, and are cross-cut by Middle Jurassic Nelson intrusions (Höy and Andrew 1989, 1990; Andrew and others 1991; Andrew and Höy 1991). Part of the Mt. Verde (Red Mountain) Fault (MVF in Figure 4), southwest of Nelson, dips steeply to the east and exhibits apparent reverse displacement, but has been interpreted as an overturned west-side-down normal fault by Höy and Andrew (1989).

2.4 EOCENE EXTENSIONAL STRUCTURES

Stratified rocks of Eocene age which can be used to measure tilts related to Eocene extension are preserved mainly to the west of the study area. Structural relationships in bedded sequences have been analysed in the vicinity of Greenwood (Monger 1968; Fyles 1990), and farther north, in klippen overlying the Granby Pluton (Carr and Parkinson 1989). These authors reported that many of the faults which comprise the Greenwood fault system (described below) are listric, and Fyles (1990) suggested that displacement on these faults is primarily responsible for eastward dips of 30 to 50° observed in Eocene stratiform rocks as well as for the tilts of similar magnitude observed paleomagnetically in the underlying Granby Pluton by Marquis and Irving (1990).

Few visible indicators of tilt related to Eocene extension are present to the east of the Granby Fault (Figures 2.2 and 2.4). About three kilometres west of

the town of Rossland, a panel of andesitic volcanics of the Marron Formation is bounded on the east by the O.K. Fault (Figure 5.6). These volcanics dip shallowly to the north, except in the immediate footwall, where they dip at moderate angles to the west, possibly the result of drag against the fault (Fyles 1984). A smaller panel of Marron volcanics is exposed about five kilometres to the northwest; these are shown on the map of Little (1982) to dip at various angles and directions. Both these bodies of Eocene volcanic rocks are intruded by syenite of the Coryell Pluton, and the smaller panel is the largest of a number of roof pendants in that area (Little 1982; Fyles 1984). Because of the intrusive nature of contacts with the Coryell Pluton, bedding in the volcanic rocks is difficult to interpret, and may not be a reliable indicator of the pre-tilt horizontal plane.

A body of Eocene volcanic and sedimentary rocks is exposed on First Thought Mountain in northeastern Washington, in the immediate hanging wall of the east-dipping Kettle River Fault (KF) (Figure 2.4). These rocks form a doubly-plunging syncline cut by two east-dipping high-angle faults (Rhodes and Cheney 1981). The syncline has apparently been tilted down-to-the-west, and Rhodes and Cheney (1981) suggest that the high-angle faults may be synthetic listric splays which merge at depth with the KF. Measurements of bedding attitude in another small panel of Eocene volcanic rocks, located five kilometres south of the border near Big Sheep Creek (~118°W), indicate that these rocks may dip at a shallow angle to the west.

In the following paragraphs, the major extensional faults of the southernmost Omineca Belt are briefly discussed, in particular, those within the

area of the present study, as recognized by Parrish and others (1988). Little is known of Eocene structures between the major extensional faults, and this general lack of fundamental structural data has been a major obstacle to the interpretation of extensional deformation in the region. The fault systems described below are illustrated in Figure 2.2; those within the sampling area of the present study are also illustrated in Figures 2.4 and 5.6. Additional information is presented, where appropriate, in Chapter 6, in which the results of the present study are interpreted in terms of the kinematics of Eocene extension.

Most major extensional faults are poorly exposed, and the approximate positions of their surface traces commonly have been inferred from contrasts in lithology and metamorphic grade between footwall and hanging wall rocks. Similarly, the dips of several of the faults have been inferred from the attitudes of mylonitic fabrics exposed in their lower plates, and, in some cases, from seismic reflection data. On the basis of Lithoprobe reflection data, some workers have suggested that most of the major extensional faults flatten into the lower crust; however, they interpret one of these, the Slocan Lake Fault, to extend into the lower crust *without* significant flattening and, possibly, to offset the Moho (Cook and others 1988, 1992; Brown and others 1991; Varsek and Cook 1992). Displacements on the major normal faults have been estimated to be of the order of 10 to 40 km, and locally up to 90 km (Parrish and others 1988). The fault configurations proposed by Parrish and others (1988) are shown in Figure 2.3.

The oldest extensional structure yet recognized is the amphibolite grade Valkyr Shear Zone (VSZ), a 2 to 3 km thick zone of ductile strain which forms the roof of the Valhalla Complex (Carr and others 1987; Parrish and others 1988).

According to these workers, kinematic indicators suggest that motion was upper-plate-to-the-east, and that the VSZ is an eastward-rooting extensional structure, although Carr and others (1987) also pointed out that it could, in fact, be a west-rooting thrust fault.

The VSZ is deformed by the ductile-brittle Slocan Lake Fault (SLF), which bounds the Valhalla Complex to the east (Carr and others 1987). These authors suggested that arching of the Valhalla Complex, during Early Eocene extension, tilted and deactivated the western flank of the VSZ while it was still beneath the brittle-ductile transition, and that normal displacement then continued on the slightly younger SLF. In its central segment, the SLF is thought to dip gently eastward (30°); farther to the south, where the SLF is known as the Champion Lakes Fault, dips are apparently 40 to 80°, according to Corbett and Simony (1984). The SLF is pinned (displacement reduces to zero) at both ends (Little 1982; Corbett and Simony 1984; Parrish and others 1985a; Carr and others 1987).

The Kettle River Fault (KF) forms the eastern boundary of the Kettle Complex. It is exposed along the Kettle River in Washington, but not in British Columbia (Parrish and others 1985b), where the position of its surface trace is inferred to correspond to the boundary between amphibolite grade metamorphic rocks of the Kettle Complex and much lower grade hanging wall rocks to the east (Preto 1970; Cheney 1980; Rhodes and Cheney 1981). Earlier workers believed the boundary to follow the west branch of the KF, but Parrish and others (1988) have assigned sillimanite-grade rocks northeast of Christina Lake to the Kettle Complex, and positioned the KF farther to the east (Figures 2.4 and

5.6). If this relationship is correct, then the trace of the fault is intersected by a westward-extending lobe of the Coryell Pluton. The pluton is thought to cross-cut the fault (Parrish and others 1988), although this relationship, like the exact position of the fault, has yet to be documented and is therefore not known with certainty (R. Parrish, personal communication 1992). In Washington, the KF is observed to be a brittle fault, which dips about 30° east; here, however, it apparently truncates mid-Eocene plutonic and volcanic rocks (Rhodes and Cheney 1981).

The Kettle Complex is bounded on its west side by the west-dipping Granby Fault (GF). The GF juxtaposes sillimanite-grade paragneiss and plutonic rocks in its footwall against unmetamorphosed and chlorite-grade rocks in its hanging wall, and truncates the Granby Pluton (Preto 1970; Carr and Parkinson 1989). The fault dips on average 25 to 35° west, but is steeper locally (Carr and Parkinson 1989). Detailed mapping in the hanging wall of the GF by these workers revealed a number of subsidiary faults. They interpreted the essentially flat-lying Jones Fault, which underlies isolated klippen of volcanic rocks of the Eocene Marron Formation (Figure 5.6), to be older than the GF. Also, they interpreted the sub-parallel set of steeply-dipping faults in the hanging wall of the GF to be younger than the GF.

Outside the study area, three other major Eocene extensional faults have been proposed: the east-dipping Purcell Trench Fault (PTF) to the east, and the west-dipping Greenwood (GWF) and Okanagan Valley (OVF) faults to the west (Figure 2.2). The PTF, which bounds the eastern side of the Priest River Complex in Idaho and northeast Washington, is thought to be a ductile-brittle

normal fault which accommodated tens of kilometres of east-directed displacement (Rehrig and Reynolds 1981; Parrish and others 1988; Harms and Price 1992). Parrish and others (1988) proposed that the PTF extends north of the international border and underlies southern Kootenay Lake (Figure 2.2). The GWF is actually a complicated west-dipping system of low and moderate angle brittle faults, which roots in the vicinity of Greenwood, and which may include the Jones Fault in the hanging wall of the GF (Parrish and others 1988). As described at the beginning of this section, many of the faults regarded by Parrish and others (1988) as segments of the GWF are listric and may be related to structural tilts observed in the Greenwood area. The OVF follows Okanagan Valley and forms the western boundary of the southern Omineca Belt. This ductile-brittle fault is believed to dip about 20 to 45° to the west, and may have accommodated up to 90 km of top-to-the-west displacement (Tempelman-Kluit and Parkinson 1986; Parrish and others 1988; Armstrong and Parrish 1989).

2.5 TIMING OF EXTENSION

The VSZ deforms 58 ± 1 Ma (U-Pb zircon) Ladybird Granite, and is intruded by late post-kinematic granite and pegmatite, which has been dated (U-Pb zircon) at 56.5 ± 1.5 Ma (Carr and others 1987; Parrish and others 1988). Deformed, synkinematic muscovite from within the Slocan Lake fault zone has been dated by Rb-Sr methods at 54.5 ± 1.5 Ma by Carr and others (1987) who interpreted this to be the age of greenschist grade mylonitization, at temperatures less than 450°C, in the fault zone. They argued that displacement on the VSZ occurred within about four million years, between 58 and 54 Ma, and that this was followed by motion on the SLF at 54 Ma. Parrish and others (1988)

suggested that motion on most of the east-dipping faults ended by 52 Ma, which would constrain the age of the SLF and KF to between 54 and 52 Ma. However, they did not report any data which firmly constrain the age of last motion on these faults. Their interpretation appears to be based mainly on Rb-Sr ages (noted above) of synkinematic muscovite from the SLF (and supporting dates from the Columbia River Fault to the north, Figure 2) which they take to indicate that much of the ductile deformation is of Early Eocene age. The SLF itself is nowhere reported to be cross-cut by rocks known to belong to the Coryell Intrusive Suite. Corbett and Simony (1984), however, observed both crushed and undeformed dykes, of presumed Eocene age, within the Champion Lakes fault zone, the southerly continuation of the SLF. They inferred that motion was broadly contemporaneous with dyke intrusion. If the undeformed dykes are related to the 52 Ma Coryell Intrusive Suite, then movement on the SLF must have ceased by approximately this time, as argued by Parrish and others (1988). No precise radiometric ages are yet available for these undeformed dykes.

As noted above, the KF *may* be intruded by the 52 Ma Coryell Pluton, and this would place a firm upper limit on the age of the KF, but this has yet to be verified (R. Parrish, personal communication 1992). South of the international border, however, the KF is believed to truncate, and hence may be younger than, mid-Eocene Coryell plutons and related volcanic rocks (Rhodes and Cheney 1981). In order to reconcile this apparent ambiguity, Parrish and others (1988) proposed that both Early and Middle Eocene displacement occurred. An alternative explanation is that the KF consists of several segments, and that displacement is older on the more northerly segments than on those farther to the south.

In summary, therefore, the age and duration of motion on the VSZ is well constrained geochronometrically between 58 and 54 Ma, and the east-dipping normal faults are generally older than the west-dipping ones. An older age limit of 54 Ma for the east-dipping SLF seems reasonably well established; a younger age limit of 52 Ma has been suggested, but the evidence for this is not strong. The west-dipping faults (GF, GWF, and OVF) apparently truncate *circa* 52 Ma Coryell intrusions or related volcanics, and hence are interpreted to be younger than this age. An older age limit of 51 Ma for the west-dipping GF seems well established by the age of the Granby Pluton (51.1 ± 0.5 Ma, U-Pb zircon, Carr and Parkinson 1989), but a younger age limit for displacement on any of the west-dipping faults has not been established.

CHAPTER 3

SAMPLING PROCEDURES

3.1 INTRODUCTION

The initial stage of sampling was carried out during August, 1990. The first two weeks were spent collecting oriented core from 19 sites along an east-west transect of the extensional zone from the Columbia River Fault to the Okanagan Valley Fault, along, or close to, the Trans-Canada Highway between the towns of Revelstoke and Sicamous (Figure 2.2). Most samples were amphibolitic metasedimentary rocks of the Monashee Complex and the overlying Selkirk Allochthon. During the last two weeks, efforts were concentrated farther south, to extend the previous collections (34 sites) made by Irving in 1985 (reported in Bardoux and Irving 1989) and by Marquis and Irving during 1987 (reported in Marquis 1988, and Marquis and Irving 1990). Metadiorites, syenites, and dyke rocks were collected from 35 sites from the hanging wall of the Kettle River Fault to the hanging wall of the Slocan Lake / Champion Lakes Fault.

The second round of sampling took place during August, 1991. Preliminary results from the 19 sites collected along the northern transect indicated that the metasedimentary rocks are, in general, too unstably magnetized to be suitable for paleomagnetic study. It was decided to abandon the northern transect and to concentrate further sampling in the area to the south. An additional 43 sites were collected in the latter during 1991, bringing the total number of sites collected in the southern area to 112. The locations of sample sites are plotted in Figure 5.6 (in back pocket), and are described in detail in Appendix A.

3.2 SAMPLING CRITERIA

There are a number of criteria which should be met for a site to be considered suitable for sample collection. First, there must be reasonable grounds for believing that the rocks cooled, and hence probably acquired their magnetization, during the mid-Eocene (approximately 54 to 47 Ma). Rocks of this age are likely to have recorded tilting due to extension, and their paleomagnetic directions (paleodirections) can be compared to the reference direction for North America, which is known with great accuracy for the mid-Eocene (Chapter 5). Plutons and related dykes of the Coryell Intrusive Suite are known to have crystallized and cooled rapidly during this interval of time. Metamorphic rocks of the Valhalla and Kettle River Metamorphic Complexes (VCx and KCx in Figure 2.2) also record mid-Eocene cooling ages. Therefore, these intrusive and metamorphic rocks were considered to be the best sampling targets.

A second criterion is that the rocks must have a mineralogical composition such that they are likely to have acted as good recorders of the geomagnetic field during cooling. Previous experience, borne out by the present work, has shown that this requirement is generally satisfied by rocks which are rich in ferromagnesian minerals. Such rocks commonly contain free magnetite or titanomagnetite, or they may contain pyroxene or hornblende, minerals which commonly contain fine inclusions of these oxides. In some areas, the margins of the Coryell plutons, as well as most of the related dykes, are quite mafic, with up to about 40% ferromagnesian minerals; these rocks were sampled preferentially

over less mafic phases. Many of the meta-igneous rocks sampled in the Valhalla Complex also are rich in pyroxene and/or hornblende.

Where detailed mapping has been carried out in this part of the southern Omineca Belt (e.g. Granby Valley (Carr and Parkinson 1989); Rossland area (Fyles 1990); eastern study area (Andrew and others 1991)), it is apparent that geological structure is complex. Hence, if paleomagnetism is to assist substantially in determining structure, a high density of samples is necessary. Ideally, sites should be evenly distributed across the area, in both the hanging walls and footwalls of mapped extensional faults. The distribution of sites, however, is controlled mainly by the availability of suitable rock types and outcrop, and by accessibility along highways and logging roads. Most sites are located in roadcuts, which provide fresh rock surfaces, and are unlikely to have been affected by lightning strikes. Because of the paucity of suitable lithologies and the lack of road access, no sites were obtained within the Kettle River Metamorphic Complex (Figure 2.2). One region of high sample density is the north shore of Arrow Lake, where almost continuous outcrop is available over long stretches of Deer Park Forest Service Road (Figure 3.1).

3.3 SAMPLE COLLECTION AND PREPARATION

A minimum of five cores, 2.5 cm in diameter and ranging from 3 to 12 cm in length, were obtained from each site using a gasoline-powered drill designed specifically for this purpose (Figure 3.2). At each outcrop, cores were spread over one to three metres, and occasionally up to ten metres.

Figure 3.1: View to the northwest, from Syringa Creek Provincial Park, showing the extent of outcrop along Deer Park Forest Service Road on the north shore of Lower Arrow Lake. This is part of the "Syringa Section" of Marquis (1988) and Marquis and Irving (1990).

Figure 3.2: The author using a gasoline-powered drill to collect core from bedrock exposed in the bed of a stream.

Each core was oriented using a sleeve-and-platform mounted Brunton compass. To ensure accuracy of measurement, bearings were measured in both directions. The magnetic readings obtained were also verified, when weather and topography permitted, using a specially-designed solar compass. In most cases, measurements by the two methods agreed to within one or two degrees. Where they differed by more than this amount, the sun reading was generally taken to be the more accurate of the two. Another common practice when orienting paleomagnetic cores, is to verify magnetic readings by taking sightings to local landmarks and comparing the bearings obtained to those expected from a topographic map. However, because of the considerable topographic relief and forest cover in most of the map area, this was not possible. Hand specimens were obtained, from all but a few sites, so that samples would be available for the purpose of radiometric dating and petrographic study as required.

One or two specimens were cut from each core, depending on its length. This was accomplished using a rock saw with special clamps designed to hold drill core. During the present study, a total of 444 cores were collected from 78 sites along the southern transect, and 818 specimens were prepared for paleomagnetic analysis.

CHAPTER 4

PALEOMAGNETIC ANALYSIS

4.1 INTRODUCTION

This chapter begins with a discussion of how primary and secondary magnetizations may be acquired by igneous and metamorphic rocks during and after cooling. This is followed by a description of the techniques by which the stable primary magnetizations of interest are isolated and their directions measured. The criteria are then described by which the magnetizations are graded according to their reliability as recorders of the paleofield. On this basis, some sites and specimens are rejected from further study. The results of the analyses are compiled in Table 4.2. An explanation of statistical parameters employed is given in Appendix B.

4.2 ACQUISITION OF REMANENCE

When the magnetic minerals (usually Fe-Ti oxides) of an igneous rock are cooled through their *Curie temperatures*, T_c, in the presence of an applied magnetic field, they acquire a spontaneous magnetization directed parallel to that field. At temperatures very near to T_c, the magnetization reaches equilibrium with, or "relaxes into", the field very rapidly, and so changes in direction if the field direction changes; the *relaxation time*, τ, is very short (microseconds). As the temperature falls, τ increases exponentially, so that at a temperature slightly below the Curie point, known as the *blocking temperature*, T_b, τ becomes very long (millions of years for fine-grained single-domain magnetite) and the magnetization becomes "frozen in"; this magnetization is called *thermoremanent*

magnetization, or TRM. Because a rock may typically contain several magnetic phases or exsolved members of solid solution series, each with different τ's and corresponding T_b's, the ensemble of grains present in a rock specimen will gain its magnetization over an interval of time. Slow rates of cooling will tend to increase τ and lower T_b, but by only a few degrees (York 1978). If the rock is essentially isotropic in character, with no preferred orientation of the crystallographic or grain shape axes of magnetic grains, its direction of magnetization will be parallel to the ambient field during cooling. Dykes and small stocks intruded into cold country rocks may acquire TRM as a result of conductive cooling. Plutonic rocks emplaced at depth into hot country rocks may become magnetized as a result of later uplift, by cooling through the isotherms corresponding to their T_b interval (Pullaiah and others 1975). Metamorphic rocks found at great depths may become magnetized in the same way as they are uplifted and cooled. It is with magnetizations acquired as a result of intrusion and cooling, or uplift and cooling, that this thesis is principally concerned.

The Curie temperature of fine-grained magnetite is approximately 580°C, and measured blocking temperatures are commonly in the range 550 to 580°C. Members of the ulvospinel-magnetite solid solution series, the titanomagnetites, form a complete solid solution above 600°C; at lower temperatures one phase forms exsolution lamellae in the other. The Curie temperature of titanomagnetite decreases in an approximately linear manner as the proportion of ulvospinel increases (Irving 1964).

In the above discussion, the acquisition of remanence has been described in terms of relaxation time and blocking temperature. The phenomenon can also

be discussed in terms of *coercive force, or coercivity,* H_c, which is defined in Figure 4.1. When the relaxation time, τ, is large, coercivity is generally large. Above T_b, and below T_c, the coercivity is small, much less than the Earth's field. As cooling takes place through T_b, the coercivity increases exponentially, within a few tens of degrees becoming two or more orders of magnitude greater than the Earth's field. The remanence is thus able to retain its memory of the field, despite later changes (such as reversals) of the ambient field. Although dependent on a variety of factors, including anisotropy and the presence of intergrowths and impurities, the main influence on coercivity is grain size and shape (Day 1977). Single domain (SD) grains are of the order of 10^{-6} m in diameter, and generally have high coercivities. Larger particles (greater than about 10^{-5} m in diameter) minimize their total energy by subdivision into multiple domains. Because it is relatively easy to move domain walls, the remanence carried by multi-domain (MD) grains is generally of lower coercivity, and hence lower stability, than that of SD grains.

Subsequent to the acquisition of TRM, considered here to be the *primary* component of magnetization, acquired during cooling from high temperature, a rock may acquire *secondary* components of magnetization. The most common type is *viscous remanent magnetization*, VRM, parallel to the ambient field, which may be acquired over long periods of time at temperatures well below T_b. This occurs if grains with τ in the order of 1 to 10^6 years are present. Such grains are either just below or just above the critical size for single domain grains. In the latter case, they are referred to as multi-domain grains. Typically a

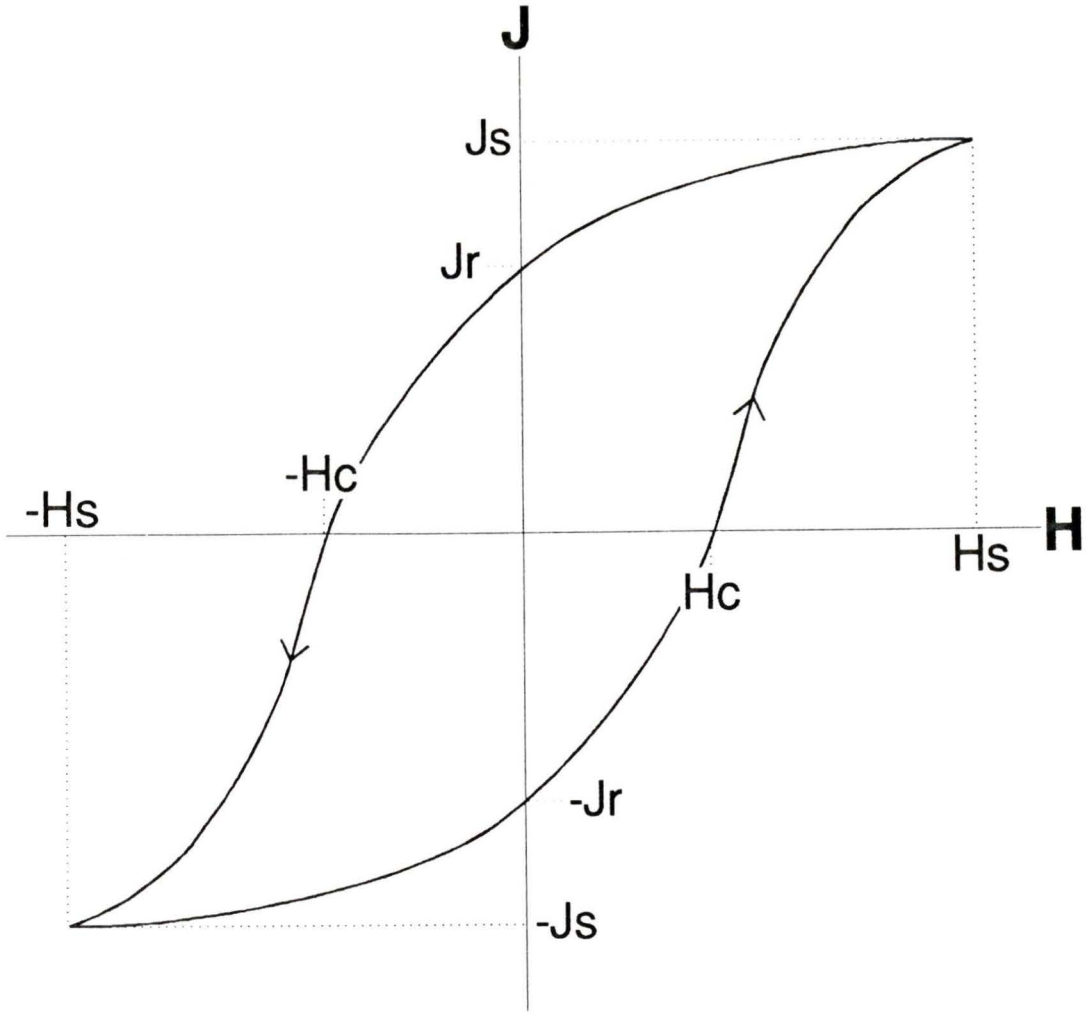

Figure 4.1: Theoretical hysteresis loop for a specimen containing an ensemble of randomly oriented magnetic grains (from Irving 1964). As an external magnetic field, *H*, is increased, the magnetization, *J*, induced in the specimen reaches a saturation value, J_S, at a field *Hs*. If the field is then removed, *J* is reduced, but not along the same path, and, in zero applied field, a magnetization, J_r, (known as an isothermal remanent magnetization, or IRM) remains. If the field is then increased in the opposite direction, *J* is reduced to zero at an applied field *-Hc*, known as the *coercive force*. If the reverse field is increased further, saturation, $-J_S$, is reached at *-Hs*. The same paths are followed during repeated oscillation of the field, forming what is referred to as a *hysteresis loop* (hysteresis ≡ memory).

relatively soft magnetization, VRM decays and reforms in a new direction when the ambient field changes. VRM's in specimens are commonly aligned parallel to the direction, at the collecting locality, of the present Earth's field (PEF) if τ is in the order of 1 to 10 years, or to the direction of the geocentric axial dipole (GAD) if τ is in the order of 10^2 to 10^6 years. Specimens from a number of the sites measured during this study exhibit, in addition to primary TRM, a secondary viscous component approximately parallel to the GAD or PEF. This is referred to as a *Bruhnes overprint*. Other spurious magnetizations of viscous origin may be acquired by specimens during storage in the laboratory or during transportation, for example.

Rocks may also acquire a remanence, parallel to the ambient field, during secondary alteration or recrystallization, at temperatures below the Curie points of their magnetic minerals. This is known as *chemical (or crystallization) remanent magnetization*, or CRM. Following nucleation, the relaxation time, τ, of a crystal increases as its size increases. As a crystal grows through its *blocking volume*, V_b, and reaches single-domain size, τ increases exponentially, and the crystal acquires a remanent magnetization of high stability. With increased growth, the crystal enters the size range for multi-domain grains, and the stability of its remanence is lowered. It is not critical, for the present study, to distinguish between TRM and CRM, provided they were acquired at the same time, during mid-Eocene cooling. The majority of specimens collected during this study were obtained from exposures of fresh, unweathered rock, and show no evidence of secondary alteration or recrystallization of magnetic minerals subsequent to Eocene cooling.

4.3 MEASUREMENT PROCEDURES

Partial demagnetization ("cleaning") of specimens is employed to remove secondary VRM's from the total magnetization (NRM) in order to isolate the primary component of interest. This technique is possible because secondary components are generally of lower *stability* (less resistant to change) than the primary component. They are, because of their lower *unblocking temperature*, T_{ub}, less resistant to heat, and because of their lower coercivity, H_c, less resistant to applied magnetic fields, than primary TRM.

During stepwise thermal demagnetization, specimens are heated to successively higher temperatures and then cooled in field-free space. Each treatment step effectively randomizes the magnetization in grains having T_{ub}'s less than the treatment temperature employed. In stepwise alternating field (AF) demagnetization, specimens are tumbled while subjected to progressively higher alternating magnetic fields, which randomizes the magnetization directions of grains which have a coercivity less than the peak field employed at each step. Bruhnes-age VRM's are commonly randomized by partial demagnetization at temperatures of about 300 to 400°C or in alternating magnetic fields (AF) of 10 to 20 mT (Irving 1964).

Measurements of initial NRM and of remanence after demagnetization were carried out using a Schonstedt SSM-2 spinner magnetometer controlled by an IBM/PC. The automated system used at the Pacific Geoscience Centre enables unattended measurement of batches of up to fifteen specimens. At least two pilot specimens per site were then chosen for detailed stepwise

demagnetization: one thermally, the other with alternating magnetic fields (AF). Thermal demagnetization was carried out using a Schonstedt TSD-1 furnace, and AF demagnetization using a Schonstedt GSD-5 AC tumbling demagnetizer. The optimum demagnetization technique and intensity for the remainder of the specimens from each site were determined through concurrent analysis of stereographic, orthogonal, and intensity versus treatment diagrams.

Examples of essentially single component magnetizations are illustrated in Figures 4.2 and 4.3. A spurious VRM component, possibly acquired during storage, is removed between room temperature and 100°C in Figure 4.2, and by 300°C in Figure 4.3. At higher temperatures, the direction of magnetization remains approximately constant, as shown in the stereographic projections. This clustering of directions during thermal demagnetization is referred to as an *endpoint*, and reflects the *thermal stability*, or resistance to heat, of the primary component. Eventually, commonly above 580°C (for magnetite), all magnetization in the specimen is destroyed. A similar endpoint is observed using AF demagnetization techniques.

On orthogonal plots (Zijderveld 1967; Dunlop 1979), which show both the direction and relative intensity of the magnetization vector during demagnetization, linear decay to the origin indicates a stable primary component has been isolated. (In practice, an orthogonal plot showing the changes in intensity and direction in a horizontal plane is used in conjunction with the plot of the north-south vertical plane shown in the figures.) When the line is well-defined (as in Figure 4.2), a treatment level can be readily determined which will remove any secondary components present. Where the line is less well defined,

the direction of the stable magnetization can be calculated by fitting a least-squares line to the points. By measuring the direction of remanence after each demagnetization step, the direction of the removed vector (M_R in Figures 4.2 to 4.6) can be calculated.

Plots of intensity versus thermal treatment reveal information about the unblocking temperature(s) (T_{ub}) of the magnetic minerals in the specimen. The example in Figure 4.2 illustrates a discrete T_{ub} above 550°C, indicating the magnetic carrier is fine-grained single-domain magnetite. The corresponding plot in Figure 4.3 shows a distributed T_{ub}, suggesting the primary magnetization is carried by both magnetite and titanomagnetite. Plots of intensity versus AF treatment (an example is given in Figure 4.6) indicate the coercivity of the magnetic carriers, or resistance of the remanent magnetization to alternating fields.

Analysis of these plots enables determination of the treatment level necessary to remove any secondary components present and isolate the principal stable component of TRM. AF demagnetization techniques are employed preferentially because they are less time-consuming than thermal methods. Because T_{ub} and H_c may be distributed over a wide range, it is, in some cases, cumbersome to use these parameters to describe or characterize the behaviour of specimens during demagnetization. A useful quantity in this regard is the median destructive temperature, MDT, which is the temperature at which the initial NRM intensity is reduced by 50%. Similarly, the median destructive field, MDF, is the AF level at which 50% of the initial NRM is destroyed.

4.4 TYPES OF MAGNETIZATIONS

A wide range of behaviour was exhibited by specimens during demagnetization. The sites are sorted into three main categories according to the median destructive temperature (MDT) and other characteristics. These categories are discussed below, and summarized in Table 4.1. The directions of the primary magnetizations obtained are compiled in Table 4.2. Data from previous studies (Marquis 1988; Bardoux and Irving 1989; Marquis and Irving 1990) has been reclassified according to the criteria described below (Table 4.3). In addition, specimens from four sites studied by Marquis, but incompletely processed, have been re-measured.

Type A behaviour is distinguished by strong, single-component magnetization. MDT's are over 500°C, producing, on a plot of intensity versus treatment, a square-shouldered curve, typical of fine-grained single-domain magnetite (Figure 4.2). Type A magnetization is characterized by a stable endpoint on stereographic projections and by linear decay to the origin on orthogonal plots, both attained after a soft viscous overprint is removed by treatment at 10 or 20 mT. MDF's are variable, but not less than 9 mT. Specimen directions are very well grouped within each site (k generally $\geq$ 100). Type A magnetization is considered to to provide a record of the paleofield during mid-Eocene cooling through T_b, either after intrusion or as a result of uplift (or both).

Type B magnetization is less ideal than type A, although it yields useful information. MDT's are less than 500°C, and T_{ub}'s are commonly distributed over a wide range between room temperature and 600°C. The magnetic carriers in these specimens are interpreted to be magnetite and/or titanomagnetite.

Table 4.1: Categories of observed magnetic behaviour

CATEGORY	MDT	CHARACTERISTICS	INTERPRETATION
A	> 500°C	Single very hard component; well-grouped directions	Record of paleofield
B1	< 500°C	Single hard component; well-grouped directions	Record of paleofield
B2		Soft component grouped around PEF; underlying hard component	Hard = record of paleofield; soft = Bruhnes overprint
C1	variable, commonly < 300°C	Very soft component; directions grouped around PEF	Bruhnes overprint only
C2		Very strong magnetization; scattered directions	Lightning magnetization only
C3		Incoherent magnetization; scattered directions	No record of paleofield
C4		Magnetizations with very low coercivity and very high T_{ub}	Not understood; not interpretable as a record of the paleofield

CATEGORY	# SITES	SITES FROM PREVIOUS STUDIES	TOTALS	
A	25	17	42	
B1	25	7	32	78
B2	1	3	4	
C1	7	5	12	
C2	2	0	2	34
C3	16	2	18	
C4	2	0	2	
A & B SITES WITH $\alpha_{95} > 12°$	2	1	3	

NOTES: Description of categories of magnetic behaviour (top); numbers of sites in each category (bottom). Of 112 sites, 34 type C sites are rejected. Of the 78 A and B sites remaining, 3 yield mean directions with $\alpha 95 > 12°$ (see Table 4.2) and are rejected. 75 sites are retained. Additional sites are from Marquis (1988, and unpublished data) and Bardoux and Irving (1989).

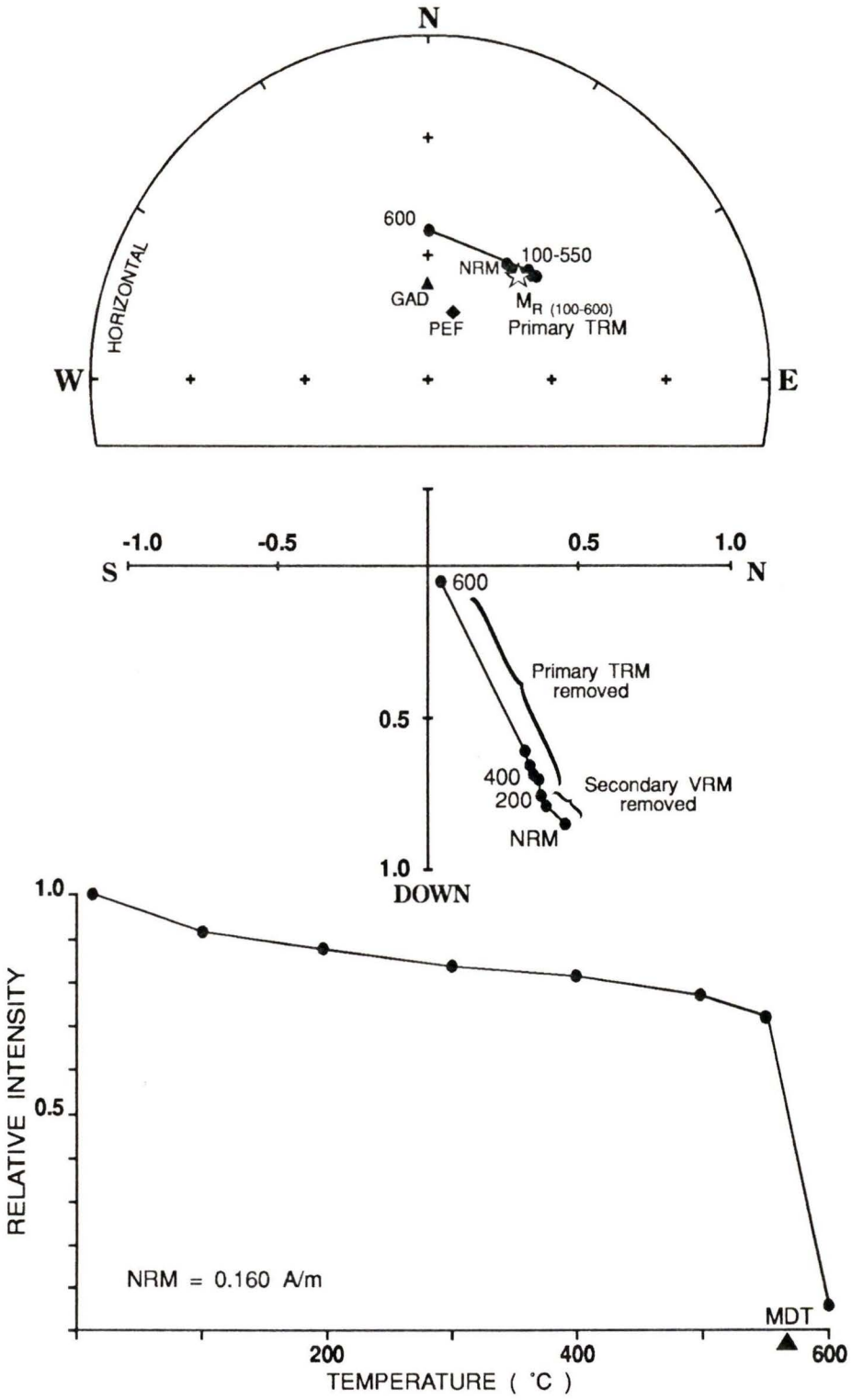

Figure 4.2: A-type magnetization, site 80. Plots show change in direction (top) and intensity (bottom) during thermal demagnetization; orthogonal plot (middle) shows trajectory of the magnetization vector endpoint projected into a north-south vertical plane. Star indicates the direction of the magnetization removed (M_R) within the interval indicated in brackets.

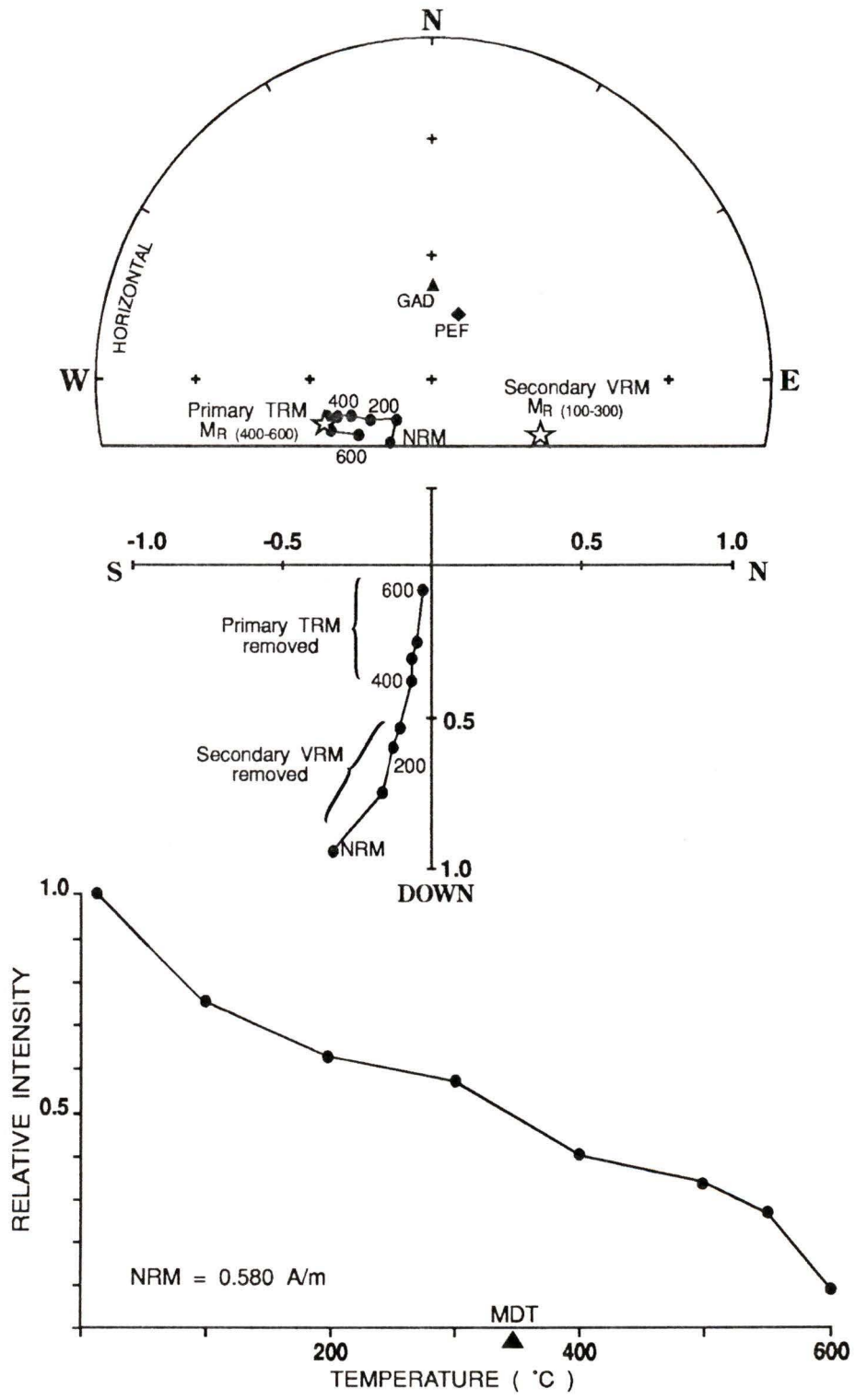

Figure 4.3: B1-type magnetization, site 98. Refer to Figure 4.2 for explanation.

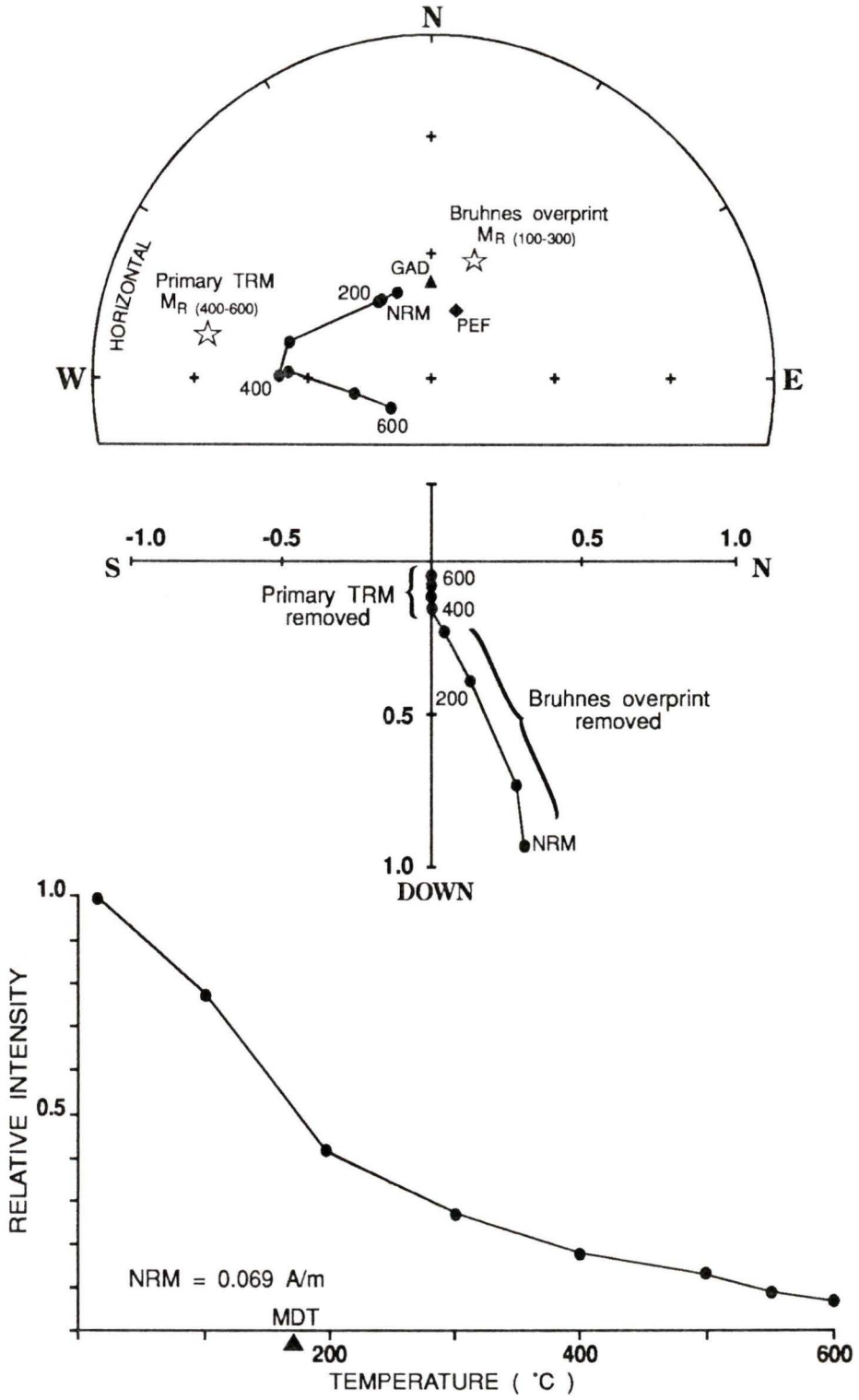

Figure 4.4: B2-type magnetization, site 78. Refer to Figure 4.2 for explanation.

MDF's range as low as 6 mT. Within-site grouping of specimen directions is generally good ($k \approx 50$).

Type B behaviour is divided into two sub-categories, on the basis of observed magnetization components, which are identified from stable endpoints or from intervals of linear decay to the origin on orthogonal plots. Sites in category B1 have essentially single-component magnetizations (Figure 4.3). Spurious VRM components, generally not aligned close to PEF, are removed by treatment at 300°C or 20 mT. On orthogonal plots, the primary TRM may decay linearly and to the origin, but the end-point is not as well-defined as in type A. B1 magnetizations are interpreted to be an adequate record of the mid-Eocene paleofield. B2 magnetizations consist of a hard component and a soft component approximately parallel to PEF ($M_{r[100\text{-}300]}$ in Figure 4.4). The former is interpreted to be a record of the paleofield, and the latter, which is removed by treatment at 10 or 20 mT, to be a Bruhnes overprint. In Figure 4.4, the secondary VRM component, removed by treatment at 300°C, is a Bruhnes overprint, aligned approximately parallel to the PEF.

MDT's of type C magnetizations are variable but generally less than 300°C; MDF's range as low as 5 mT. There are four sub-categories. Type C1 sites possess only a soft component approximately parallel to the PEF (Figure 4.5); this is interpreted to be entirely a Bruhnes overprint. Type C2 sites exhibit a very high-intensity NRM, which decays quickly during treatment. Although thermal treatment sometimes may produce apparently good results (see Figure 4.6), no useful linear decay or endpoint can be obtained by AF demagnetization. C2 sites are interpreted to have been affected by lightning, which has obliterated all record of the paleofield. C3 magnetizations are incoherent, with highly scattered directions. Finally, two sites (49 and 96, both from the western edge of the

Coryell Pluton) exhibit peculiar magnetizations with very low coercive force and very high unblocking temperature. The magnetic carrier in these rocks has not been identified, and the results cannot readily be interpreted. These two sites are classified as type C4. Sites exhibiting type C behaviour are not considered to provide a reliable record of the Eocene paleofield and are rejected from further study.

The criteria for rejection of type C sites are also applied to the rejection of individual specimens within type A and B sites. Specimens are also abandoned where it is apparent that they have suffered gross orientation errors. Details of the rejection of individual specimens are given in Table 4.2. In addition, three sites are rejected because the errors in measurement (α_{95}) are large, greater than an arbitrary limit of 12°.

Three sites are found to possess both normal and reverse polarity magnetizations, the directions of which are approximately antiparallel. In two of these sites (63 and M10), the site mean direction is based on the average of the normal and reverse components. In site 16, only the normal polarity components yield a site mean direction of sufficient precision to be useful. Sites M10 and 16 consist of some specimens with normal magnetizations and others which yield reverse magnetizations; both polarities are obtained at the same demagnetization levels. The specimens from site 63, however, yield a normal polarity high T_{ub} component and a reversed polarity low T_{ub} component. These dual polarity magnetizations constitute very important pieces of information (this will be made more apparent in the next chapter), because if both low and high T_{ub} components yield the same paleodirection, then the rock must have cooled to the temperature of the low T_{ub} component before any tilting occurred.

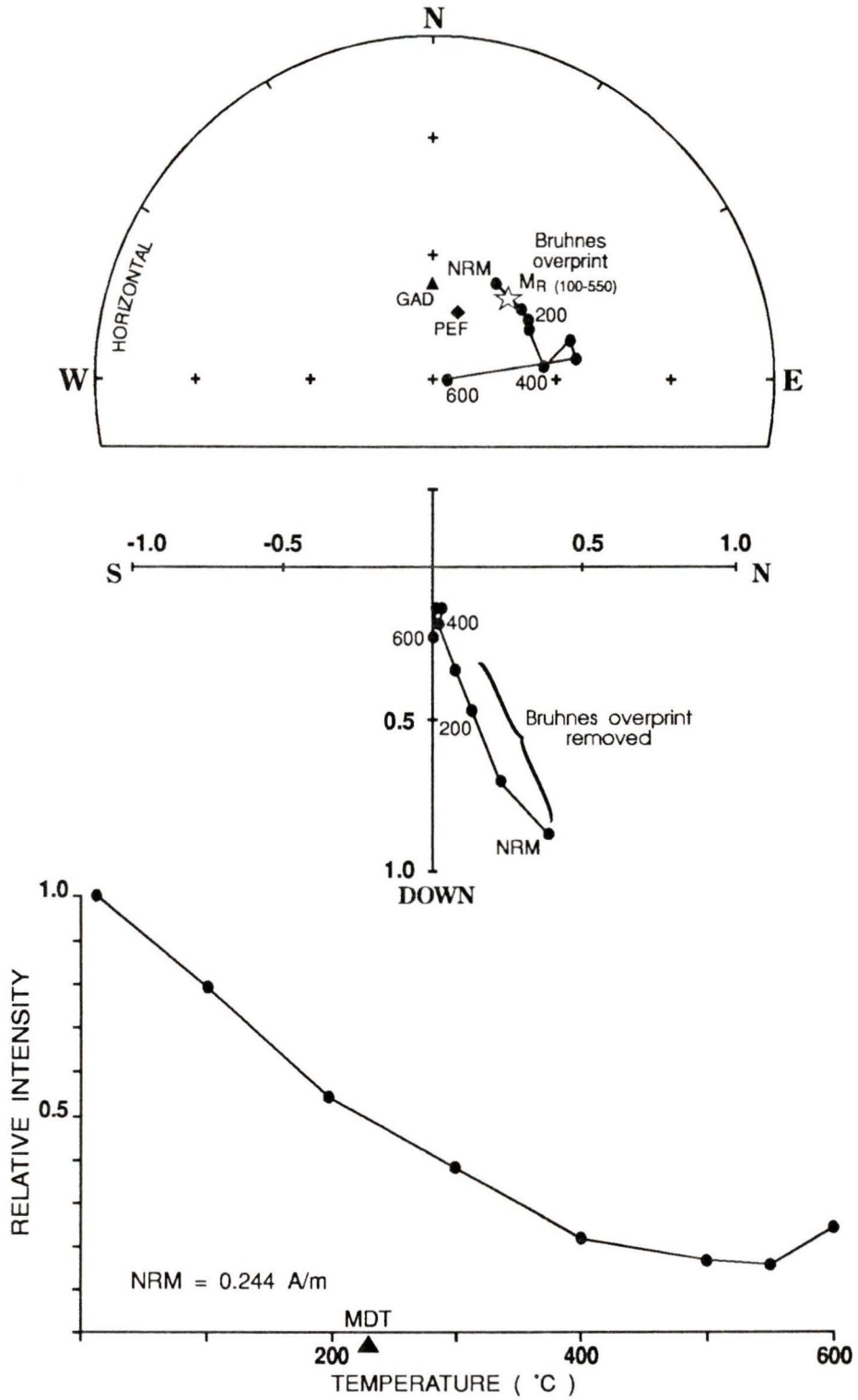

Figure 4.5: C1-type magnetization, site 20. Refer to Figure 4.2 for explanation.

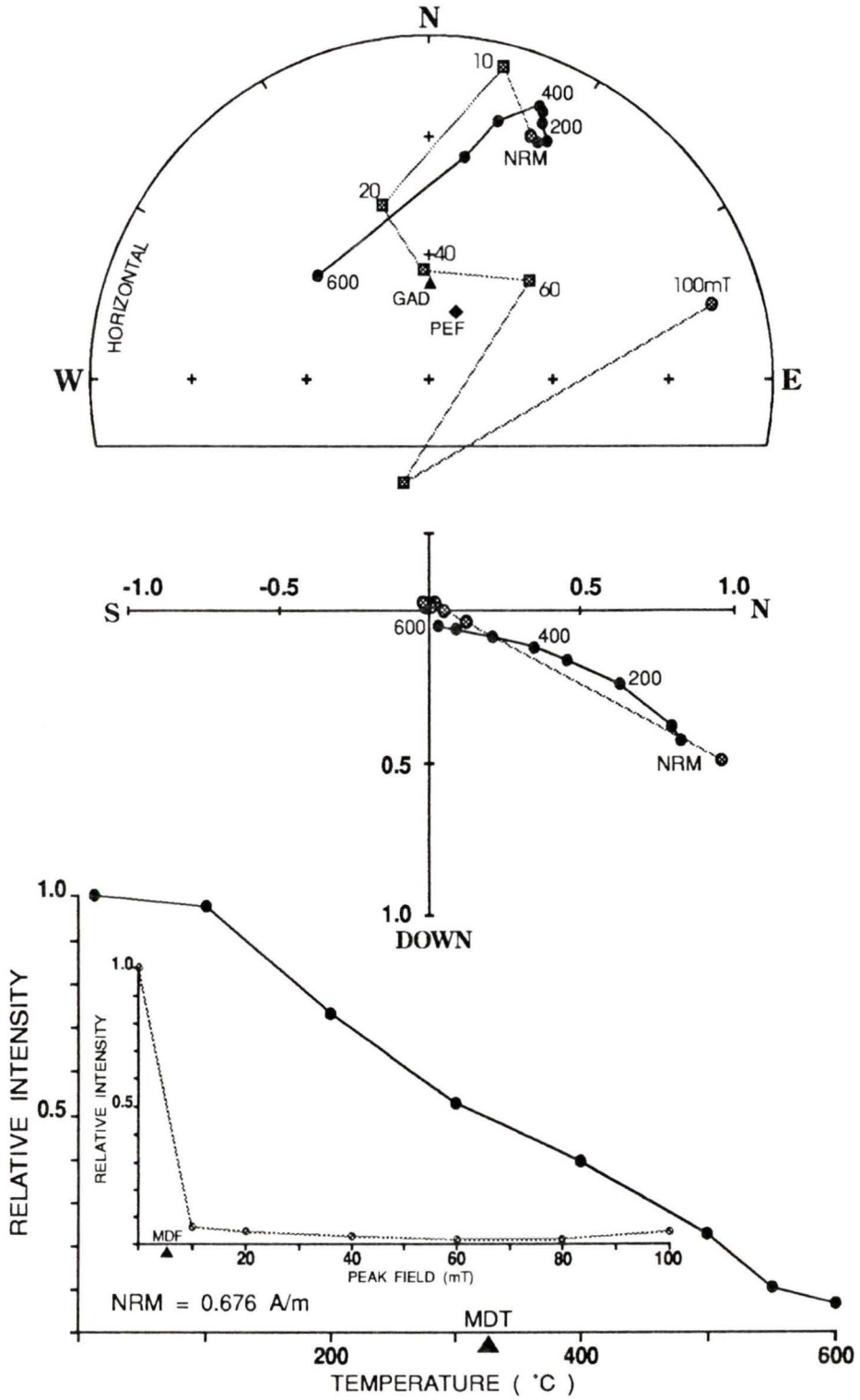

Figure 4.6: C2-type magnetization, site 44. Refer to Figure 4.2 for explanation. Also shown are the changes in direction (square symbols indicate upwards inclination) and intensity during AF demagnetization.

Table 4.2: Data by sites

SITE	CATEGORY	*c, s, s'*	*M* (A/m)	*D,I* (°)	*k*	α_{95} (°)
1	B1	6, 12, 12	3.47	068, 71	115	4
2	A	6, 12, 12	1.47	034, 62	178	3
3	B1	5, 10, 10	1.25	051, 65	137	4
4	C2	5, 10, 0				
5	A	6, 12, 12	1.08	293, 81	819	2
6	A	5, 10, 6[c]	.00626	188,-74	151	6
7	C1	6, 12, 0				
8	B1	5, 9, 9	.0702	230,-40	53	7
9	B1	7, 12, 12	.940	051, 66	493	2
10	C3	6, 11, 0				
11	C1	5, 10, 0				
12	C3	7, 12, 0				
13	B1	5, 9, 5[b]	2.34	273, 41	98	8
14	B1	5, 10, 8[c]	.300	324, 65	126	5
15	A	5, 10, 10	.866	284, 39	383	3
16N	B1	2, 4, 4	-	026, 64	91	10
16R	B1	3, 6, 4[a]	-	147, -62	25	19
16N+R	B1	5, 10, 8[a]	.148	356, 66	20	13
17	C3	5, 10, 0				
18	C3	5, 10, 0				
19	B1	5, 10, 10	.316	327, 60	30	9
20	C1	5, 10, 0				

NOTES: Site numbers with N or R refer to normal or reverse components; CATEGORY= magnetization category; *c, s, s'*= #cores, #specimens, #specimens used in calculations (criteria for rejection of individual specimens within site: a= C1, b= C2, c= C3, d= core orientation error); *M*= NRM mean intensity; *D,I* = observed site mean direction; *k*= Fisher's precision parameter; α_{95} = half-angle of cone of 95% confidence about site mean direction. Sites 54 and 63 incorporate data from sites 54 and 6, respectively, of Marquis (1988). Shaded entries which contain data are results rejected due to large errors (α_{95} > 12°). TREATMENT (# specimens in brackets): **3**, **15**, **21**, **27, 42, 45, 60, 70, 76, 83, 85, 88, 90, 91, 93, 94**: 20mT(9), 550°C(1); **1**, **2**: 20mT(11), 550°C(1); **5**: 10mT(11), 550°C(1); **6**: 10mT(4), 300°C(2); **8**: 10mT(1), 200-400°C(8); **9**: 20mT(11), 200°C(1); **13**: 20mT(5); **14**: 20-40mT(7), 500-600°C(1); **16:** 20mT(8); **19**: 10-20mT(1), 400-600°C(8), 300-500°C(1),; **22**: 20mT(13), 500°C(1); **23**: 20mT(7), 550°C(1); **25**: 20mT(13), 550°C(1); **26**: 10mT(3), 300-400°C(3); **27**: 20mT(7), 550°C(1); **28**: 20mT(8), 550°C(1); **29**: 20mT(8), 550°C(1); **43**: 20mT(10), 550°C(1); **46**: 10mT(12), 550°C(1); **54**: 20mT(5), 550°C(2), 80mT(9); **63N**: 500°C(6), 10-60mT(1), 10-40mT(1), 5-60mT(1); **63R**: 3-500°C(5), 5-60mT(2), 5-40mT(1), 5-20mT(1); **64**: 10mT(10), 550°C(1); **66**: 20mT(9), 400°C(1); **68**: 20mT(9), 500°C (1); **72**: 20mT(4), 550°C(1); **73**: 20mT(9), 300°C(2); **75**: 80mT(7); **77**: 20mT(10), 550°C(1); **78**: 80-100mT(1), 400-600°C(5); **79**: 20(4), 300°C(2); **80**: 20mT(9), 550°C(2); **84**: 10-20mT(7), 100-400°C(1);**95**: 20mT(11), 550°C(1); **98**: 20mT(6), 550°C(1).

Table 4.2: Data by sites, continued.

SITE	CATEGORY	*c, s, s'*	*M* (A/m)	*D,I* (°)	*k*	α_{95} (°)
21	A	5,10,10	.733	304, 40	34	8
22	A	7, 14, 14	.388	046, 60	62	5
23	A	5, 10, 8[c]	25.5	048, 53	188	4
24	C3	10, 19, 0				
25	A	8,16,14[d]	.698	254, 58	344	2
26	B1	5, 9, 6[c]	.0611	233, -63	80	8
27	B1	5, 10, 10	.676	321, 67	288	3
28	B1	5, 10, 8[d]	.509	336, 72	57	7
29	B1	5, 10, 9[c]	.0953	267, 31	91	5
42	A	5, 10, 10	3.23	003, 57	510	2
43	A	6, 11, 11	.457	009, 66	105	5
44	C2	6, 11, 0				
45	B1	5, 10, 10	.368	356, 69	126	4
46	B1	7, 13, 13	.471	010, 40	89	4
47	A	5, 10, 10	1.71	325, 69	213	3
48	C3	7, 11, 0				
49	C4	5, 10, 0				
50	C3	5, 10, 0				
54	A	9,17,16[c]	.101	050, 57	38	6
60	A	5, 10, 10	1.21	296, 42	205	3
61	C3	5, 10, 0				
62	C3	5, 10, 0				
63N	B1	7,11,9[c]	-	303, 56	53	7
63R	B1	5, 9, 9	-	102, -46	8	19
63N+R	B1	9,20,18[c]	1.62	292, 52	14	10
64	B1	6, 11, 11	.199	040, 49	82	5
65	C1	5, 10, 0				
66	B1	5, 10, 10	.934	063, 47	520	2
67	A	5,10, 3[c]	.390	039, 57	30	23
68	A	5, 10, 10	.121	055, 36	92	5
69	C3	5, 10, 0				

Table 4.2: Data by sites, continued.

SITE	CATEGORY	*c, s, s'*	*M* (A/m)	*D,I* (°)	*k*	α_{95} (°)
70	A	5, 10, 10	.316	014, 39	48	7
71	C3	5, 10, 0				
72	A	5, 10, 6	.119	357, 65	33	12
73	B1	6, 12, 12	.428	353, 72	195	3
74	C1	5, 9, 0				
75	B1	7, 11, 7[a]	.995	094,-77	350	3
76	B1	5, 10, 10	.381	285, 65	75	6
77	B1	6, 11, 11	.182	299, 68	33	8
78	B2	4, 7, 6[a]	.0992	280, 34	18	16
79	A	7, 12, 6[c]	.0145	266, 38	198	5
80	A	6, 11, 11	.123	066, 51	53	6
81	C3	5, 9, 0				
82	C3	5, 10, 0				
83	A	5, 10, 10	2.26	236,-42	298	3
84	B1	5, 10, 8[d]	.372	143, 73	86	6
85	B1	5, 10, 10	1.22	020, 68	55	7
86	C3	5, 10, 0				
87	C1	5, 10, 0				
88	A	5, 10, 10	.601	282, 43	40	8
89	C3	5, 10, 0				
90	A	6,12,10[d]	.451	037, 75	159	4
91	B1	5, 10, 10	.723	314, 52	18	12
92	C3	5, 10, 0				
93	A	5, 10, 10	2.01	300, 46	224	3
94	A	5, 10, 10	1.63	287, 43	300	3
95	A	6, 12, 12	.758	300, 43	155	4
96	C4	5, 9, 0				
97	C1	5, 10, 0				
98	B1	5, 9, 7[d]	.240	261, 67	207	4

Table 4.3: Data from earlier studies.

SITE	CATEGORY	*c, s, s'*	*M* (A/m)	*D,I* (°)	*k*	α_{95} (°)
M1	B1	7,14,12[d]	.654	285, 25	59	6
M2	B1	6,12,12	.919	339, 72	181	3
M3	A	5,10, 5	.761	331, 49	24	16
M4	C1	5,10, 0				
M5	B1	5, 9, 9	.495	018, 65	59	7
M6	see site 63 in Table 4.2					
M7	C3	6,10, 0				
M8	C1	5,10, 0				
M9	C1	5,10, 0				
M10N	B1	3, 4, 4		340, 59	13	26
M10R	B1	5, 9, 8[c]		220, -61	11	17
M10N+R	B1	7,13,12[c]	.180	009, 59	17	11
M11	A	6,12,10[d]	1.19	310, 40	124	4
M12	A	7,13,13	.861	302, 31	83	5
M13	B1	8,15,12	.521	318, 66	64	6
M14	B1	6,12,12	.443	303, 43	49	6
M15	C3	6,11, 0				
M16	A	6,12,11	3.60	327, 58	50	7
M17	A	8,16,16	.493	304, 27	79	4
M18	A	5, 7, 7	2.85	308, 16	119	6
M19	A	6,12,8	1.72	340, 41	31	10
M20	A	5,10,10	1.72	304, 44	179	4
M21	B1	5,10,10	.525	308, 40	139	4
M22	B2	5, 9, 9	.653	283, 20	59	7

Refer to Table 4.2 for explanatory notes. Sites with prefix M are from Marquis (1988, and unpublished data); those with B are from Bardoux and Irving (1989, and unpublished data (site B1)). SS = data from Summit Stock (Irving and Archibald, 1990). Sites M6 and M54 were resampled during the present study, and the data are incorporated into sites 63 and 54, respectively, in Table 4.2. Unpublished data of Marquis reported here include four sites remeasured during this study. TREATMENT (for four sites measured during this study): **M2**: 20mT(11), 550°C(1); **M5**: 20mT(6), 30mT(1), 550°C(2); **M10**: 20mT(9), 550°C(3); **M51**: 20mT(8), 550°C(1).

Table 4.3: Data from earlier studies, continued.

SITE	CATEGORY	*c, s, s'*	*M* (A/m)	*D,I* (°)	*k*	α_{95} (°)
M51	A	5, 9, 9	.757	265, 35	57	7
M52	B2	5,10,10	.161	057, 56	39	8
M53	C1	5, 9, 0				
M54	see site 54 in Table 4.2					
M55	C1	6,12, 0				
M56	A	5,10,10	.272	245, -54	95	5
M57	A	5,10,10	.113	235, -40	201	3
M58	A	5,10,10	.498	050, 42	368	3
M59	A	9,14,13	.335	038, 42	79	5
B1	A	5,10,10	.0422	227, -34	74	6
B5	B2	6,12,12	.861	068, 51	14	12
B6	A	5,10,9(?)	.182	065, 37	77	6
B7	A	5,10,10	.324	052, 54	20	11
B51	A	5,10,10	.620	057, 63	154	4
SS	---	9 SITES	---	048, 72	290	3

CHAPTER 5

APPARENT TILT

5.1 INTRODUCTION

Only if certain conditions are met, can aberrant paleodirections be used to calculate tilt. This chapter begins by discussing these conditions. Then the procedures are described by which the mid-Eocene reference direction is determined. The chapter ends with descriptions of the inferred tilts and of their significance, judged according to statistical and geological criteria.

5.2 CAUSES OF ABERRANT PALEODIRECTIONS

Tectonic motions can be expressed as rotations. Because inclination increases northward and southward from the geomagnetic equator, rocks which acquired magnetization at low latitudes, and were then translated to higher latitudes, will preserve inclinations shallower than those expected from their present positions (Figure 5.1, top). Such latitudinal displacements may be expressed as rotations about Euler poles situated on the equator, at a longitude 90° from that of the locality. Rotations about a pole that is vertical and close by produces aberrant declinations (Figure 5.1, middle). Rotations about horizontal axes, referred to as tilts, can produce aberrant inclinations and declinations (Figure 5.1, bottom). In practice, an aberrant paleodirection can be caused by any of these three types of rotation, either singly or in combination. Tilts become acceptable as a general explanation of aberrancy when the other two forms of rotation can be shown to be unlikely.

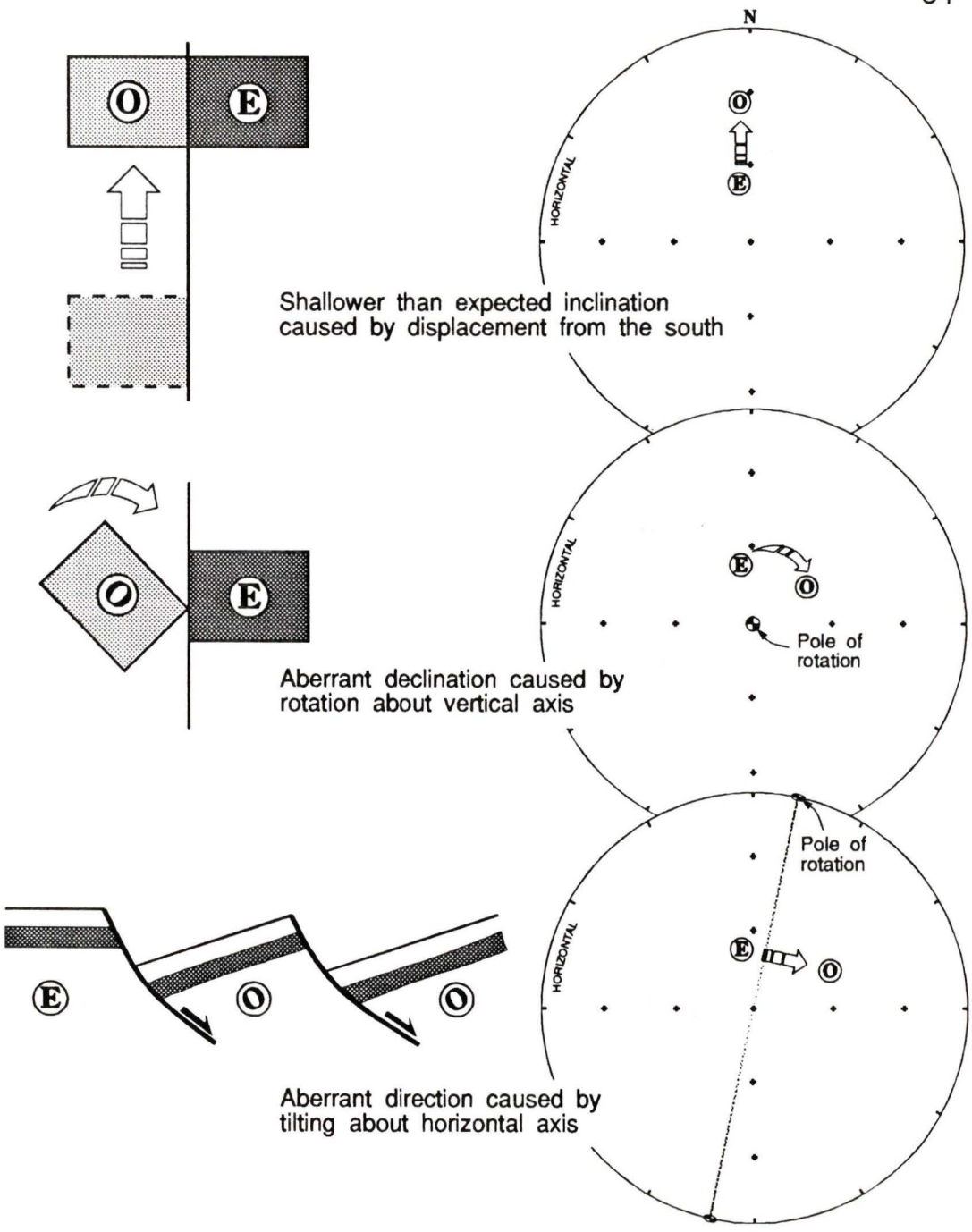

Figure 5.1: Schematic illustration of how latitudinal displacement (top), rotation about a local vertical axis (middle), and tilting about a horizontal axis (bottom) affect the observed paleodirection. Aberrant paleodirections can be caused by any combination of these three mechanisms. Note that the aberrant paleodirections produced by displacement and rotation in the first two examples could also be produced by tilting to the south and to the west-northwest, respectively.

To explain the aberrancy of paleodirections observed in this study by the first two types of motion requires that rotations of up to 60°, and/or latitudinal displacements of 30° or more, have involved rocks of Middle Eocene age in the southern Omineca Belt. Displacement in a latitudinal sense of the region since the Early Eocene is precluded by the excellent paleolatitudinal conformity demonstrated between rocks of Eocene age both to the west of the sampling area, and to the east, on the craton (Figure 5.2). Middle Eocene volcanic rocks of the Kelowna outlier (Bardoux and Irving, 1989), at the western edge of the Omineca Belt, and of the Kamloops area (Symons and Wellings 1989), in the Intermontane Belt, yield paleomagnetic poles (paleopoles) in excellent agreement with those obtained from igneous rocks of similar age in the Bearpaw and Highwood Mountains (Diehl and others 1983) in Montana, and the Absaroka Mountains (Shive and Pruss 1977) in Wyoming. The inference drawn from these data is that these five localities were part of stable North America by Eocene time, and therefore, no large-scale translation or rotation of the present sampling area has occurred since the final accretion of allochthonous terranes in the Paleocene.

5.3 MIDDLE EOCENE REFERENCE DIRECTION

In order to calculate apparent tilt for each site, the site mean direction is compared to a reference direction. This is the direction of magnetization expected in rocks of the sampling area which acquired their magnetization during the Middle Eocene and which have not undergone any tectonic disturbance since that time. The data employed in its calculation consist of 127 site mean directions from the five localities discussed in section 5.2.

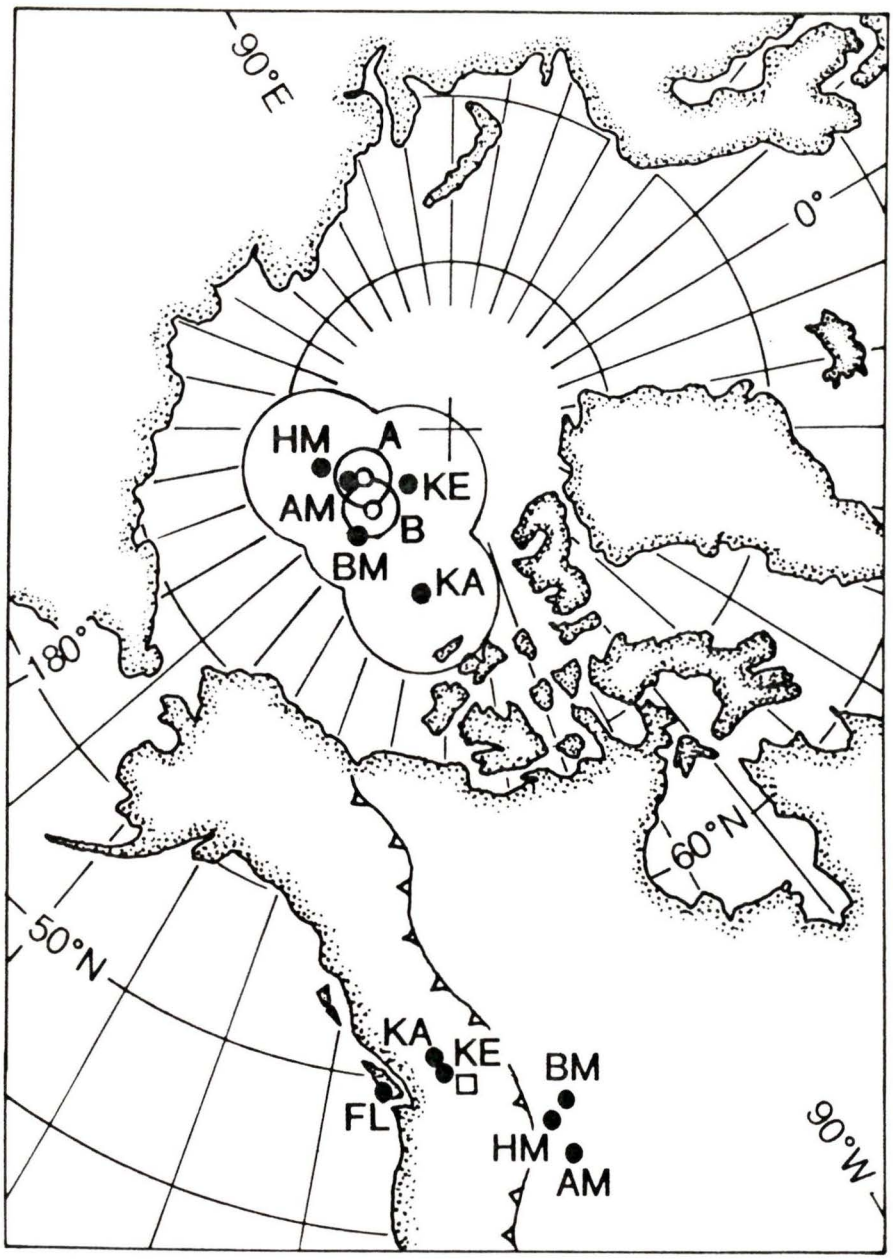

Figure 5.2: Locations and paleopoles of the five localities employed in calculation of the mid-Eocene reference direction. A and B are the mean poles determined according to calculations A and B in table 5.1. Standard error circles (α_{63}) are shown. Open square shows the location of the present study area. KA = Kamloops volcanics, KE = Kelowna volcanics, BM = Bearpaw Mountains alkalic complex, HM = Highwood Mountains volcanics, AM = Absaroka Mountains volcanics, FL = Flores volcanics (only the location is shown; data from this locality was not employed in calculations). Refer to section 5.3 and Table 5.1 for details. Ornamented line indicates the approximate eastward limit of Cordilleran deformation.

These measurements are of rocks of mid-Eocene age (54 to 48 Ma), which either are flat-lying, or have known bedding attitudes, so that appropriate dip corrections have been applied. Data from the Middle Eocene Flores volcanics of Vancouver Island (Irving and Brandon 1990) are in good agreement with results from the other five localities, but are not included here because this locality is west of the Fraser Fault System, which is known to have been active during Eocene time (Monger and Price 1979). To have included these data would not have significantly affected the results. The data employed in these calculations, and details of the calculations themselves, are given in Appendix C.

The general method of calculating the reference direction is to first determine the mean of the poles corresponding to the site mean directions. (The mean pole cannot be calculated from the mean of the site directions themselves because the directions are obtained from five geographically separate localities.) The direction of magnetization expected at the present sampling locality is then calculated from this mean pole and its precision corrected for latitude. There are, however, two ways of performing this calculation (Figure C1), each of which depends on several assumptions. The first method is to take each site mean direction individually, giving each unit weight in the calculations (entry 6, Table 5.1). This assumes that the 127 site mean directions, regardless of locality or rock unit, constitute a random sample of the paleofield over the entire interval of time which they represent. The resultant reference direction will not be a single direction, but rather a distribution of directions which reflects the dispersion due to paleosecular variation (PSV) in mid-Eocene time. The second approach is to calculate the mean of the paleopoles corresponding to the five locality mean directions (entry 7, Table 5.1). This, however, gives each locality unit weight,

and assumes that the data from each locality constitute a random sample over the entire interval of time spanned by all five localities, which clearly is incorrect. The precision of locality paleopoles is very high (much higher than the precision of individual site poles, because PSV is averaged out), but the accuracy with which the reference direction is defined remains the same; the greater precision compensates for the lower *N*.

The first approach yields a reference direction with the appropriate precision, to which individual site mean directions can be compared. The high precision obtained by the second method is not meaningful when making comparisons to individual site directions, which are spot readings of the Eocene paleofield, and subject to the full range of PSV. The second method yields the precision appropriate for comparing *locality* mean directions to a reference direction. The results of calculations by both methods are shown graphically in Figure 5.2 and listed in Table 5.1. The two procedures produce slightly different results. Although the first method (which gives each site unit weight) yields the correct precision, the mean pole differs from that obtained by the second method (which gives unit weight to each of the five localities). This is because the 127 site mean directions are not evenly distributed among the five localities, and this imposes a bias on the position of the mean pole calculated from the individual site data. The problem can be overcome by taking the same number of site mean directions from each locality (which would discard 25% of the data), or by using the direction calculated by the second method. The second method is therefore considered to provide the best estimate of the reference direction, while the first method gives the best estimate of its precision. This is a

Table 5.1: Early to Middle Eocene data and reference direction.

#	ROCK UNIT	Location		Age	*N*	Mean Pole		*K*	A_{95}	A_{63}
		Lat	Long	(Ma)		Lat	Long			
1	Kamloops Group volcanics	50.8°N	109.6°W	49±2	24	80°N	128°W	19	11	6
2	Kelowna volcanics	49.9°N	120.8°W	52±2	24	86°N	157°W	20	7	4
3	Bearpaw Mountains alkalic complex	48.2°N	109.6°W	50-54	30	82°N	161°W	31	7	4
4	Highwood Mountains volcanics	47.5°N	110.5°W	49-53	30	82°N	194°W	27	11	6
5	Absaroka Mountains volcanics	44.5°N	109.6°W	48	19	83°N	181°W	15	11	6
6	Mean of 1 - 5; calculation A (sites)				127	83°N	164°W	11	4	2
7	Mean of 1 - 5; calculation B (localities)				5	84°N	180°W	369	4	2
8	Best estimate of reference direction	$D = 351°$, $I = 69°$, $k = 28$, $\alpha_{95} = 2°$								

NOTES: N = number of sites (localities in entry 7); K = Fisher's precision parameter; A_{95} (A_{63}) = half-angle of cone of 95% (63%) confidence about mean paleopole. Entries 6 and 7 give the mean poles based on 127 sites and 5 localities, respectively. Entry 8 is the best estimate of the reference direction expected at the centre of the present study area. References are as follows: 1) Symons and Wellings (1989), 2) Bardoux and Irving (1989), 3) and 4) Diehl and others (1983), 5) Shive and Pruss (1977).

compromise solution which is adequate for present purposes. The reference direction thus determined is given in entry 8, Table 5.1.

The angular dispersion of the geomagnetic field is strongly latitude dependent, and the precision of the reference direction may be corrected from the precision of the mean pole according to the relation (Cox 1970):

$$\frac{k_s}{K_p} = \frac{2\left[1+3\sin^2\lambda_p\right]^2}{\left[5+3\sin^2\lambda_p\right]}$$

where k_S is the precision at the sampling area, K_p the precision of the pole (K_p = 11.2), and λ_p the paleolatitude of the sampling area (53.7°N). The corrected precision of the reference direction is therefore k = 28 (entry 8, Table 5.1).

5.4 APPARENT TILT

Apparent tilt can be determined graphically (Figure 5.3). Both the Eocene reference direction and the observed site mean direction are plotted on a stereonet. The angular distance measured along a small circle between these two points gives the magnitude of tilt; the direction is given by the azimuth of the principal plane parallel to the small circle. This method assumes that tilting occurred about axes which were close to horizontal. Apparent tilts are calculated in this manner for all those sites not rejected according to the procedures outlined in the previous chapter. The results are illustrated graphically in Figure 5.4 and compiled in Table 5.2, grouped into regions. These groupings are arbitrary to a degree, but they correspond to structural domains with apparent

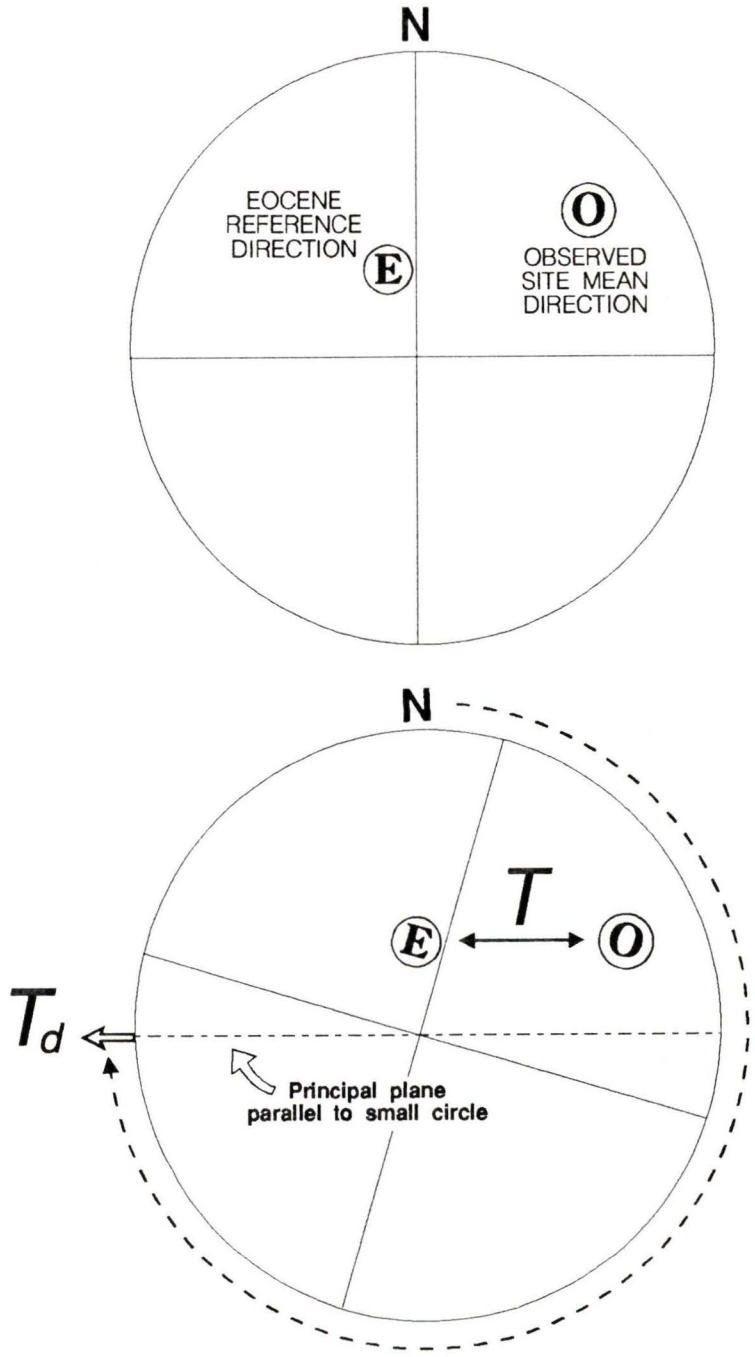

Figure 5.3: Graphical technique for the determination of apparent tilt. Both the observed site mean direction and expected reference direction are plotted on a stereonet. The points are rotated so that they both lie on a small circle. The magnitude of apparent tilt, T, is given by the angular distance along the small circle between the two points; the direction of tilt, T_d, is given by the azimuth of the principal plane parallel to the small circle.

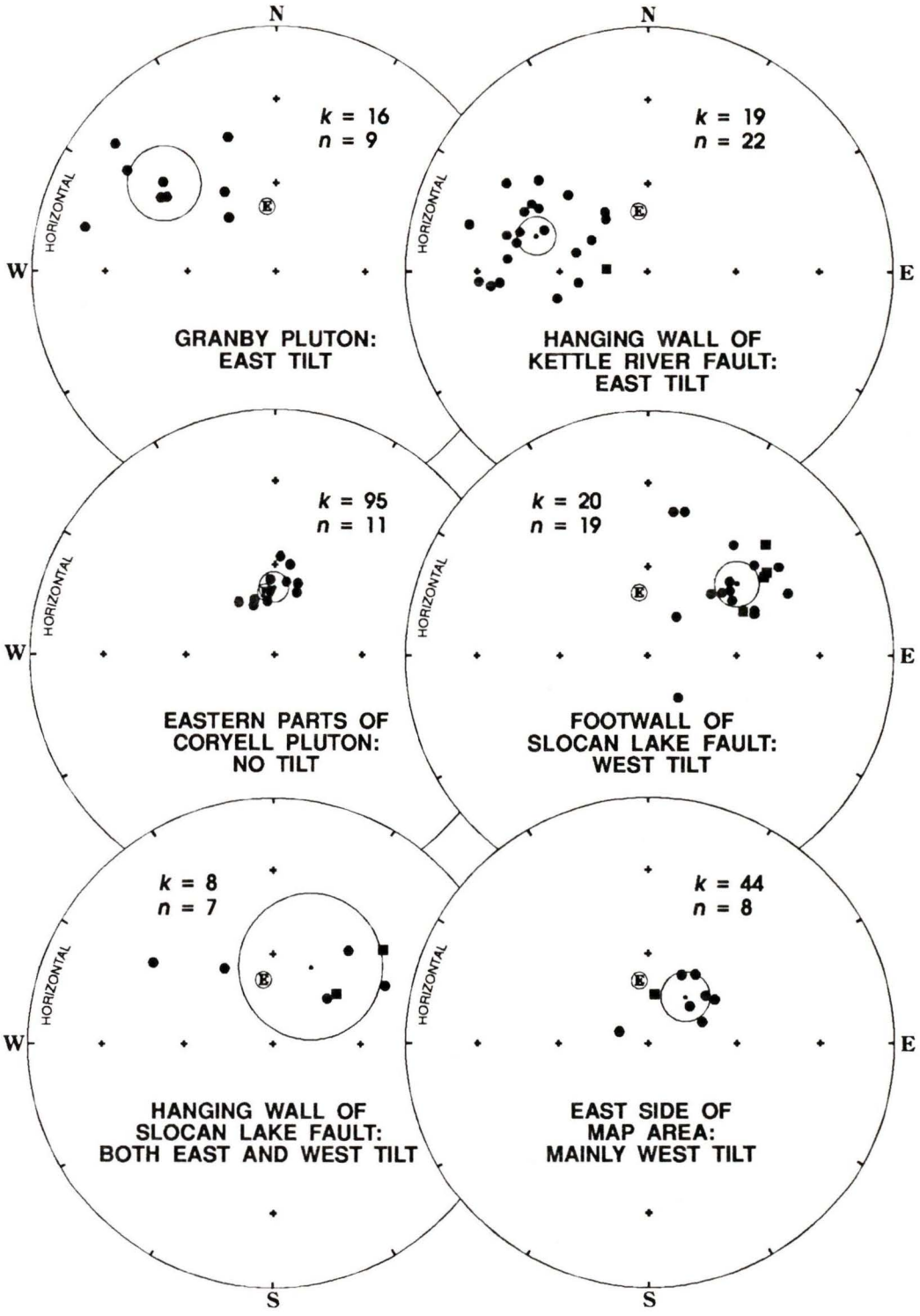

Figure 5.4: Site mean directions grouped according to sampling region; those with negative inclination have been inverted through the origin and are displayed using square symbols. E is the Eocene reference direction (D = 351°, I = 69°, k = 28, α_{95} = 2°) expected at the centre of the map area. Regional mean directions are shown with α_{95} error circle. k = Fisher's precision parameter, n = number of sites. Refer to Tables 5.2 and 5.3 for details.

Table 5.2: Apparent tilt for sites grouped by sampling region.

SITE	T, T_d (°)	SIGNIFICANT ?	SITE	T, T_d (°)	SIGNIFICANT ?
GRANBY PLUTON					
M13	13, 078	N	**M19**	29, 151	Y
M14	38, 094	Y	**M20**	37, 095	Y
M16	16, 122	P	**M21**	39, 102	Y
M17	53, 102	Y	**M22**	65, 091	Y
M18	63, 109	Y			
HANGING WALL OF KETTLE RIVER FAULT					
13	51, 066	Y	**79**	56, 062	Y
14	12, 086	N	**88**	46, 075	Y
15	49, 077	Y	**91**	26, 102	P
25	41, 042	Y	**93**	37, 090	Y
27	11, 074	N	**94**	44, 080	Y
29	62, 063	Y	**95**	39, 092	Y
60	41, 087	Y	**98**	32, 040	Y
63N+R	34, 078	Y	**M1**	62, 084	Y
75	22, 026	P	**M11**	38, 106	Y
76	26, 055	P	**M12**	50, 100	Y
77	19, 058	P	**M51**	61, 062	Y
EASTERN PARTS OF CORYELL PLUTON					
28	06, 044	N	**73**	03, 325	N
42	13, 204	N	**85**	11, 272	N
43	06, 246	N	**M2**	05, 050	N
45	02, 281	N	**M5**	12, 257	N
47	09, 078	N	**M10N+R**	13, 221	N
72	05, 199	N			

NOTES: T, T_d = Magnitude and direction of apparent tilt; SIGNIFICANT ? = result of test to determine if the observed site mean direction is significantly different from the Eocene reference direction; Y=Yes, P=Probably, N=No (refer to text). Eocene tilt of the Summit Stock (SS) is inferred from comparison of mid-Cretaceous paleodirections with the mid-Cretaceous reference field (Irving and Archibald, 1990).

Table 5.2, continued.

SITE	T, T_d (°)	SIGNIFICANT ?	SITE	T, T_d (°)	SIGNIFICANT ?
FOOTWALL OF SLOCAN LAKE / CHAMPION LAKES FAULT					
22	26, 271	P	**B1**	50, 252	Y
23	32, 264	Y	**B5**	41, 280	Y
46	32, 206	Y	**B6**	53, 271	Y
54	30, 271	Y	**B7**	33, 270	Y
68	50, 261	Y	**M52**	32, 276	Y
70	34, 211	Y	**M56**	38, 280	Y
80	37, 271	Y	**M57**	47, 263	Y
83	45, 265	Y	**M58**	43, 259	Y
84	36, 339	Y	**M59**	38, 245	Y
90	16, 305	P			
HANGING WALL OF SLOCAN LAKE / CHAMPION LAKES FAULT					
8	45, 258	Y	**26**	26, 281	P
9	24, 285	P	**64**	33, 253	Y
19	14, 117	N	**66**	44, 274	Y
21	41, 098	Y			
EASTERN MAP AREA					
1	25, 303	P	**6**	08, 308	N
2	20, 264	P	**16N**	17, 266	P
3	24, 283	P	**B51**	28, 284	Y
5	18, 016	P	**SS**	23, 283	P

Table 5.3: Mean directions and apparent tilt by sampling region.

REGION entry	*n*	*D, I* (°)	*k*	α_{95} (°)	*T* (°)	T_d (°)
GRANBY PLUTON[a]						
1	9	309, 41	16	14	38 ± 14	103 ± 27
HANGING WALL OF KETTLE RIVER FAULT[a]						
2	22	287, 50	19	7	38 ± 7	074 ± 15
EASTERN PARTS OF CORYELL PLUTON[a]						
3	11	359, 68	95	5	03 ± 6	244
FOOTWALL OF SLOCAN LAKE / CHAMPION LAKES FAULT[a,b]						
4	19	051, 51	20	8	35 ± 8	267 ± 18
5	15	055, 48	57	5	39 ± 6	268 ± 12
HANGING WALL OF SLOCAN LAKE / CHAMPION LAKES FAULT						
6	5	051, 53	44	12	33 ± 12	268 ± 27
EASTERN MAP AREA[b,c]						
7	8	039, 71	44	8	17 ± 8	292 ± 38

NOTES: *n* = number of sites; *D, I* = region mean direction; *k* = Fisher's precision parameter; α_{95} = half-angle of cone of 95% confidence about region mean direction; *T* = magnitude of mean apparent tilt for region; *Td* = direction of mean apparent tilt for region. 95% confidence interval indicated on magnitude and direction of apparent tilt. Entry 5 excludes outlying sites 46, 70, 84, 90; entry 6 excludes sites 19 and 21. Refer to section 5.4 for details. [a,b,c] = incorporating data of Marquis (1988), Bardoux and Irving (1989), Irving and Archibald (1990).

tilts of similar sense. The mean paleodirection and the mean apparent tilt for each region are summarized in Table 5.3, and discussed in section 5.4.

The range of apparent tilts is wide, 2 to 65°. These apparent tilts have been determined for individual sample sites, each of which represents a spot reading of the field and not the full range of secular variation. The reference direction is itself not a single direction, but rather a distribution of directions reflecting secular variation in middle Eocene time. There is need, therefore, for a definition of what can (or cannot) be regarded as a significant departure from the reference direction.

Figure 5.5 is a histogram in which the calculated apparent tilts are plotted in five degree intervals away from the reference direction. The probability of observing a direction which makes an angle θ_0 or more with the true mean is given by the equation (Watson and Irving 1957):

$$1-\cos\theta=\frac{-\ln\left[P\left\langle\theta>\theta_0\right\rangle\right]}{k}$$

From this equation are derived two quantities useful in paleomagnetism, θ_{63} and θ_{95}, which represent the radii of the circles about the true mean direction which contain 63% and 95% of the individual directions. θ_{63} and θ_{95} are analogous to the standard deviation and 1.96 times the standard deviation of the normal distribution, respectively (Irving 1964). For the Eocene reference direction (Table 5.1, entry 8), the equation above, using k = 28, yields θ_{63} = 15.3° and θ_{95} = 26.7°.

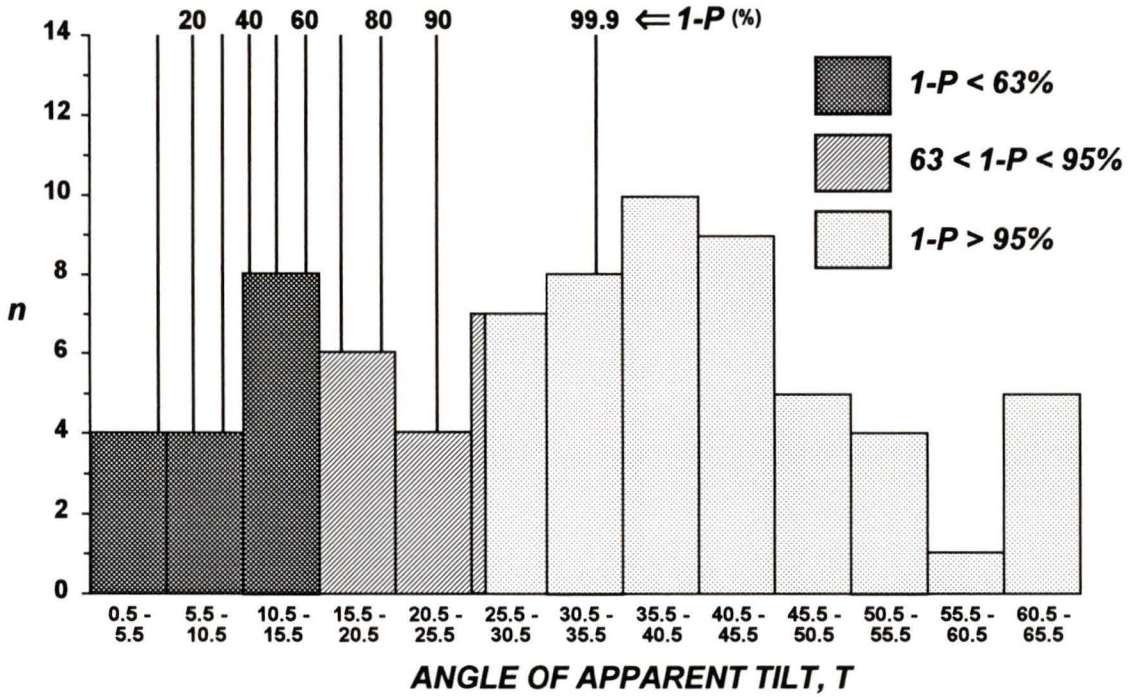

Figure 5.5: Histogram showing the number of sites, ***n***, with angles of apparent tilt, ***T***, plotted in five degree intervals away from the Eocene reference direction. The scale in the background gives the probability, ***1 - P***, that an observed site mean direction is significantly different from the reference direction at a particular angle of departure. Sites with departure angles in the interval *1 - P* < 63% (less than 15.3° from the reference direction) are not statistically significant; those in the interval *1 - P* > 95% (more than 26.7°) are highly significant. There are fourteen sites whose mean directions lie in the interval *1 - P* = 63% to 95% (15.3° to 26.7° from the reference direction). These are probably significant, although this is best decided by geological, rather than statistical, criteria.

The scale in the background of Figure 5.5 indicates the probability that an observed site mean direction is significantly different from the reference direction, and therefore indicative of tilt. Referring to Figure 5.5, the probability, *P*, of observing, in untilted rocks, a site mean direction which deviates by 27° or more from the reference direction is only 5%. Therefore, the probability (1 - *P*) is 95% that such an angle of departure is significantly different from the reference direction, and the rocks are presumed to be tilted. Angles of departure less than 15° are not considered to be significant, and these sites are believed not to have been tilted. The significance of departure angles is less certain for 14 sites whose mean directions lie in the interval 15° to 27° from the reference direction. Although these departure angles are probably significant, this is best determined by geological criteria and by comparison with neighbouring sites, rather than through statistical procedures.

5.5 RESULTS

The apparent tilts are plotted by sites and by regions in Figure 5.6 (located in back pocket), and in simplified form in Figure 5.7. Two first-order features are immediately apparent upon examination of these tilt maps. The first is that easterly apparent tilts, which dominate the west half of the map area, are juxtaposed, in the vicinity of Arrow Lake, against westerly apparent tilts of similar magnitude in the east half of the map area. Farther south, these opposing tilts are separated by a region of apparently untilted rocks comprising the eastern parts of the Coryell Pluton. Secondly, over considerable areas, tilts are remarkably consistent in direction. In general, tilt direction is orthogonal to the mapped traces of the major faults, justifying the assumption that tilt occurred

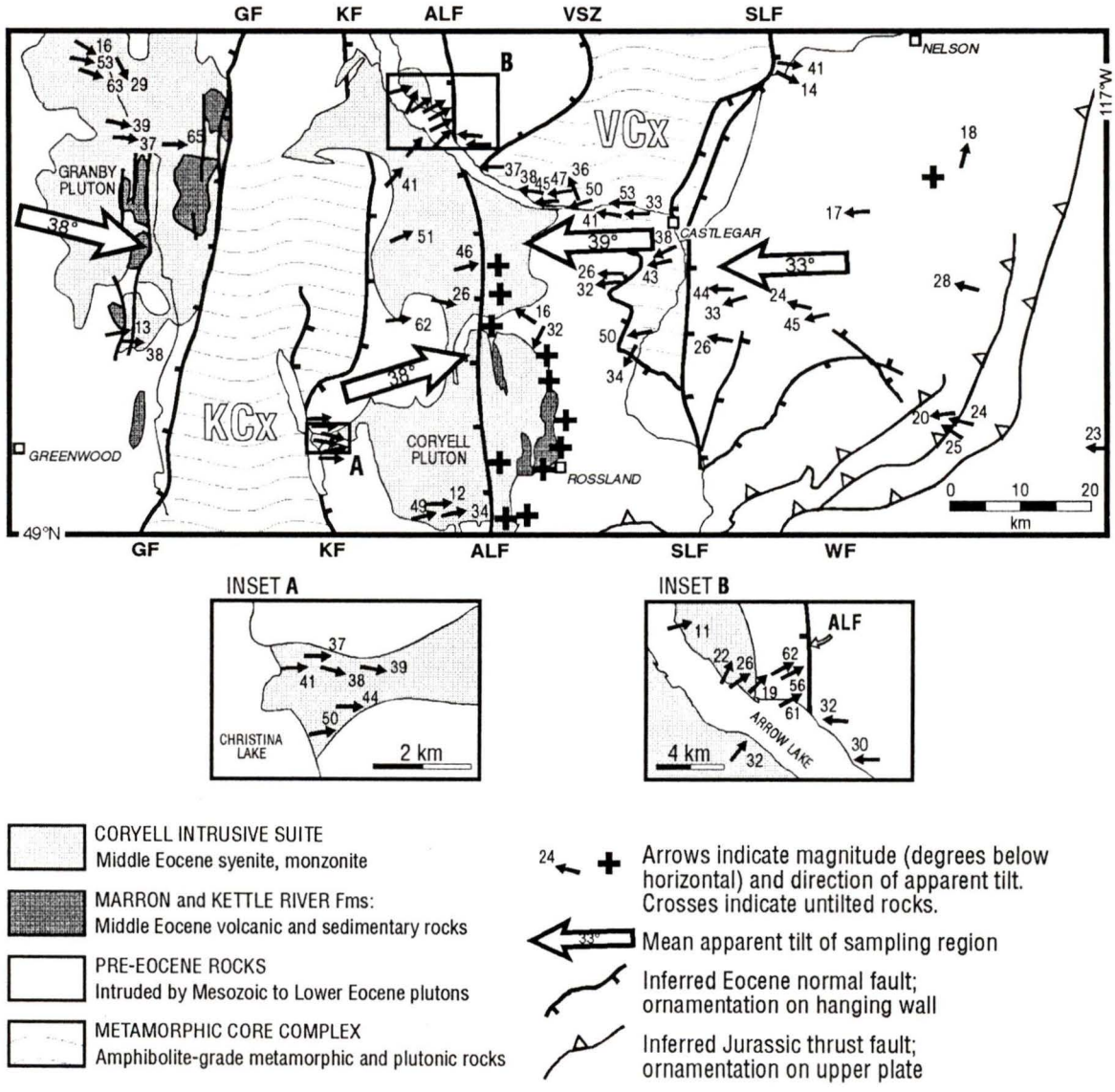

Figure 5.7: Map of the study area (simplified from Figure 5.6), showing the magnitude and direction of apparent tilt.

about axes which are close to horizontal. The magnitude of apparent tilt is more variable, but it too is commonly consistent amongst groups of adjacent sites. The general consistency of apparent tilts, which are inferred from magnetizations acquired over a range of blocking temperatures, implies that the tilted regions had cooled to the lower end of the blocking temperature range (approximately 300°C) before tilting occurred (Figure 5.8). The remainder of this section provides justification for the grouping of sites into regions, describes briefly the results from each region, and interprets those results of probable significance. The value of k for each region, listed in Table 5.3, is utilized as a crude indicator of the internal strain undergone by each region. Detailed geological analysis of the results is offered in Chapter 6.

All data for the hanging wall of the Granby Fault are from Marquis (1988) and Marquis and Irving (1990). These sites have a consistent sense of apparent tilt, generally eastward, but the site mean directions are relatively scattered (k = 16). The large scatter of the data may be a reflection of the structural complexity of the region (see Figure 5.6), made apparent by detailed mapping in the area by Carr and Parkinson (1989). These authors have observed at least two generations of normal faults in the hanging wall of the Granby Fault. The departure angles are statistically significant for all but two sites. Site M13, for which the angle is not significant, is located in one of a series of small fault blocks between west-dipping normal faults (Figure 5.6), and is likely to have been tilted. The adjacent block to the east, containing site M14, is tilted 38° to the east. Site M16 is of probable significance, from an area north of the limit of detailed mapping undertaken by Carr and Parkinson (1989). This site may be

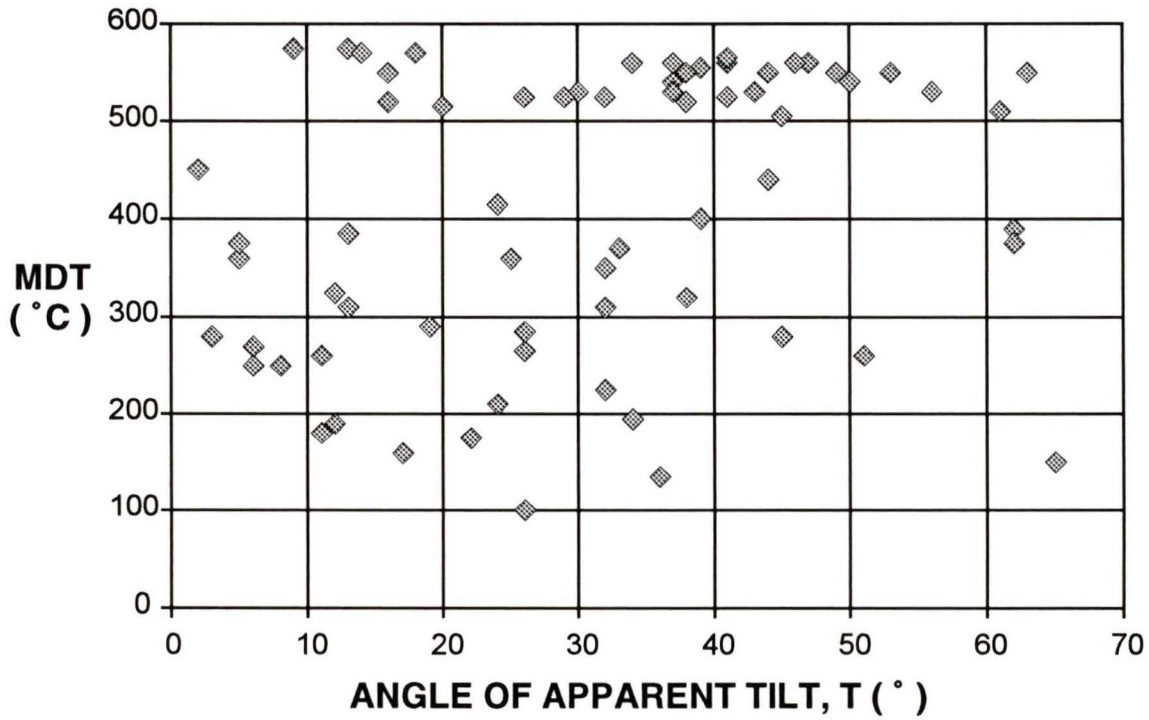

Figure 5.8: Variation of the magnitude of apparent tilt, T, with median destructive temperature, MDT. The absence of a correlation between T and MDT lends support to the hypothesis that the region cooled to the lower end of the magnetic blocking temperature range (< 300°C) before tilting occurred.

separated by an unmapped structure from adjacent sites M17 and M18, which are tilted at 53/102 and 63/109 (T/T_d), respectively.

Sites in the hanging wall of the Kettle River Fault are tilted to the east, in the opposite direction to that expected in the hanging wall of an east-dipping normal fault. The implications of this are discussed in detail in the next chapter. Based on the large size of the area and the moderate amount of scatter (k = 19), it is presumed to be composed of several smaller fault-bounded blocks. The departure angles for sites 14 and 27 are not significant; those for sites 75, 76, and 77 are of probable significance. Sites adjacent to site 14 exhibit significant apparent tilt, suggesting that site 14 is tilted also. Along the north shore of Arrow Lake, west of the inferred trace of the Arrow Lake Fault (Figure 5.6), the departure angles increase crudely over a distance of about four kilometres, from site 27 (11°) eastward to site M51 (61°), suggesting the existence of smaller faults or perhaps a fold in the hanging wall of the main fault. The directions of tilt are consistently to the east or northeast, suggesting all the apparent tilts are real.

Data from the eastern parts of the Coryell Pluton are remarkably well grouped (k = 95), and indicate no apparent tilt. This implies that the area behaved as a stable, coherent block which was not tilted during extension. In addition, the value of k is considerably higher than that expected due to secular variation, suggesting that the magnetizations were acquired in an extremely short interval of time.

Sites in the footwall of the Slocan Lake / Champion Lakes Fault (SLF) are, with the exception of four outlying sites, generally well grouped. Statistics and

mean apparent tilts are calculated for the entire group and for the group minus the four outliers (entries 4 and 5, respectively, in Table 5.3). Including the outliers, k = 20; without them, k = 57. The higher value is similar to the k of 63 obtained from 11 sites along the "Syringa section" by Marquis (1988), and indicates that the Syringa section, most of which is in the footwall of the Valkyr Shear Zone (VSZ), was (as suggested by Marquis 1988) either tilted as a coherent block or sustained tilts of similar magnitude and direction in several smaller blocks. No obvious change in the degree of apparent tilt occurs across the trace of the Valkyr Shear Zone (VSZ); this is to be expected, because the VSZ has been interpreted as a ductile, amphibolite-grade structure (Carr and others 1987), presumably created at temperatures above T_b, so the magnetizations post-date motion along the VSZ.

Three of the outlying sites (46, 70, and 90) are geographically distant from the main group. Site 70 is relatively isolated at the southern end of the region and is tilted to the southwest, rather than to the west. The cores at site 46 were drilled from the centre of a 5m-wide mafic dyke intruding a 10m-wide body of what appears to be a fine-grained, porphyritic marginal phase of the Coryell Pluton. Together, these lithologies are enclosed by pre-Eocene volcanics(?) and banded marble. The contacts between the intrusives and country rocks are poorly-exposed, but calc-silicate skarn assemblages in the adjacent marble unit may suggest that the contacts are intrusive rather than faulted. Other nearby exposures of Coryell syenite, and the dykes intruding them, show no significant tilt. If the porphyry hosting the site 46 dyke is indeed the same age as the rest of the pluton, then no tilt should be expected. It is possible that the fine-grained porphyry represents an early phase which cooled and acquired its magnetization

before the main phase of Coryell plutonism. For this reason site 46 is included with the sites in the footwall of the SLF rather than with those in the pluton. The fourth outlier, site 84, is situated in the Syringa section, between two sites which exhibit reverse polarity magnetizations, and may represent a transitional magnetization direction acquired during a reversal of the geomagnetic field. Sites 22 and 90 have departure angles of probable significance. Site 22 is believed to be tilted, because it exhibits apparent tilt of similar magnitude and direction as site 23, which is a sample from the same syenite stock. There is inadequate control to confidently interpret the significance of site 90, which is a dyke intruding Middle Jurassic diorite near the eastern margin of the Coryell Pluton. The calculated direction of tilt, however, is broadly consistent with that of the region as a whole, and probably is real.

Two sites in the hanging wall of the SLF (19 and 21), which are located north of the main group, on the Kootenay River, are tilted to the east, in the opposite sense to those farther south, and probably represent a separate block. The value of k obtained for the five southern sites is 44 (entry 6, Table 5.3), and suggests that this area was tilted down-to-the-west, either as a coherent block, or as several smaller blocks with tilts of similar magnitude. The abundance of enclaves of gneiss in the western part of the Middle Jurassic Bonnington Pluton (Figure 2.4) is consistent with westward tilt (P.S. Simony, personal communication 1991). Sites 9, 19, and 26 have departure angles of probable significance. Sites 9 and 26 are believed to be tilted, based on comparison with nearby sites, all of which yield westerly tilts. Site 19 is believed to be tilted to the east, in a similar direction to site 21.

The sites along the eastern side of the map are spread over too large an area for the calculated *k* of 44 to be considered valid. Three sites (1, 2, and 3) in the Tramway Stock, which indicate a westerly apparent tilt, are in good agreement with results from the Ymir (site B51) and Summit Stocks (site SS in Table 5.2). Sites 5, 6, and 16, which are dykes intruding pre-Eocene rocks, are not only relatively isolated geographically, but also are not situated close to any mapped extensional structures. Interpretation of the results from these sites is therefore difficult. It should be noted that the error in determining an individual site mean direction consists not only of experimental and statistical error (an estimate of this, α_{95}, is given in Table 4.2), but also the much larger contribution ($\approx$15°) from secular variation. Because of this, results from isolated sites are not, by themselves, necessarily very useful.

CHAPTER 6

KINEMATIC AND TECTONIC IMPLICATIONS

6.1 INTRODUCTION

During the course of interpreting the paleomagnetic evidence, it will be found necessary to invoke two separate phases of magnetization of Coryell intrusive rocks: dykes and smaller bodies in the east most likely cooled before the large plutons in the western and central parts of the study area, although all may have been emplaced during the same interval of time. It will also be found necessary to invoke the existence of a major, west-dipping normal fault, named here the Arrow Lake Fault (ALF), which extends from Lower Arrow Lake southward to the international border. The ALF may be connected to the north with a west-dipping normal fault, inferred by Parrish and others (1988) to extend along the east side of Lower Arrow Lake (Figure 2.2). The existence of the ALF necessitates modification of the interpreted extensional history of the study area. The inferred apparent tilts are used to constrain several aspects of the kinematics of extension, including the subsurface geometry of major faults, and the magnitude and timing of extension. Finally, the effects of restoring older several structures to their pre-extensional attitudes are considered.

6.2 INFERRED STRUCTURES

Where apparent tilts of substantially different magnitude and/or direction are observed in adjacent sites, it is both intuitive and reasonable to assume that the disparity reflects the existence of an unmapped structure of some sort. It has

already been suggested that sites in different parts of the map area may be separated by a fault or perhaps are located in different parts of a fold (section 5.5). Such interpretations can only be made with any degree of confidence, however, if the apparent tilts differ by an amount greater than that attributable to secular variation, and if several sites with contrasting apparent tilts are observed on either side of the proposed structure.

Of greater significance are structures of major proportion whose existence can be inferred from the first-order pattern of apparent tilt exhibited by entire sampling regions. As noted in section 5.5, and illustrated in Figures 5.6 and 5.7, easterly apparent tilts in the hanging wall of the Kettle River Fault (KF) are juxtaposed, in the vicinity of Arrow Lake, against westerly apparent tilts of similar magnitude in the footwall of the Slocan Lake Fault (SLF). Farther south, these regions of opposing tilt are separated by an apparently untilted region comprising the eastern parts of the Coryell Pluton. In order to account for the easterly apparent tilts in the hanging wall of the KF, it is necessary to infer the existence of a west-dipping normal fault, or "breakaway zone", along their eastern limit. This fault, called here the Arrow Lake Fault (ALF), is of major dimensions, extending from the north shore of Lower Arrow Lake to the international boundary, bisecting the Coryell Pluton (Figure 5.6).

The position of the ALF is relatively well-controlled, within about two kilometres, between sites 79 and M52 and between sites 88 and 85. Farther south, it is suggested that the fault passes beneath parts of the valleys which contain Lamb Creek and Big Sheep Creek. The Big Sheep Creek valley trends, in a linear fashion, more than 15 kilometres north from the international

boundary, and is of impressive proportions, averaging more than one kilometre in width, with mountains on each side rising steeply to more than 800 metres above the valley floor (Figure 6.1). Site 28 is the only site in the valley, located on the east side of the valley floor, and exhibits no apparent tilt. No evidence to indicate proximity to a major fault was observed at this site, although the outcrop is both badly weathered and poorly exposed. Due mainly to time constraints and to the lack of accessible outcrop, only a short time was expended during fieldwork to look for geological evidence which might indicate the existence of the ALF, and none has been discovered.

The differences in tilt could mean that the east and west parts of the Coryell Pluton might actually be separate igneous bodies. There appears to be no evidence for this, however. Although some margins are finer-grained and more mafic and several porphyritic hypabyssal phases are present, the pluton is fairly homogeneous in character over much of its extent. Petrographic and chemical analyses of samples from both the east and west parts of the Coryell Pluton, reported by Daly (1912), are similar. However, even if the eastern parts of the pluton did, in fact, acquire their magnetization some time after the western parts, this would explain only the region of no apparent tilt, and it would still be necessary to infer the existence of a fault, such as the ALF, in order to account for the easterly apparent tilt observed in the west.

A third mechanism was considered which potentially could explain the difference in apparent tilt observed across the pluton. This involves tilt occurring at the same time as uplift and magnetization (Figure 6.2). Although the entire pluton may actually be tilted by the same amount, those parts which are

Figure 6.1: View to the southwest across Big Sheep Creek valley, taken from a vantage point on its east side, about four kilometres north of the international boundary.

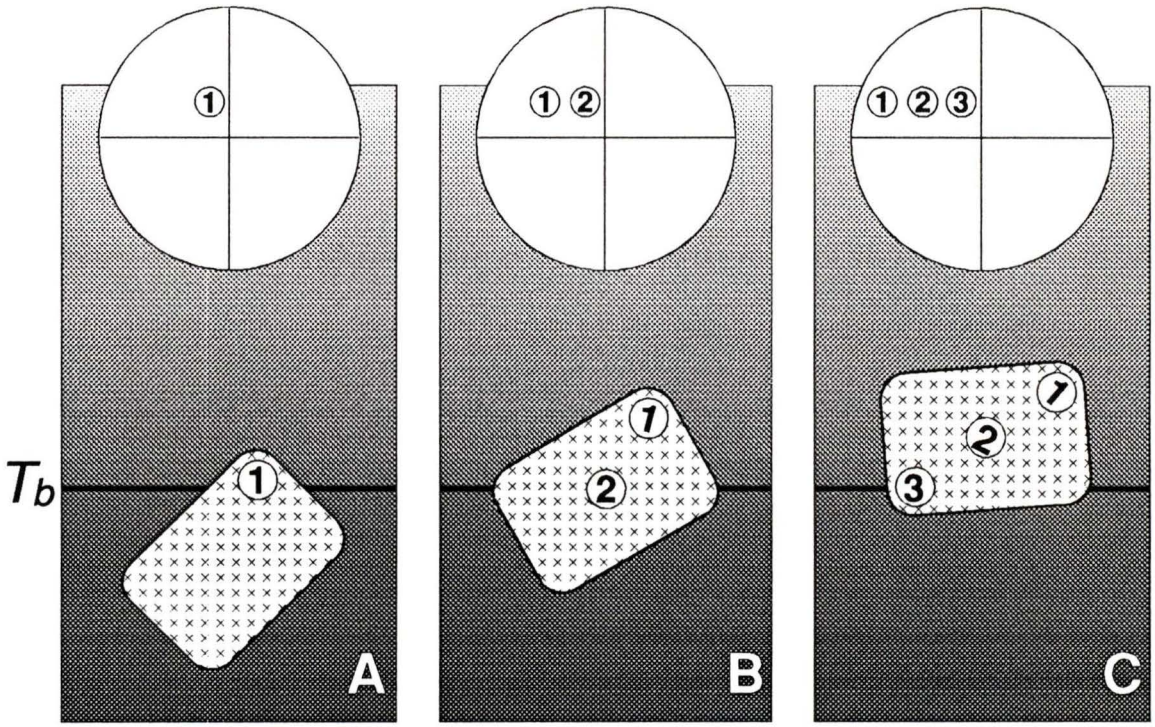

Figure 6.2: Schematic illustration of a pluton undergoing tilt during the process of uplift and magnetization. In A, the uppermost portion (point 1) of the pluton is magnetized as it rises through the isotherms corresponding to the range of blocking temperatures, T_b. In B, point 1 records apparent tilt while point 2 acquires magnetization. In C, points 1 and 2 record apparent tilt, while point 3 acquires magnetization. If tilting ceases at this time, point 3 will not record apparent tilt.

uplifted and acquire magnetization first will record a greater amount of apparent tilt than the lower regions of the pluton which acquire their magnetization at a later time. This may result in a region of no apparent tilt at one end of the pluton and apparent tilt directed *outwards* from the centre at the other end of the pluton. This mechanism cannot, however, account for the observed map pattern in which the apparent tilt is directed *inwards,* toward the centre of the pluton.

6.3 A MODIFIED EXTENSIONAL MODEL

The inferred existence of the ALF necessitates modification of previous interpretations of the extensional history of the map area. Within the following paragraphs, a re-interpretation of the extensional history is presented, in order to account for the observed pattern of apparent tilts. This may be considered to be a "model", in that its predictions are testable through detailed geological mapping, geochronological investigations, and further paleomagnetic studies. The model is illustrated schematically in Figure 6.3.

It is hypothesized that the dykes and small stocks sampled in the eastern half of the map area were cooled and acquired their magnetization prior to cooling, and possibly prior to emplacement, of the large plutons sampled in the west. These eastern regions were then tilted down-to-the-west as a result of displacement along the east-dipping Kettle River and Slocan Lake Faults. The cessation of motion on these faults (at about 52 Ma) was followed by the cooling and magnetization of the large Coryell and Granby Plutons in the central and

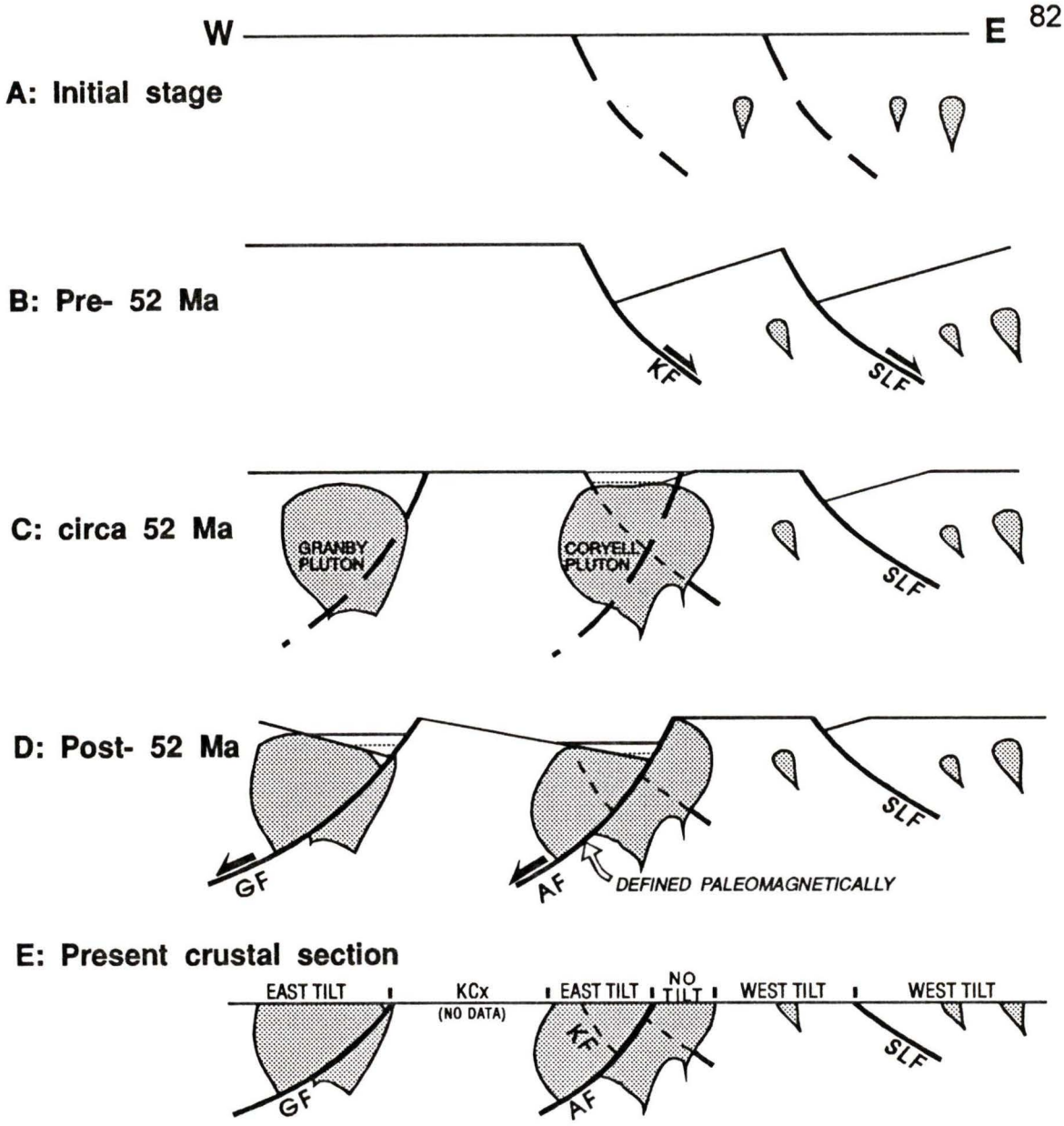

Figure 6.3: Series of schematic cross-sections illustrating the sequence of Eocene extensional events in the map area as inferred from the paleomagnetic data. A: cooling and magnetization of small stocks and dykes in the eastern part of the map area; B: normal displacement on east-dipping faults causes down-to-the-west tilting of terranes east of the Kettle River Fault; C: large plutons in the central and western parts of the area are cooled and magnetized; D: normal displacement on west-dipping faults produces down-to-the-east tilting of terranes west of the Arrow Lake Fault, leaving the eastern parts of the Coryell Pluton untilted; E: this section illustrates the regions of observed apparent tilt at the present level of erosion. (GF=Granby Fault, KF=Kettle River Fault, ALF=Arrow Lake Fault, SLF=Slocan Lake/Champion Lakes Fault)

western parts of the map area. Normal displacement on the west-dipping Granby Fault and the paleomagnetically-defined Arrow Lake Fault then produced the down-to-the-east apparent tilts observed in the west, leaving the eastern parts of the Coryell Pluton untilted.

Radiometric ages obtained from intrusive rocks of the Coryell Intrusive Suite in this part of the southern Omineca Belt tend to cluster around 52 Ma. Their precisions are such that it is not possible to determine accurately the relative ages of plutons and dykes in different parts of the map area. Because of this, the possibility that the intrusive rocks sampled in the eastern half of the area were emplaced or cooled prior to the main phase of Coryell plutonism cannot, at present, be tested by the existing geochronological data, although such a test in principle could be made. If the dykes and small stocks in the eastern half of the area were emplaced at the same time as the large plutons farther west, it is to be expected that they would nevertheless record slightly older cooling ages and magnetizations than the plutons, because they were intruded into higher structural levels in the hanging wall of the SLF, while the plutons are not only much larger, but also were intruded at greater depth into hotter rocks in the footwall of the fault, and hence cooled more slowly. The westerly apparent tilt observed in the eastern map area, as well as in metamorphic rocks in the footwall of the SLF, was presumably caused by motion on the east-dipping faults, which are interpreted to have been active prior to emplacement of the Coryell plutons (Parrish and others, 1988). The absence of apparent tilt in the eastern parts of the Coryell Pluton constrains the last motions on the east-dipping faults as having occurred prior to its cooling and

magnetization (and possibly its emplacement) at about 52 Ma, thus providing independent confirmation of the interpretations of Parrish and others (1988).

One might expect that normal displacement along the east-dipping Kettle River Fault (KF) would have produced down-to-the-west tilting of rocks in its hanging wall. This relationship was predicted by Parrish and others (1988, see their Plate 2), and has been observed in Eocene stratiform rocks in northeastern Washington (Rhodes and Cheney 1981). Within the area of the present study, however, tilts are observed of opposite sense to that expected, and it is this that is the basis for inferring the existence of the west-dipping Arrow Lake Fault. All but four of the twenty-two sites which yield useful results are from intrusive rocks within the Coryell Pluton. Because cooling and magnetization of these rocks postdates displacement on the KF, they should not record apparent tilt related to motion on the fault. One might expect, however, to have observed westerly tilts in the four sites which are located within older country rocks on the north shore of Arrow Lake. In fact, the paleomagnetically observed tilts are to the east, in the opposite sense. There are a number of plausible explanations. The first is that the country rocks at this location may be close enough to the margin of the Coryell Pluton for their magnetizations to have been thermally reset during its emplacement. Several workers have proposed similar explanations to account for anomalously young K-Ar ages observed in pre-Eocene rocks of the area (e.g. Thorpe and Little 1973, Parrish and others 1988). Other authors have noted, however, that where observed, the contact aureole around the Coryell plutons is narrow, between 150 and 600 metres (Daly 1912; Fyles 1984). Nevertheless, this possibility cannot, at present, be discounted, especially since the sub-surface geometry of the pluton margin is unknown, and remagnetization may

have occurred outside the petrologically visible aureole. A second possible explanation is that the country rocks do, in fact, preserve pre-Coryell magnetizations, and have been tilted first to the west by motion on the KF, and then to the east by motion on the ALF. If this is true, then samples from the plutons should exhibit a greater degree of apparent tilt than adjacent country rocks. This is unlikely, because the degree of apparent tilt increases away from the pluton, towards the fault. It is also possible, however, that the country rocks were jostled considerably during intrusion of the Coryell Pluton, and then tilted eastward during displacement on the ALF.

6.4 FAULT GEOMETRY AND MAGNITUDE OF EXTENSION

The sub-surface geometry of the major extensional faults recognized within the map area is not well constrained. Because of a lack of evidence indicating that the faults are listric, and because some are known to have penetrated well into the region of ductile strain, Parrish and others (1988) interpreted them to be essentially planar crustal-scale detachments, which may extend to middle or lower crustal depths without significant flattening. They suggested that this view may be supported by seismic reflection data across several of the faults, although they note that the interpretations of the seismic data are largely conjectural below about five kilometres. The high heat flow measured across the southern Omineca Belt (Davis and Lewis 1984; Lewis and others 1985) suggests that the lower crust is weak and ductile, and that it may be unlikely that the faults could extend as coherent structures through the middle crust.

The similarity in apparent tilt observed in the hanging wall and footwall of the SLF suggests that it may be a planar rotational fault (as defined by Wernicke and Burchfiel 1982). If the major faults in the study area are planar, as suggested by Parrish and others (1988), then the similarity of apparent tilts observed in their hanging walls and footwalls demands that significant tilting of the major blocks has occurred during extension. This is essentially the "card deck" simple shear model, the geometry of which is illustrated, in simplified fashion, in Figure 6.4, and expressed by the equation (LePichon and Sibouet 1981; Wernicke and Burchfiel 1982):

$$\%Extension = 100\left[\sin\phi/\sin\langle\phi-\theta\rangle - 1\right]$$

The initial dip, ϕ, of the faults is given by the sum of the inferred apparent tilt, θ, and their present dip. Although this geometric model is most likely over-simplified and unrealistic, it can be used to provide first-order estimates of the amount of extension accommodated by the major faults across the southern Omineca Belt. Table 6.1 is a summary of data on the major extensional faults, compiled from the recent literature. Several of the parameters listed are the result of interpolation into the plane of section at 49°20'N. All estimates are conservative. The line of section does not necessarily correspond to the latitude at which the maximum displacement on any particular fault is interpreted to have occurred. For example, Carr and others (1987) and Parrish and others (1988) infer perhaps twenty kilometres of displacement on the central section of the Slocan Lake Fault, but this is reduced to about six kilometres at the latitude of the line of section (Carr and others 1987). Using the dip of 30° assumed for the Slocan Lake Fault by Parrish and others (1988), the geometric model gives a value of about 78% extension across the fault. At the latitude of the plane of

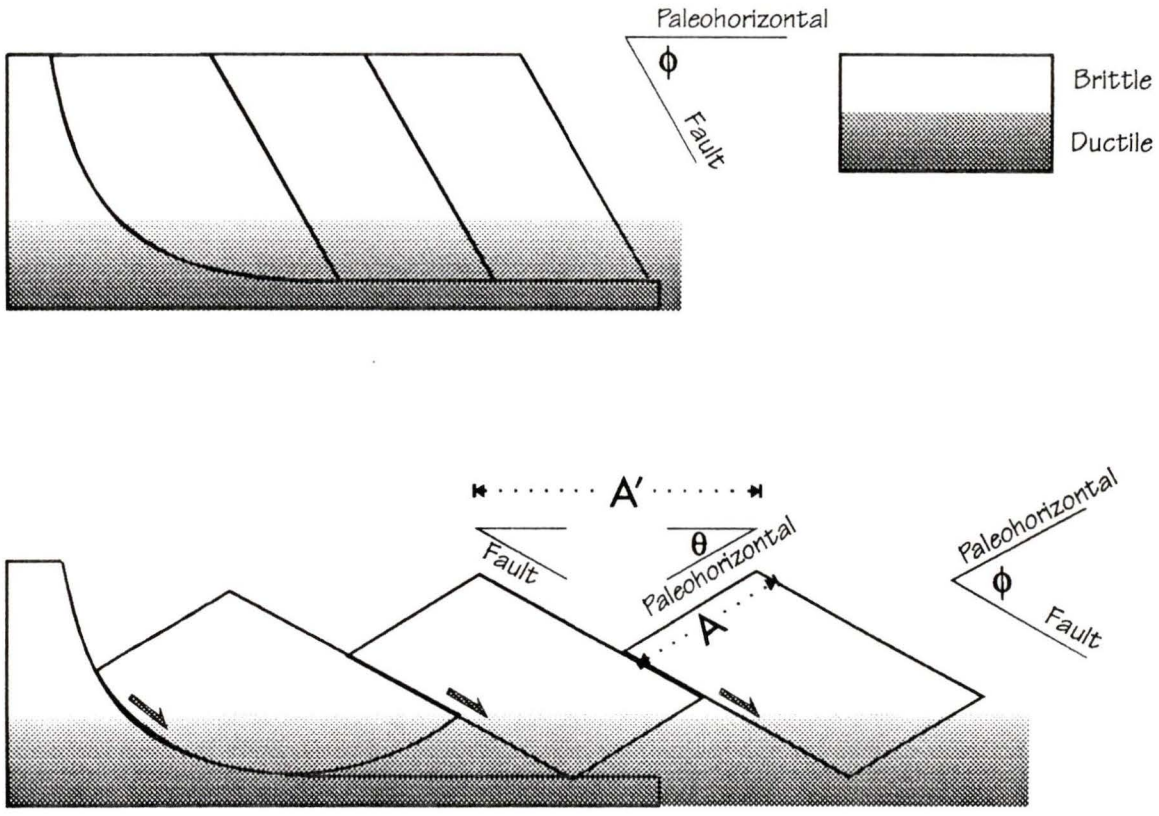

$$\%E = 100(A' - A) = 100[(\sin \phi / \sin (\phi - \theta)) - 1]$$

Figure 6.4: Schematic illustration of the geometry of planar rotational fault blocks, bounded here by a listric normal fault.

Table 6.1: Fault parameters used to estimate extension along latitude 49°20'N

	A	B	C	D	E	F
FAULT SYSTEM	**PRESENT DIP (°)**	**APPARENT HW TILT(°)**	**ORIGINAL DIP (A+B)**	**DISPLACE-MENT (km)**	**HEAVE, h (km)**	**EXTENSION (%)**
OKANAGAN VALLEY	20W[4]	20E[4]	40W	80[4,6]	75	----
GREENWOOD	40W[6,8]	40E[8]	80W	15[6]	11	53
GRANBY	30W[7,8]	38E[9]	68W	15[6,7,8]	13	85
ARROW LAKE	45W[?]	38E[10]	83W	10[?]	7	40
KETTLE RIVER	45E[1]	39W[10]	84E	15[6]	11	41
CHAMPION LAKES	45E[2,3,5]	33W[10]	78E	6[5]	4	38

CUMULATIVE HEAVE, Σh = 121km

NOTES: Data from published results are interpolated estimates into line of section at 49°20'N. Heave is calculated using present dip of faults. %Extension calculated using the equation presented in section 6.3 and illustrated in Figure 6.4; all faults are assumed planar. Refer to text for explanation. REFERENCES: 1, Preto (1970); 2, Corbett and Simony (1984); 3, Carr (1985); 4, Tempelman-Kluit and Parkinson (1986); 5, Carr and others (1987); 6, Parrish and others (1988); 7, Carr and Parkinson (1989); 8, Fyles (1990); 9, Marquis and Irving (1990); 10, this study; ?, assumed.

section, however, the present dip of the fault is interpolated to be about 45° (giving a value of 38% extension), based on measured dips of up to 80° reported farther south, on the Champion Lakes Fault, by Corbett and Simony (1984). No value has been calculated in Table 6.1 for the Okanagan Valley Fault because the shallow dip of rocks in the hanging wall, the very low angle of the fault zone, and the large amount of displacement (up to 90 km) inferred by Tempelman-Kluit and Parkinson (1986), are not compatible with the geometric model described by the equation. Valid estimates are given in Table 6.1 for the values of extension on the remaining faults, assuming a planar geometry in all cases.

The values of extension calculated for each fault using the above equation (column F in Table 6.1) should be considered as minimum estimates. In addition, due to rotation of the major faults to shallower angles as extension continues, displacement becomes increasingly difficult, and motion may proceed on second- and third-generation fault sets which may account for a large amount of the total extension (Angelier and Colletta 1983). The values of k reported in Table 5.3, as well as the consistency of apparent tilt observed over large areas, suggest that second-order faults of this type are likely to be present. Several generations of normal faults have been mapped in the hanging wall of the Granby Fault (Carr and Parkinson 1989), in Eocene stratified rocks of the Greenwood area (Monger 1968; Fyles 1990), and in the hanging wall of the Okanagan Valley Fault (Tempelman-Kluit and Parkinson 1986).

If the major faults are, in fact, listric at depth, then tilting is an immediate consequence of fault displacement, and the amount of extension may have been considerably less than has been calculated in Table 6.1 (see Figure 10 of

Wernicke and Burchfiel 1982). Another important potential source of error in all of these estimates of extension is the unknown geometry of the *upper* reaches of the major faults, which have been removed by erosion. If it is assumed that the presently observed fault planes are the flat basal portions of listric faults, then the degree of extension will be less than has been estimated by assuming a planar geometry.

There is evidence to suggest that the Arrow Lake Fault is listric. If the fault is planar, then the same degree of apparent tilt should be observed in its footwall as in its hanging wall. The absence of tilt in the eastern parts of the Coryell Pluton suggests, therefore, that the fault may be listric at depth. If so, the ALF may serve to solve the "space problem" at the eastern end of the west-dipping fault set (see the listric bounding fault in Figure 6.4). Seismic reflection data from northeastern Washington (COCORP profile W3; Potter and others 1986) could be interpreted to indicate that the KF flattens at mid-crustal depths, possibly forming a listric bounding fault to accommodate tilt related to displacement on the east-dipping faults. This is very speculative, however, because only the westernmost portion of the KF is imaged in the profile. No paleomagnetic data have been obtained from the Kettle River Complex, which forms the footwall of the Granby Fault and of the Kettle River Fault, and therefore it is difficult to speculate on the sub-surface geometry of these faults.

The total extension across the southern Omineca Belt can also be calculated from estimates of the displacement on each fault. The present distance between the Purcell Trench and the hanging wall of the Okanagan Valley Fault is about 200 km, and the cumulative heave on the major faults is

121 km (Table 6.1), indicating a total extension of about 150%. This value is much greater than the estimates of extension calculated using the geometric model, but likely is more realistic. It should be regarded as a minimum value, because it is based on conservative estimates of displacement, does not include Early Eocene displacement on the Valkyr Shear Zone, and because displacements on numerous minor faults have been omitted from the calculation. Also omitted are the effects of dilation due to mid-Eocene intrusion of plutons and dykes of the Coryell Intrusive Suite.

6.5 TIMING AND DURATION OF EXTENSION

Displacement on the major faults of the map area may have taken place over a very short interval of time. Motion on the Slocan Lake Fault occurred over a maximum of about four million years; synkinematic muscovite porphyroclasts, dated by the Rb-Sr technique, indicate the fault was active at 54.5 ± 1.5 Ma (Carr and others 1987), and displacement is inferred to have ended by about 52 Ma (section 6.3). It is suggested here that motion on the Kettle River Fault was approximately contemporaneous with displacement on the SLF, in order for it to have accommodated uplift and westward tilt of the footwall of the SLF. The very high value of k (95; Table 5.3) calculated for the eastern parts of the Coryell Pluton implies that these rocks cooled with extreme rapidity and therefore displacement on the Arrow Lake Fault may have occurred very soon after 52 Ma. Displacement on the Granby Fault also occurred after the acquisition of magnetization, between 51 and 52 Ma, by syenites of the Granby Pluton (Marquis and Irving 1990). The age of last motion on the west-dipping faults is poorly constrained.

Further evidence concerning the duration of extension is supplied by the polarity of the magnetizations. During much of mid-Eocene time, the geomagnetic field was reversed (Figure 6.5), and normal polarity chrons between 49 and 56 Ma are less than 1 Ma in length (Harland and others 1982). Therefore, if the collection spans more than about 4 Ma, the majority of samples should exhibit reverse polarity magnetizations. In fact, only 11 out of 78 sites (14%) exhibit reverse polarity magnetizations (Tables 4.2 and 4.3). Of 26 sites in the footwall and hanging wall of the Slocan Lake / Champion Lakes Fault, 20 are normal and 6 reversed. Chron 24r spans the interval 56 to 53.5 Ma, and so the normal polarity magnetizations likely were acquired after 53.5 Ma, during Chron 24. The reversed magnetizations may have been acquired during Chron 24r, or somewhat later during Chron 23r at about 52.5 Ma. These proposed correlations are necessarily tentative, but if correct, constrain the duration of motion on the SLF and KF to between 54 and 52 Ma (Figure 6.5).

All samples from the hanging wall of the Granby Fault are normally magnetized. This suggests that these rocks acquired their magnetization during Chron 22 or 23. In either case, cooling of the pluton was rapid, because these two polarity chrons are both less than 1 Ma in length. The closeness in time of crystallization and cooling ages obtained from syenites of the Granby Pluton (Marquis and Irving 1990) also suggests very rapid cooling, and that the magnetizations were likely acquired during Chron 23 at about 52 Ma (Figure 6.5). In summary, the data indicate that motion on the east-dipping KF and SLF occurred in the interval between 54 and 52 Ma, and on the west-dipping ALF and GF after 52 Ma.

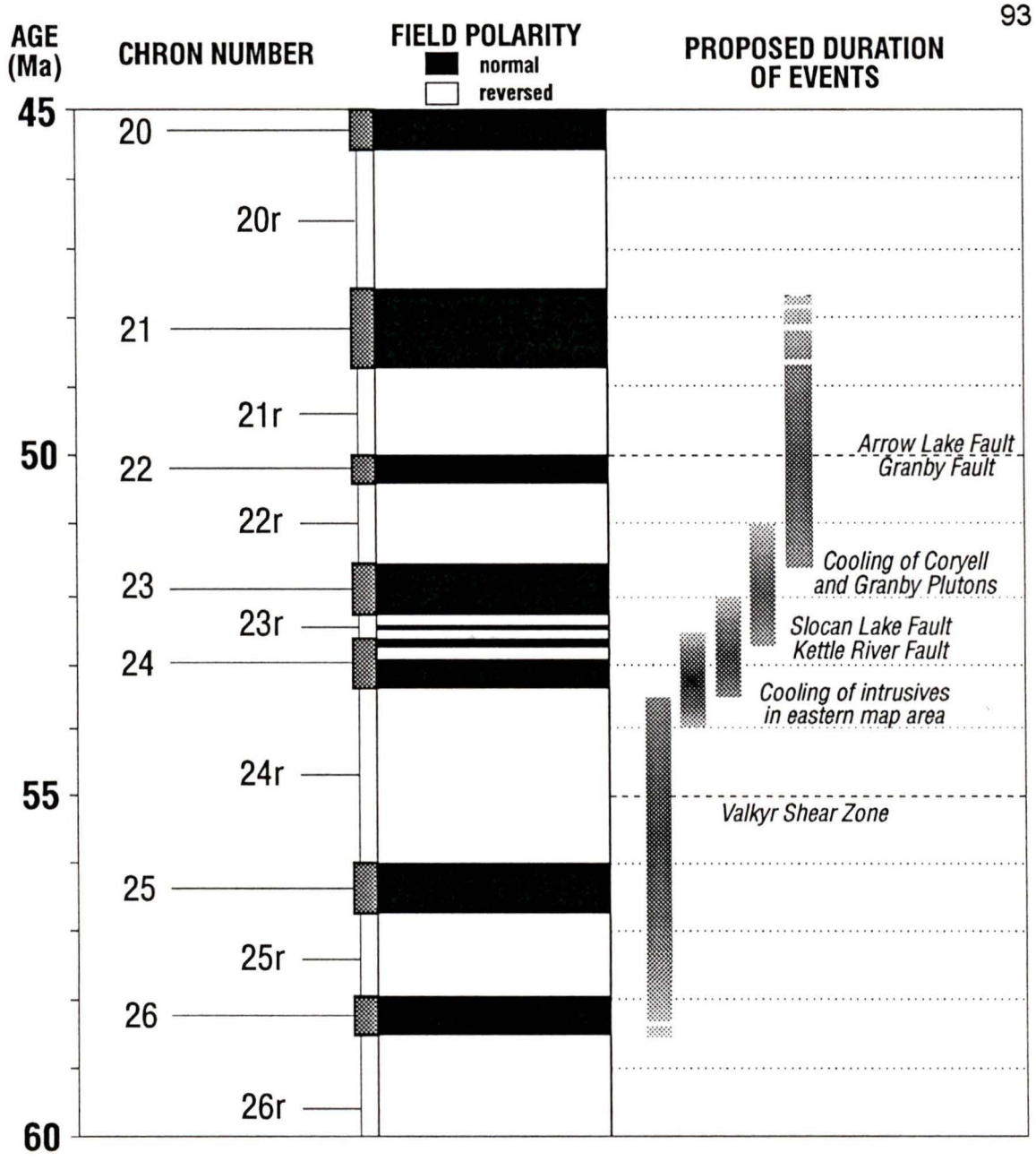

Figure 6.5: Proposed correlation of mid-Eocene extensional events with polarity chrons, based on geological, geochronological, and paleomagnetic data. Refer to text for discussion.

6.6 RESTORATION OF OLDER STRUCTURES

By removing the effects of inferred tilting, older structures can be restored to their pre-tilt configurations. There are several structural elements which predate displacement on the major mid-Eocene extensional faults: the Jones Fault (JF) in the hanging wall of the Granby Fault, the Early Eocene Valkyr Shear Zone (VSZ), the Jurassic Mt. Verde Fault (MVF) southwest of Nelson, and the Waneta Fault (WF) and other related thrusts of Jurassic age located in the southeast corner of the study area (Figures 2.4 and 2.5). Other pre-Eocene structures in the study area, such as the Jurassic thrust faults south of Greenwood and segments of the Waneta Fault south of the termination of the SLF (Figure 2.4), are not considered, because they are located far from any sites sampled during this study and it is not reasonable to extrapolate the paleomagnetic data over such distances.

Carr and Parkinson (1989) describe the JF as presently flat-lying or dipping gently to the east or west. Restoration of bedding, measured in supracrustal rocks of the upper plate, suggests that the fault originally dipped 60 to 80° to the west (Carr and Parkinson 1989). The eastward apparent tilts observed in underlying crystalline rocks of the Granby Pluton (Marquis 1988; Marquis and Irving 1990) tend to confirm this interpretation. The mean apparent tilt for the region is 38 ± 14°, and three of the sites are apparently tilted by more than 50°, of the same order as predicted by Carr and Parkinson (1989).

Both Carr and others (1987) and Parrish and others (1988) interpret the VSZ to be an eastward-rooting extensional normal fault. Carr and others (1987), however, point out that the top-to-the-east kinematic indicators and the present antiformal attitude of the VSZ do not preclude its interpretation as a westward-

rooting thrust fault. The paleomagnetic data can be employed to eliminate this possibility. After removing about 40° of down-to-the-west tilt caused by motion on the SLF, the restored VSZ dips 40° to the east, and therefore, is not likely to be a westward-rooting thrust fault.

As described in section 2.3, parts of the MVF (Figure 2.4) dip steeply to the east and their apparent sense of displacement is reverse. Höy and Andrew (1989), however, interpreted this structure to be a listric normal fault which is overturned to the west at higher structural levels, and which places volcanic rocks of the Upper Elise Formation in its western hanging wall against more deformed Archibald Formation rocks to the east. Although paleomagnetic observations are sparse in this area, the general sense of apparent tilt is down-to-the-west. Site 16, which is located just west of the MVF, records westward apparent tilt of 17° at 266°. Removal of about 20° of westward tilt would confirm the interpretation of Höy and Andrew (1989) that the MVF is an overturned normal fault.

Similarly, where the Waneta (WF) and Tillicum Creek Faults (TCF) dip steeply to the southeast (Figure 2.5), they have been interpreted to be overturned (Höy and Andrew 1990; Einarson 1991). Several of the slightly younger north-trending thrust faults in this region dip steeply to the east and also have been interpreted to be overturned (Höy and Andrew 1990). These interpretations may be supported by the paleomagnetic evidence. Results from the Tramway Stock suggest that this region was tilted down-to-the-west by about 25° (Figure 5.6). Although the WF and TCF strike obliquely to the observed direction of apparent tilt, removing a component of the inferred tilt, perhaps 10°, might restore the steeper segments of these faults to a steeply northwest-

dipping configuration. The effect, on the north-trending thrusts, of removing about 20° of westward tilt is illustrated in Figure 6.6. The strike of these faults is approximately perpendicular to the direction of tilt of the Tramway Stock, and to the line of cross-section (Figure 2.5). After restoration, the steeply west-dipping fault in the section dips more gently to the west, and the two east-dipping faults attain west-dipping configurations, at least at the present level of erosion.

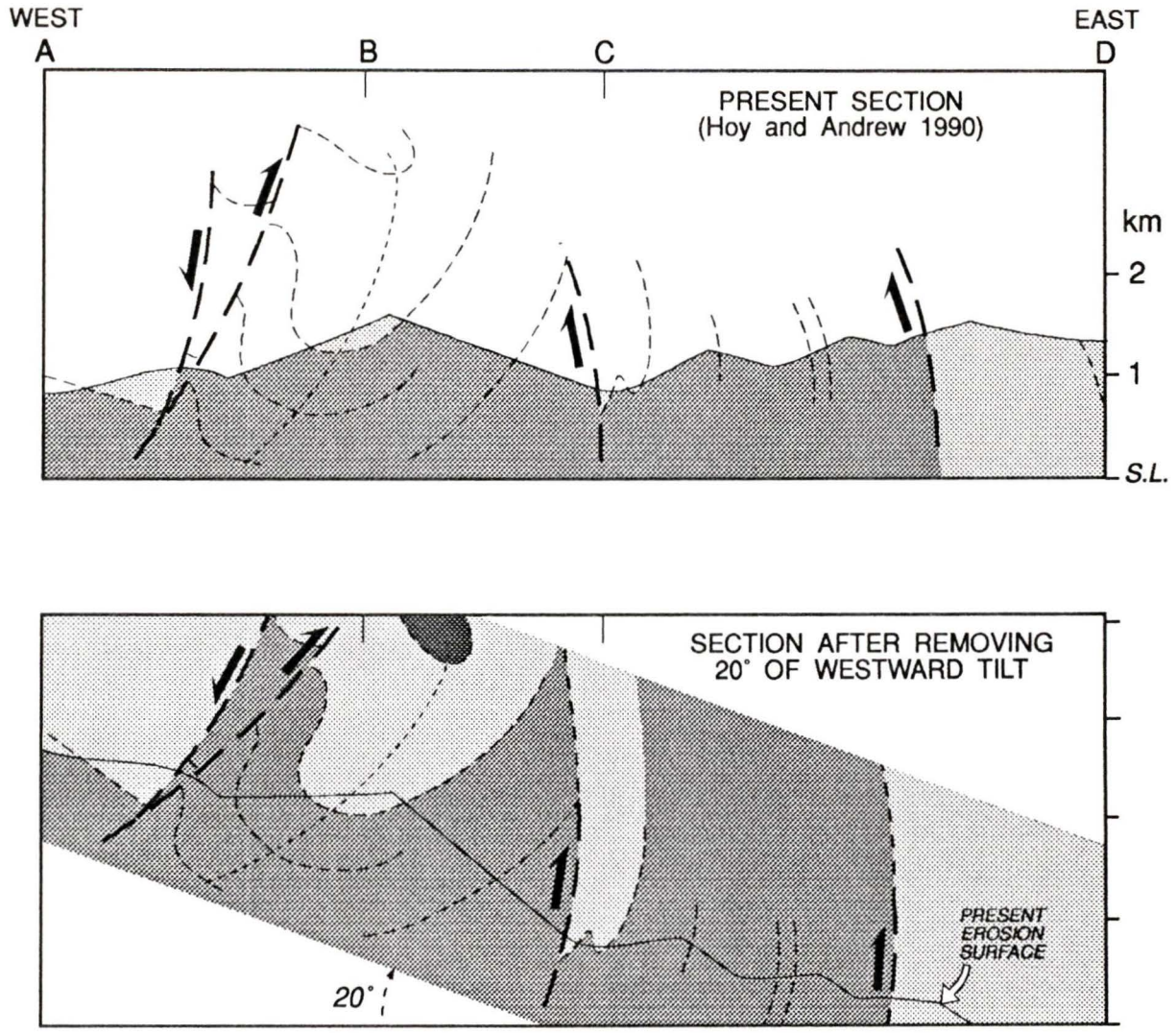

Figure 6.6: The effect of removing 20° of westward tilt on the attitude of east-dipping faults of Middle Jurassic age which cut rocks of the Rossland Group. Legend and location of present cross-section (top) are given in Figure 2.5. East-dipping faults restore to west-dipping configurations after removal of westward tilt (bottom).

CHAPTER 7

CONCLUSIONS

This project has demonstrated the utility of paleomagnetism in regional structural and tectonic studies in high-grade metamorphic and plutonic terranes. The inferred tilts provide some of the fundamental data required for accurate analysis of the kinematics of the extensional process. A map of the apparent tilts (Figure 5.6) has been produced, and the first-order patterns of tilt suggest the existence of a previously undiscovered major Eocene normal fault. Inferences regarding the timing of acquisition of magnetization with respect to tilting supply important constraints on the timing and duration of extension. The following paragraphs summarize the main conclusions of this study:

1. Apparent tilts are generally orthogonal to the mapped traces of the major extensional faults, justifying the assumption that tilting occurred about axes which were close to horizontal.

2. Mid-Eocene dykes and small stocks intruded into the hanging wall and footwall of the SLF, which record westward apparent tilt, were presumably magnetized prior to tilting due to displacement on the SLF and KF. Intrusive rocks sampled in the hanging wall may have cooled rapidly by conduction, rather than as the result of uplift, because these country rocks were less than 300°C during the Eocene (Parrish and others 1988). In the footwall of the SLF, the consistency of apparent tilt, derived from magnetizations acquired over a range of blocking temperatures, suggests the rocks cooled to the lower end of the T_b range before tilting occurred. It is hypothesized that these lower plate rocks were

cooled as a result of rapid uplift, which also served to "lock up" the VSZ and initiate motion on the SLF and KF.

3. Polarity evidence suggests that most of the magnetizations in the footwall and hanging wall of the SLF were acquired during the normal polarity chron 24, and therefore that motion on the SLF commenced close to 53 Ma. In order to have accommodated tilting of the footwall of the SLF, it is hypothesized that displacement on the KF was synchronous with motion on the SLF.

4. The value of k (= 95) observed in the eastern parts of the Coryell Pluton is considerably higher than that expected from secular variation (k = 28). This suggests that the pluton was cooled with extreme rapidity, presumably the result of rapid and substantial uplift. Such rapid cooling is also indicated by the closeness in time of radiometric crystallization and cooling ages, all of which cluster around 52 Ma. The predominance of normal polarities in samples from the Coryell Pluton suggests magnetization was acquired during chron 23.

5. The absence of apparent tilt in the eastern parts of the Coryell Pluton confirms that displacement on the SLF ended before cooling and magnetization of the pluton at about 52 Ma. Parrish and others (1988) reached this same conclusion, but their arguments were incomplete, because although they did produce evidence that the VSZ (and possibly the KF) is intruded by the 52 Ma Coryell suite, they did not demonstrate that the SLF, in particular, is cross-cut by 52 Ma intrusions.

6. A previously undiscovered, major Eocene extensional fault, named here the Arrow Lake Fault, has been defined paleomagnetically. Marquis (1988)

speculated that such a fault may exist east of the Coryell Pluton, but did not have sufficient sample density or coverage to define such a structure. The same degree of apparent tilt indicated by the high T_b normal and low T_b reversed magnetization components of site 63 indicates the pluton had cooled through the T_b range before motion occurred on the AF. Rapid cooling of the Coryell Pluton at about 52 Ma indicates that motion on the AF may have commenced very soon after this date. If the western parts of the Coryell Pluton were magnetized with the same rapidity as the eastern parts, then the much lower value of *k* determined for the west is likely a reflection of deformation in the hanging wall of the AF.

7. Apparent tilt data allow inferences to be made regarding the sub-surface geometry of the major extensional faults. The similarity of apparent tilt in the hanging wall and footwall of the SLF suggest that it is a planar rotational fault. Conversely, the absence of apparent tilt in the footwall of the AF suggest that it may have a listric geometry. The data also allow estimates of the amount of extension on the major faults to be calculated using a simple geometric model. The model predicts extension on the major faults to average about 50%. A review of published estimates of fault displacements suggests the amount of extension across the southern Omineca Belt, between the footwall of the PTF and the hanging wall of the OVF, may be closer to 150%.

8. By removing the effects of inferred tilting, older structures can be restored to their pre-tilt configurations. Eastward apparent tilts observed in syenites of the Granby Pluton confirm the interpretation of Carr and Parkinson (1989) that the Jones Fault, which presently is flat-lying, dipped originally to the west. The

footwall of the SLF is interpreted to be tilted down-to-the-west by about 40°. Restoration of this inferred tilt indicates that, during the Early Eocene, the VSZ dipped about 40° to the east, and is indeed an east-rooting extensional fault, thus making unlikely the possibility (raised by Carr and others 1987) that the VSZ is a west-rooting thrust fault. The Mount Verde normal fault, and the Waneta, Tillicum Creek, and other thrust faults, all of Jurassic age, are believed by some to be overturned to the west (Höy and Andrew 1990; Einarson 1991); down-to-the-west apparent tilts observed in the eastern part of the study area tend to support this interpretation.

REFERENCES

Andrew, K.P.E., Höy, T., and Simony, P. 1991. Geology of the Trail Map Area, southeastern British Columbia, British Columbia Ministry of Energy, Mines, and Petroleum Resources, Open File 1991-16.

Andrew, K.P.E., and Höy, T. 1991. Geology of the Rossland Group in the Erie Lake area, with emphasis on stratigraphy and structure of the Hall Formation, southeastern British Columbia, British Columbia Ministry of Energy, Mines, and Petroleum Resources, Geological Fieldwork, Paper 1991-1, p. 9-20.

Angelier, J., and Colletta, B. 1983. Tension fractures and extensional tectonics, Nature, **301**: 49-51.

Archibald, D.A., Glover, J.K., Price, R.A., Farrar, E., and Carmichael, D.M. 1983. Geochronology and tectonic implications of magmatism and metamorphism, southern Kootenay Arc and neighbouring regions, southeastern British Columbia. Part 1: Jurassic to mid-Cretaceous, Canadian Journal of Earth Sciences, **20**: 1891-1913.

Armstrong, R.L., and Parrish, R.R. 1989. A geological excursion across the Canadian Cordillera near 49°N (special Paleogene version), Vancouver, British Columbia.

Ash, C.H., MacDonald, R.W.J., and Reynolds, P.R. 1992. Ophiolite-related mesothermal lode gold in British Columbia: a deposit model, *in preparation*.

Bardoux, M., and Irving, E. 1989. Paleomagnetism of Eocene rocks of the Kelowna and Castlegar areas, British Columbia: studies in determining paleohorizontal, Canadian Journal of Earth Sciences, **26**: 829-844.

Beck, M.E., Jr., Burmester, R.F., Engebretson, D.C., Schoonover, R. 1981. Northward translation of Mesozoic batholiths, western North America: paleomagnetic evidence and tectonic significance, Geofisica International, **20**: 144-162.

Beck, M.E., Jr. 1992. Some thermal and paleomagnetic consequences of tilting a batholith, Tectonics, **11(2)**: 297-302.

Brown, R.L., and Read, P.B. 1983. Shuswap Terrane of British Columbia: a Mesozoic "core complex", Geology, **11**: 164-168.

Brown, R.L., Journeay, J.M., Lane, L.S., Murphy, D.C., Rees, C.J. 1986. Obduction, backfolding, and piggyback thrusting in the metamorphic

hinterland of the southeastern Canadian Cordillera, Journal of Structural Geology, **8**: 255-268.

Brown, R.L., and Journeay, J.M. 1987. Tectonic denudation of the Shuswap metamorphic terrane of southeast British Columbia, Geology, **15**: 142-146.

Brown, R.L. and Carr, S.D. 1990. Lithospheric thickening and orogenic collapse within the Canadian Cordillera, Proceedings of the Pacific Rim 90 Congress, Australian Institute of Mining and Metallurgy, Volume II, p.1-10.

Brown, R.L., Carr, S.D., Johnson, B.J., Coleman, V.J., Cook, F.A., and Varsek, J.L. 1991. The Monashee Décollement of the southern Canadian Cordillera: a crustal-scale shear zone linking the Rocky Mountain Foreland Belt to lower crust beneath accreted terranes, *in*: McClay, K.R. (ed.), Thrust Tectonics, Chapman and Hall, p.344-347.

Butler, R.F, Gehrels, G.E., McClelland, W.C., May, S.R., Klepacki, D. 1989. Discordant paleomagnetic poles from the Canadian Coast Plutonic Complex: Regional tilt rather than large-scale displacement?, Geology, **17**: 691-694.

Carr, S.D. 1985. Ductile shearing and brittle faulting in Valhalla gneiss complex, southeastern British Columbia, *in*: Current Research, Part A, Geological Survey of Canada, Paper 85-1A, p. 89-96.

Carr, S.D., Parrish, R., and Brown, R.L. 1987. Eocene structural development of the Valhalla complex, southeastern British Columbia, Tectonics, **6**: 175-196.

Carr, S.D., and Parkinson, D.L. 1989. Eocene stratigraphy, age of the Coryell batholith, and extensional faults in the Granby Valley, southern British Columbia, *in*: Current Research, Part E, Geological Survey of Canada, Paper 89-1E, p. 79-87.

Cheney, E.S. 1980. Kettle dome and related structures of northeastern Washington, *in*: M.D. Crittenden, P.J. Coney, and G.H. Davis, (eds.), Cordilleran Metamorphic Core Complexes, Geological Society of America, Memoir 153, p.463-482.

Coney, P.J. 1980. Cordilleran metamorphic core complexes: an overview, *in*: M.D. Crittenden, P.J. Coney, and G.H. Davis, (eds.), Cordilleran Metamorphic Core Complexes, Geological Society of America, Memoir 153, p.7-31.

Coney, P.J., and Harms, T.A. 1984. Cordilleran metamorphic core complexes: Cenozoic extensional relics of Mesozoic compression, Geology, **12**: 550-554.

Cook, F.A., Green, A.G., Simony, P.S., Price, R.A., Parrish, R.R., Milkereit, B., Gordy, P.L., Brown, R.L., Coflin, K.C., and Patenaude, C. 1988. Lithoprobe seismic reflection structure of the southern Canadian Cordillera: initial results, Tectonics, **7**: 157-180.

Cook, F.A., Varsek, J.L., Clowes, R.M., Kanasewich, E.R., Spencer, C.S., Parrish, R.R., Brown, R.L., Coflin, K.C., and Patenaude, C. 1992. Lithoprobe crustal reflection cross-section of the southern Canadian Cordillera: foreland thrust and fold belt to Fraser River Fault, Tectonics, **11**: 12-35.

Corbett, C.R., and Simony, P.S. 1984. The Champion Lake Fault in the Trail - Castlegar area of southeastern British Columbia, *in*: Current Research, Part A, Geological Survey of Canada, Paper 84-1A, p. 103-104.

Cox, A. 1970. Latitude dependence of the angular dispersion of the geomagnetic field, Geophysical Journal of the Royal Astronomical Society, **20**: 253-269.

Crittenden, M.D., Coney, P.J., and Davis, G.H. 1978. Tectonic significance of metamorphic core complexes in the North American Cordillera, Geology, **6**: 79-80.

Crittenden, M.D., Coney, P.J., and Davis, G.H. (eds.). 1980. Cordilleran Metamorphic Core Complexes, Geological Society of America, Memoir 153.

Daly, R.A. 1912. Geology of the North American Cordillera at the forty-ninth parallel, Memoir No. 38, Canada Department of Mines, p. 358-376.

Davis, E.E., and Lewis, T.J. 1984. Heat flow in a back-arc environment, Intermontane Belt, southern Canadian Cordillera, Canadian Journal of Earth Sciences, **21**: 715-726.

Day, R. 1977. TRM and its variation with grain size, *in*: D.J. Dunlop (ed.), Advances in Earth and Planetary Sciences, v.1: Origin of Thermoremanent Magnetization, Japan Scientific Societies Press, Tokyo, p. 1-33.

Diehl, J.F., Beck, M.E. Jr., Beske-Diehl, S., Jacobson, D., and Hearn, B.C. Jr. 1983. Paleomagnetism of the Late Cretaceous - Early Tertiary north-central Montana alkalic province, Journal of Geophysical Research, **88[B12]**: 10,593-10,609.

Drysdale, C.W. 1915. Geology and ore deposits of Rossland, British Columbia, Geological Survey of Canada, Memoir 77, 317p.

Dunlop, D.J. 1979. On the use of Zijderveld vector diagrams in multicomponent paleomagnetic studies, Physics of the Earth and Planetary Interiors, **20**: 12-24.

Einarson, J.M. 1991. Structural geology of the terrane accretion boundary in the southern Kootenay Arc, Proceedings of the Lithoprobe Southern Canadian Cordillera Transect Workshop, Calgary, p. 100-103.

Fisher, R.A. 1953. Dispersion on a sphere, Proceedings of the Royal Society of London, **A217**: 295-305.

Fyles, J.T. 1984. Geological Setting of the Rossland Mining Camp, Bulletin 74, British Columbia Ministry of Energy, Mines, and Petroleum Resources, 61p.

Fyles, J.T. 1990. Geology of the Greenwood - Grand Forks Area, NTS 82E/1,2, Open File 1990-25, British Columbia Geological Survey Branch, 19p.

Gabrielse, H., Monger, J.W.H., Wheeler, J.O., and Yorath, C.J. 1991. Part A. Morphogeological belts, tectonic assemblages, and terranes, *in*: H. Gabrielse and C.J. Yorath, (eds.), Chapter 2 of Geology of the Cordilleran Orogen in Canada, Geological Survey of Canada, Geology of Canada, No. 4, p. 15-28.

Gabrielse, H., and Yorath, C.J. 1989. DNAG #4, The Cordilleran Orogen in Canada, Geoscience Canada, **16**: 67-83.

Halls, H.C., and Shaw, E.G. 1987. Paleomagnetism and orientation of Precambrian dykes, eastern Lake Superior region, and their use in estimates of crustal tilting, Canadian Journal of Earth Sciences, **25**: 732-743.

Harland, W.B., Cox, A.V., Llewellyn, P.G., Pickton, C.A.G., Smith, A.G., and Walters, R. 1982. A geologic time scale, Cambridge University Press, 131p.

Harms, T.A., and Price, R.A. 1992. The Newport Fault: Eocene listric normal faulting, mylonitization, and crustal extension in northeast Washington and northwest Idaho, Geological Society of America Bulletin, **104**: 745-761.

Holder, R.W., and Holder, G.A.M. 1988. The Colville Batholith - Tertiary plutonism in northeast Washington associated with graben and core complex (gneiss dome) formation, Geological Society of America Bulletin, **100[12]**: 1971-1980.

Hood, P.J. 1961. Paleomagnetic study of the Sudbury Basin, Journal of Geophysical Research, **66[4]**: 1235-1241.

Höy, T., and Andrew, K.P.E. 1989. The Rossland Group, Nelson map area, southeastern British Columbia, British Columbia Ministry of Energy, Mines, and Petroleum Resources, Geological Fieldwork, Paper 1989-1, p. 33-42.

Höy, T., and Andrew, K.P.E. 1990. Structure and tectonic setting of the Rossland Group, Mount Kelly - Hellroaring Creek area, southeastern British Columbia, British Columbia Ministry of Energy, Mines, and Petroleum Resources, Geological Fieldwork, Paper 1990-1, p. 11-17.

Höy, T., and Andrew, K.P.E. 1991. Geology of the Rossland Area, southeastern British Columbia, British Columbia Ministry of Energy, Mines, and Petroleum Resources, Geological Fieldwork, Paper 1991-1, p. 21-31.

Höy, T., Dunne, K.P.E., and Wehrle, D. 1992. Tectonic and stratigraphic controls of gold-copper mineralization in the Rossland Camp, southeastern British Columbia (82F/4), British Columbia Ministry of Energy, Mines, and Petroleum Resources, Geological Fieldwork, Paper 1992-1, p.261-272.

Hunt, P.A., and Roddick, J.C. 1987. A compilation of K-Ar ages, Report 17, *in*: Radiogenic Age and Isotopic Studies, Report 1, Geological Survey of Canada, Paper 87-2, p.143-210.

Hunt, P.A., and Roddick, J.C. 1988. A compilation of K-Ar ages, Report 18, *in*: Radiogenic Age and Isotopic Studies, Report 2, Geological Survey of Canada, Paper 88-2, p.127-153.

Hunt, P.A., and Roddick, J.C. 1990. A compilation of K-Ar ages, Report 19, *in*: Radiogenic Age and Isotopic Studies, Report 3, Geological Survey of Canada, Paper 89-2, p.153-190.

Hunt, P.A., and Roddick, J.C. 1991. A compilation of K-Ar ages, Report 20, *in*: Radiogenic Age and Isotopic Studies, Report 4, Geological Survey of Canada, Paper 90-2, p.113-143.

Irving, E. 1964. Paleomagnetism and its application to geological and geophysical problems, John Wiley and Sons, New York, 399p.

Irving, E., Baker, J., Wright, N., Yorath, C.J., and York, D. 1992. Magnetism and age of the Porteau Pluton, southern Coast Plutonic Complex, British Columbia: evidence for tilt and translation, *submitted to* Canadian Journal of Earth Sciences.

Irving, E., and Archibald, D.A. 1990. Bathozonal tilt corrections to paleomagnetic data from mid-Cretaceous plutonic rocks: examples from the Omineca Belt, British Columbia, Journal of Geophysical Research, **95**: 4579-4585.

Irving, E., and Brandon, M.T. 1990. Paleomagnetism of the Flores volcanics, Vancouver Island, in place by Eocene time, Canadian Journal of Earth Sciences, **27**: 811-817.

Irving, E., Woodsworth, G.J., Wynne, P.J., and Morrison, A. 1985. Paleomagnetic evidence for displacement from the south of the Coast Plutonic Complex, British Columbia, Canadian Journal of Earth Sciences, **22**: 584-598.

Journeay, J.M. 1983. Progressive deformation and inverted regional metamorphism associated with Mesozoic emplacement of the Shuswap-Monashee complexes, southeast British Columbia, Geological Society of America, Abstracts with Programs, **15**: 606.

Journeay, J.M. 1986. Stratigraphy, internal strain, and thermo-tectonic evolution of northern Frenchman Cap dome: an exhumed basement duplex structure, unpublished Ph.D. dissertation, Queen's University, Kingston, Ontario, 401p.

LeCouteur, P.C., and Agar, C.A. 1972. Paleomagnetism of the Triassic Guichon Batholith and rotation in the Interior Plateau, British Columbia: Discussion, Canadian Journal of Earth Sciences, **9**: 1341-1343.

LePichon, X., and Sibouet, J. 1981. Passive margins: a model of formation, Journal of Geophysical Research, **86**: 3708-3720.

Lewis, T.J., Jessop, A.M., and Judge, A.S. 1985. Heat flux measurements in southwestern British Columbia: the thermal consequences of plate tectonics, Canadian Journal of Earth Sciences, **22**: 1262-1273.

Little, H.W. 1957. Kettle River, east half, British Columbia, Map 6-1957, Geological Survey of Canada.

Little, H.W. 1960. Nelson map area, west half, British Columbia, Memoir 308, Geological Survey of Canada, 205p.

Little, H.W. 1982. Geology of the Rossland-Trail map area, British Columbia, Geological Survey of Canada, Paper 79-26, 38p.

Marquis, G. 1988. Aberrant paleomagnetic directions in the Canadian Cordillera, M.Sc. thesis, University of Victoria, Victoria, British Columbia, 97p.

Marquis, G., and Irving, E. 1990. Observing tilts in midcrustal rocks by paleomagnetism: examples from southeast British Columbia, Tectonics, **9[5]**: 925-934.

Monger, J.W.H. 1968. Early Tertiary stratified rocks, Greenwood map area, (82 E/2), British Columbia, Geological Survey of Canada, Paper 67-42, 39p.

Monger, J.W.H., and Price, R.A. 1979. Geodynamic evolution of the Canadian Cordillera - progress and problems, Canadian Journal of Earth Sciences, **16**: 770-791.

Monger, J.W.H., Price, R.A., and Tempelman-Kluit, D.J. 1982. Tectonic accretion and the origin of the two major metamorphic and plutonic welts in the Canadian Cordillera, Geology, **10**: 70-75.

Parrish, R.R., Carr, S.D., and Brown, R.L. 1985a. Valhalla gneiss complex, southeast British Columbia: 1984 field work, *in*: Current Research, Part A, Geological Survey of Canada, Paper 85-1A, p.81-87.

Parrish, R.R., Carr, S.D., and Parkinson, D.L. 1985b. Metamorphic complexes and extensional tectonics, southern Shuswap Complex, southeastern British Columbia, in: Tempelman-Kluit, D.J., (ed.), Field Guides to Geology and mineral Deposits in the Southern Canadian Cordillera, Geological Society of America, Cordilleran Section, Vancouver, British Columbia, p.12.1-12.15.

Parrish, R.R., Carr, S.D., and Parkinson, D.L. 1988. Eocene extensional tectonics and geochronology of the southern Omineca Belt, British Columbia and Washington, Tectonics, **7[2]**: 181-212.

Potter, C.J., Sanford, W.E., Yoos, T., Prussen, E., Keech, R. II, Oliver, J.E., Kaufman, S., and Brown, L.D. 1986. COCORP deep seismic reflection traverse of the interior of the North American Cordillera, Washington and Idaho, Tectonics, **5**: 1007-1027.

Preto, V.A. 1970. Structure and Petrology of the Grand Forks Group, Geological Survey of Canada, Paper 69-22, 80p.

Price, R.A., and Mountjoy, E.W. 1970. Geologic structure of the Canadian Rocky Mountains between Bow and Athabaska Rivers - a progress report, *in*: Wheeler, J.O., (ed.), Geological Association of Canada, Special Paper 6, 7-25.

Pullaiah, G., Irving, E., Buchan, K.L., and Dunlop, D.J. 1975. Magnetization changes caused by burial and uplift, Earth and Planetary Science Letters, **28**: 133-143.

Read, P.B., and Brown, R.L. 1981. Columbia River Fault Zone: southeastern margin of the Shuswap and Monashee Complexes, southern British Columbia, Canadian Journal of Earth Sciences, **18**: 1127-1145.

Rehrig, W.A., and Reynolds, S.J. 1981. Eocene metamorphic core complex tectonics near the Lewis and Clarke zone, western Montana and northern Idaho, Geological Society of America, Abstracts with Programs, **13**: 102.

Rhodes, B.P., and Cheney, E.S. 1981. The low-angle Kettle River Fault: the eastern contact of Kettle Dome, northeast Washington, Geology, **9**: 366-369.

Shaver, S.A., and McWilliams, M. 1987. Cenozoic extension and tilting recorded in Upper Cretaceous and Tertiary rocks at the Hall molybdenum deposit, northern San Antonio Mountains, Nevada, Geological Society of America Bulletin, **99**: 341-353.

Shive, P.N., and Pruss, E.F. 1977. A paleomagnetic study of basalt flows from the Absaroka Mountains, Wyoming, Journal of Geophysical Research, **82[10]**: 3039-3048.

Simony, P.S. 1979. Pre-Carboniferous basement near Trail, British Columbia, Canadian Journal of Earth Sciences, **16**: 1-11.

Stoffel, K.L. 1990. Geologic map of the Republic 1:100,000 quadrangle, Washington, Washington Division of Geology and Earth Resources, Open File Report 90-10, 62p.

Symons, D.T.A. 1971. Paleomagnetism of the Triassic Guichon Batholith and rotation in the Interior Plateau, British Columbia, Canadian Journal of Earth Sciences, **8**: 1388-1396.

Symons, D.T.A. 1972. Paleomagnetism of the Triassic Guichon Batholith and rotation in the Interior Plateau, British Columbia: Reply, Canadian Journal of Earth Sciences, **9**: 1343-1347.

Symons, D.T.A., and Wellings, M.R. 1989. Paleomagnetism of the Eocene Kamloops Group and the cratonization of Terrane 1 of the Canadian Cordillera, Canadian Journal of Earth Sciences, **26**: 821-828.

Tarling, D.H. 1983. Paleomagnetism: principles and applications in geology, geophysics and archeology, Chapman and Hall, London, 379p.

Tempelman-Kluit, D., and Parkinson, D. 1986. Extension across the Eocene Okanagan crustal shear in southern British Columbia, Geology, **14**: 318-321.

Thorpe, R.I., and Little, H.W. 1973. The age of sulphide mineralization at Rossland, British Columbia: discussion, Canadian Journal of Earth Sciences, **8**: 1337-1346.

Varsek, J.L., and Cook, F.A. 1992. Regional three-dimensional crustal structure of the eastern Cordillera, southern Canada and northwestern United States, Proceedings of the Lithoprobe southern Cordillera transect workshop and Cordilleran tectonics workshop, Report No. 24, Edmonton, Alberta, p. 19-33.

Watson, G.S., and Irving, E. 1957. Statistical methods in rock magnetism, Monthly Notices, Royal Astronomical Society Geophysical Supplement, **7**: 289-300.

Wernicke, B., and Burchfiel, B.C. 1982. Modes of extensional tectonics, Journal of Structural Geology, **4[2]**: 105-115.

York, D. 1978. Magnetic blocking temperature, Earth and Planetary Science Letters, **39**: 94-97.

Zijderveld, J.D.A. 1967. A.C. demagnetization of rocks: analysis of results, *in*: D.W. Collinson, K.M. Creer, and S.K. Runcorn (editors), Methods in Paleomagnetism, Elsevier, Amsterdam, p. 254-286.

APPENDIX A

SAMPLE LOCATIONS

Table A1: Location and lithological description of sites sampled for paleomagnetic study

SITE	LITHOLOGY	UTM Coordinates (Zone 11u)	LOCATION
1	c/g pyroxene-biotite Coryell syenite	4823E 54385N	Tramway Stock; at N end of tailings, 3 km E on abandoned mine road to Iron Mtn; 11 km S of Salmo on Hwy 3,6
2	c/g pyroxene-biotite Coryell syenite	4822E 54385N	150m W of Site 1; 20m N of, and 10m above tailings
3	c/g pyroxene-biotite Coryell syenite	4824E 54385N	120m E of Site 1; 5m above tailings; 15m W of contact with L. Camb. seds
4	f-m/g syenite; contact phase?	4821E 54384N	250m SW of Site 1, on SW side of tailings
5	f/g dark green mafic dyke, 3-4m wide; 335/st	4848E 54710N	NW side of Hwy 6, S of Nelson, 2.1 km N of Hall Siding Rd., 2.75 km N of Hall Creek
6	f/g mafic dyke, 4m wide, fp glomerocrysts replaced by qtz-calcite-epidote; 341/83	4822E 54680N	W side of Hwy 6, 600m S of Hall Creek, at entrance to gravel road
7	f/g biotite ± px/hb(?) diorite dyke; attitude unknown	4738E 54534N	exposed in roadway, 6.1 km N from Hwy 3 on 2nd Relief Rd.
8	f/g lamprophyre dyke; 325/78	4644E 54525N	NE side of Hwy 3, 7.6 km NW from jcn with Hwy 3B
9	f/g mafic dyke; contact-parallel bands of qtz ± epidote amygdules; 012/71	4638E 54527N	NE side of Hwy 3, 8.2 km NW from jcn with Hwy 3B; 600m NW of Site 8
10	f/g mafic dyke; attitude unknown	4581E 54544N	N side of Hwy 3, 10.6 km SE of Columbia Rd., Castlegar; 4.1 km W of power lines

NOTES: Attitudes of dykes and other planar features are given as strike/dip using right-hand rule (i.e. dip on right hand side of strike direction); Abbreviations: bio: biotite; fp: feldspar; Kfp: alkali feldspar; px: pyroxene; hb: hornblende; qtz: quartz; f-, m-, c/g: fine-, medium-, coarse-grained; JR: Jurassic; N, S, E, W: compass directions; st: steep dip

Table A1: Location and lithological description of sites, continued

11	f/g lamprophyre sill/dyke (?), intrudes JR diorite and earlier dykes; attitude unknown	4555E 54547N	N side of curve on Hwy 3, 7.6 km SE of Columbia Rd., 25m W of Cai Creek Forest Service Rd.
12	m/g lamprophyre dyke intruding Coryell syenite, 3m (?) wide; 124/st	4234E 54597N	Bulldog Forest Service Rd., 3.6 km N from Hwy 3
13	c/g Coryell syenite	4230E 54602N	Bulldog Forest Service Rd., 4.5 km N from Hwy 3
14	c/g Coryell syenite	4252E 54307N	Cascade Highway; outcrop in road at hairpin turn; 1.2 km W of Site 63
15	m-c/g Coryell syenite	4242E 54302N	Cascade Highway; 1.25 km W of Site 14
16	feldspar-porphyritic aphanitic dyke, 5m wide; 354/74	4691E 54621N	Granite Creek logging road, 2.95 km W of bridge
17	f/g mafic dyke, 1-2m wide; 118/63	4705E 54613N	exposed in bed of Granite Creek, 10m N of bridge 400m from start of south fork of Granite Creek logging road
18	similar to Site 16; 187/80	4720E 54578N	0.9 km from start of Granite Creek logging road at Craigtown Jcn.
19	f/g mafic dyke, 3m wide; attitude unrecorded (strikes N)	4658E 54779N	located in S bank of Kootenay Canal, 15m E of bridge
20	m/g mafic dyke, 3m wide; intruding diorite mapped as Eocene(?); 002/75	4660E 54799N	top of large roadcut on N side Hwy 3A, across from rest area above Cora Lynn Dam
21	similar to Site 20, 5m wide; 209/83	4660E 54799N	70m W of Site 20
22	m-c/g Coryell syenite	4457E 54572N	poorly exposed in ditch on S side of College Creek Forest Service Rd., 4.05 km from start of road
23	c/g Coryell syenite	4456E 54571N	outcrop 25m E of road in bush on inside of curve, 0.3 km SW of Site 22
24	c/g syenite, and mafic dyke(?) rocks	4237E 54546N	poorly exposed outcrop area in clearcut, 2.85 km S on Bonanza Rd. from Hwy 3, 1.3 km past Bonanza Ck.

Table A1: Location and lithological description of sites, continued

25	pyroxene-rich mafic dyke (?) intruding Coryell syenite at W contact of Coryell Pluton	4196E 54674N	large cutting on abandoned railway 10.6 km N of Farron
26	f-m/g diorite dyke, 10m wide; attitude unknown (strikes N)	4571E 54477N	750m E of boundary of Champion Lakes Provincial Park, on Champion Lakes Road
27	aphanitic dark green dyke intruding c/g Coryell syenite; 234/31	4217E 54770N	8m above road, 1.9 km NW from jcn at Deer Park
28	c/g Coryell syenite	4311E 54362N	outcrop in bush 20m E of 2nd cabin in clearing, 8.7 km N from start of road in Big Sheep Creek Valley
29	aphanitic px-porphyritic volcanic; L. Paleozoic age	4259E 54744N	outcrop 10m above, and 500m from start, of Deer Creek Forest Service Rd.; 200m W of Site 79
42	m/g Coryell syenite	4403E 54364N	N side of Hwy 22, 200m W of Hwy 3B/22 jcn., 200m E of Rossland Lions campground entrance
43	m/g Coryell syenite	4404E 54408N	E side of Hwy 3B, 1 km N of Topping Creek, 5.4 km N of Hwy 3B/22 jcn.
44	c/g Coryell syenite, very mafic	4385E 54455N	W side Hwy 3B, 2.3 km N of Hanna Creek, 12.8 km N of Hwy 3B/22 jcn.
45	m/g Coryell syenite	4360E 54489N	halfway along long linear roadcut on W side Hwy 3B, 0.6 km S of start of passing lane
46	f-m/g mafic dyke, 7m wide; intruding Coryell syenite; 316/74	4339E 54507N	E side of Hwy 3B at S end of sharp corner, 7.95 km S of Hwy 3/3B jcn.; 500m N of logging road entrance
47	f-m/g Coryell syenite (?)	4329E 54518N	roadcut opposite rest area on Hwy 3B, 5.4 km S of Hwy 3/3B jcn.
48	Fp- and hb/px(?)- porphyritic dyke(?)	4312E 54561N	W end of roadcut on S side Hwy 3, 500m W of entrance to Nancy Greene Provincial Park
49	m-c/g megacrystic Coryell syenite; mafic contact phase	4194E 54466N	long roadcut on N side Hwy 3, 5.2 km W of Paulson Bridge, 5.1 km E of Lafferty Pit Rd.
50	weakly foliated f-m/g hb-bio rock	4100E 54407N	E side of East Lake Rd., opposite cottage driveway marked "Whitley's #3249)

Table A1: Location and lithological description of sites, continued

54	m/g bio-px-fp rock with pink granitoid veins	4297E 54703N	N side of Deer Park Forest Service Rd., 8.75 km E of Deer Park jcn, 4.05 km E of Little Cayuse Creek
60	m/g Coryell syenite	4103E 54405N	base of 15m-high cliffs, 1.2 km NW along McRae Rd., from start at East Lake Rd.
61	f/g mafic dyke, 3m wide; fp- and hb-porphyritic; 178/43	4234E 54546N	N side of Hwy 3, 50m E of rest area, 6.4 km E of Walker Creek rest area
62	m-c/g Coryell syenite	4218E 54320N	Cascade Highway; N side of road, near steel culvert, 20 km E of Christina Lake
63	c/g Coryell syenite, in contact with fp-hb-porphyritic hypabyssal phase	4253E 54305N	Cascade Highway; 28.2 km E of Christina Lake
64	f/g mafic sill, 3.5m thick; attitude unrecorded	4573E 54541N	N side of Hwy 3, 9.6 km E of Columbia Rd., Castlegar; 1.3 km E of Site 66.
65	m/g hb-porphyritic dyke, 3m wide; contact-parallel amygdules/vesicles; 325/67	4600E 54542N	N side of Hwy 3, 12.6 km E of Columbia Rd., Castlegar; 3 km E of Site 64
66	f-m/g mafic sill, 1m thick, amygdaloidal; attitude unrecorded	4559E 54543N	N side of Hwy 3, 8.3 km E of Columbia Rd., Castlegar; 1.3 km W of Site 64
67	m/g, massive amphibolite/ diorite, intruded by granitoid veins	4515E 54541N	W side of Hwy 22, 1 km S of 100th St., 300m N of Fairview Rd.
68	boudinaged layer of bio-px rock in amphibolitic/dioritic gneiss; layering 183/21	4484E 54501N	W side of Hwy 22, 15m-high roadcut on curve, 600m S of 12th Ave.
69	m/g, massive amphibolite layer in deformed granitoid gneiss; layering 172/23	4479E 54488N	W side of Hwy 22, 1.4 km S of Site 68, across from rest area with litter barrel
70	m/g, moderately foliated (172/54), amphibolite/diorite; similar to Site 69	4472E 54466N	W side of Hwy 22, on curve 400m S of Buckley Rd.
71	f-g mafic dyke intruding porphyritic Coryell syenite; 010/84	4326E 54279N	Cascade Highway; E side of road, 2.5 km E of Corral Creek
72	f/g fp-bio-px/hb porphyry; hypabyssal phase of Coryell(?, may be a dyke)	4330E 54287N	Cascade Highway; E side of road, 5.5 km E of Corral Creek

Table A1: Location and lithological description of sites, continued

73	f/g mafic dyke, 3m wide; 180/84	4387E 54363N	Cascade Highway; N side of road, immediately W of adit into roadcut; 2.2 km W of jcn with Hwy 22
74	f/g, hb-px-porphyritic mafic dyke, 6m-wide; intrudes Coryell syenite; strikes N	4233E 54749N	Lower Arrow Lake; 1.6 km W of Deer Park Jcn.
75	6m-wide, f-m/g, mafic dyke; intruding Coryell syenite; 354/85	4238E 54746N	Lower Arrow Lake; 0.9 km W of Deer Park Jcn.
76	c/g Coryell syenite	4243E 54743N	Lower Arrow Lake; large outcrop area, 0.4 km W of Deer Park Jcn.
77	f-m/g, pyroxene-porphyritic volcanic(?)	4253E 54742N	Lower Arrow Lake; inside of curve on uphill side of Deer Park Road; 1.0 km E of Deer Park Jcn.
78	massive feldspar-pyroxene porphyry	4259E 54740N	Lower Arrow Lake; uphill side of curve on Deer Park Road, 1.9 km E of Deer Park Jcn on Deer Park Road.
79	massive feldspar-pyroxene porphyry	4261E 54742N	Lower Arrow Lake; Deer Park Forest Service Rd., 200m from jcn with Deer Park Rd
80	m/g biotite-pyroxene-feldspar rock, agmatized by pink syenite veins	4296E 54702N	Lower Arrow Lake; on Deer Park Road, 6.5 km W of jcn at Syringa Ck. Park; 4.4 km E of Cayuse Ck.
81	m/g biotite-pyroxene diorite(?) agmatized by pink porphyritic syenite	4332E 54676N	Lower Arrow Lake on Deer Park Road; 2.7 km W of jcn at Syringa Ck. Park; 8.2 km E of Cayuse Ck.
82	m/g biotite-pyroxene diorite(?) agmatized by pink porphyritic syenite	4338E 54675N	Lower Arrow Lake; on Deer Park Road 2.3 km W of jcn at Syringa Ck. Park; 8.6 km E of Cayuse Ck.
83	foliated (347/82E) biotite-pyroxene-feldspar rock	4341E 54675N	Lower Arrow Lake; on Deer Park Road 1.9 km W of jcn at Syringa Ck Park; 9.0 km E of Cayuse Ck.
84	f-m/g, massive, pyroxene-porphyritic diorite	4360E 54664N	Lower Arrow Lake; 0.4 km E of jcn at Syringa Ck Park
85	f/g biotite-pyroxene syenite	4312E 54579N	Shields Rd.; 1 km N of Hwy 3; 115m E of road
86	f/g mafic dyke; 5-15% biotite, 5-20% phenocrysts of fp (+ px?)	4308E 54587N	Shields Rd.; 1.9 km N of Hwy 3

Table A1: Location and lithological description of sites, continued

87	lamprophyre dyke (?)	4304E 54597N	Shields Rd.; 3.1 km N of Hwy 3
88	m-c/g Coryell syenite	4303E 54600N	Shields Rd.; 3.4 km N of Hwy 3; 100m W of road
89	m-c/g Coryell syenite	4300E 54605N	Shields Rd.; 4.75 km N of Hwy 3
90	f/g mafic dyke, 5m wide; 340/82	4328E 54535N	E side of Hwy 3B, 3.9 km S of jcn with Hwy 3
91	f/g mafic dyke, 3m wide; strikes N, dip steep	4274E 54548N	Big Sheep Ck rest area, N side of Hwy 3, 5.2 km W of jcn with Hwy 3B, east end of roadcut
92	lamprophyre dyke (sill?); attitude unknown	4235E 54548N	Paulson Summit, E side of Hwy 3, 1.25 km SW of Bulldog Forest Service Road
93	m/g Coryell syenite	4106E 54402N	McRae Rd., quarry on inside of curve, 0.7 km W of jcn with Hwy 3
94	m-c/g Coryell syenite	4113E 54390N	outcrop on inside of curve on abandoned rail line, 4.5 km N of Fife Rd.
95	m-c/g Coryell syenite	4116E 54400N	outcrop in centre of straight stretch of abandoned rail line, 5.4 km N from Fife Rd.
96	m-c/g Coryell syenite, similar to Site 49	4194E 54443N	outcrop forms a cliff 8-10m in height, on abandoned rail line, 5.45 km NE of Lafferty Station, 400m S of Site 49
97	aphanitic dark grey dyke, fp-(and px?) porphyritic, intruding Coryell syenite	4260E 54702N	outcrop on abandoned rail line, 1.65 km NW of Coykendahl Station
98	dyke 15m wide intruding Coryell syenite; centre pink and Kfp porphyritic, margins darker with less Kfp, but also px/hb(?),phenocrysts	4248E 54715N	outcrop on curve on abandoned rail line, 2.65 km NW from Coykendahl Station; bearing 005° to Deer Park

APPENDIX B

STATISTICAL ANALYSIS

In paleomagnetic studies, the basic unit of information obtained from a specimen is the magnetization vector, which has both a direction and an intensity. These two quantities bear no relation to each other; a rock poor in magnetic minerals which exhibits low intensity can record the direction of the geomagnetic field just as well (provided it has an appropriate composition and grain size) as a rock rich in magnetic minerals which displays high intensity. For the purpose of analysis, therefore, paleomagnetic directions (paleodirections) are normally represented as unit vectors (Figure B1). A paleodirection is usually described in terms of spherical coordinates: its declination, *D*, which is the azimuth of its projection (H) into the horizontal plane, and inclination, *I*, from the horizontal, designated positive downwards. Paleodirections can then be illustrated graphically, usually as points in the lower hemisphere of an equal-area stereographic projection. Declination and inclination can also be illustrated on a cartesian projection, referred to as an orthogonal, or Zijderveld, plot (described in Chapter 4).

At each of the sites sampled for paleomagnetic analysis during this study, at least ten specimens were obtained. Analysis of these specimens yields ten different paleodirections, regarded as unit vectors, from which the mean direction for the site is determined. Several site means may then, in the same manner, be combined to give the mean direction for a region, locality, or rock unit. A statistical model defining the distribution of unit vectors, represented as points on the surface of a sphere of unit radius, was described in 1953 by Sir

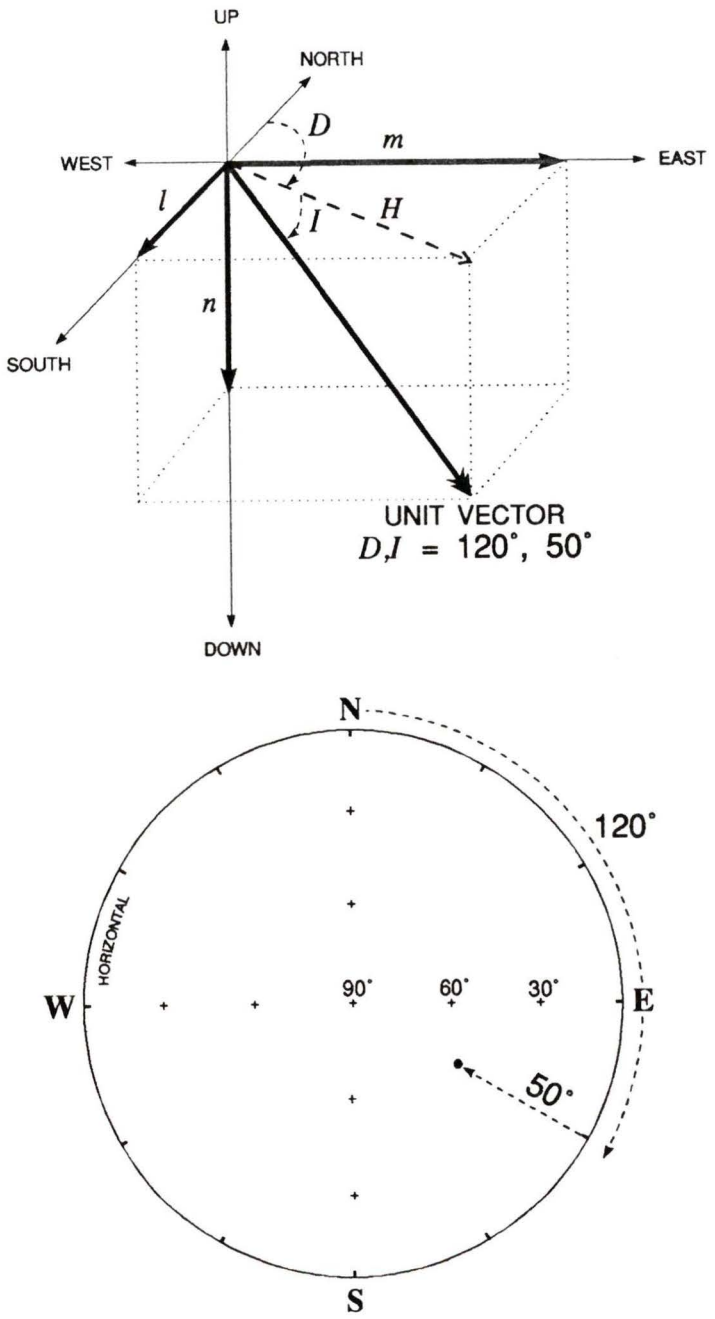

Figure B1: Paleodirections are vectors of unit length, with spherical coordinates *D*,*I*, and cartesian coordinates *l*, *m*, and *n*. The example illustrated has a declination of 120° and inclination of +50° (top). This paleodirection is illustrated on a stereographic projection as a solid circle, which indicates positive (downwards) inclination (bottom). Paleodirections with negative (upward) inclination are commonly denoted by open symbols.

Ronald Fisher, specifically to aid in the analysis of paleodirections. Fisher's distribution is a three dimensional analogue of a two-dimensional Gaussian distribution. Only a brief overview of Fisher's statistics is offered here; more complete treatments are available in the original article by Fisher (1953), and in works by Irving (1964), Tarling (1983), and others.

Fisher proposed that a population of unit vectors, when regarded as points on the surface of a sphere, would be distributed with a probability density:

$$P = \frac{K}{4\pi \sinh K} e^{[K \cos\theta]}, 0 \leq K \leq \infty$$

where K is Fisher's precision parameter, (K / 4π sinh K) normalizes the density to unity over the entire surface of the sphere, and θ is the angle between an individual point and the true mean. The density is axially symmetrical about the true mean. K is a measure of how tightly grouped the points are about the true mean, and varies from zero when the points are uniformly distributed, to infinity when they are identical to the mean. K may be thought of as analogous to the invariance (variance^{-1}) of the normal distribution.

The directional cosines, or cartesian components, of an individual unit vector are illustrated in Figure B1, labelled l, m, and n, where:

l = cos I cos D *(northward component)*

m = cos I sin D *(eastward component)*

n = sin I *(downward component)*

Fisher (1953) showed that the best estimate of the mean of N directions is the vector sum of the N individual directions. This mean direction has cosines:

$$X = \Sigma l_i / R \qquad Y = \Sigma m_i / R \qquad Z = \Sigma n_i / R$$

where R is the length of the resultant vector [XYZ] (which, of course, must always be $\leq N$):

$$R = \{(\Sigma l_i)^2 + (\Sigma m_i)^2 + (\Sigma n_i)^2\}^{1/2}$$

The declination, D_m, and inclination, I_m, of the mean direction are given by:

$$D_m = \tan^{-1} (\Sigma m_i / \Sigma l_i) \qquad I_m = \sin^{-1} (\Sigma n_i / R)$$

and the best estimate, k, of the precision parameter, K, is:

$$K \approx k = (N - 1) / (N - R), \quad \text{for } N > 7,\ K > 3$$

As an estimate of the reliability of the calculated mean direction, Fisher (1953) demonstrated that, at a probability level 1 - P, the true mean direction of N directions lies within a circular cone having a half-angle, α, given by:

$$\cos^{-1} \alpha_{1-P} = 1 - \frac{N-R}{R}\left\langle [\tfrac{1}{P}]^{1/(N-1)} - 1 \right\rangle$$

It is common to set P equal to 0.37 or 0.05, such that α_{63} and α_{95} give the half-angles of the cones of confidence about the observed mean which have 63% and 95% probability, respectively, of containing the true mean direction.

The probability of observing a paleodirection which makes an angle θ_0 or more with the true mean is given by the equation (Watson and Irving 1957):

$$1 - \cos\theta = \frac{-\ln\left[P\left\langle \theta > \theta_0 \right\rangle\right]}{k}$$

From this equation are derived two quantities useful in paleomagnetism, θ_{63} and θ_{95}, which represent the angular radii of the circles about the true mean direction which contain 63% and 95% of the individual directions. θ_{63} and θ_{95} are analogous to the standard deviation and 1.96 times the standard deviation of the normal distribution, respectively (Irving 1964).

α_{63} and α_{95} are measures of the *reliability* of an estimated mean direction; the values of these parameters decrease as N increases (as N increases to infinity, α becomes infinitely small). θ_{63}, θ_{95}, and k are measures of the angular dispersion, or *scatter*, of unit vectors about the mean direction, and are relatively independent of N (as N increases to infinity, k approaches the true value, K).

APPENDIX C

CALCULATIONS

1. MID-EOCENE REFERENCE DIRECTION

As described in section 5.2, the reference direction at the centre of the present study area was determined from 127 site mean directions from 5 localities. These data are given in Table C1. The two different methods by which the data were utilized are illustrated schematically in Figure C1. The procedure employed in estimating the mean of a set of paleodirections (or poles) has been described in Appendix A. Two calculations not described previously are: a) mapping a paleodirection to a paleopole, and b) mapping a paleopole to a paleodirection.

a) Mapping a paleodirection (D, I) to a paleopole (λ', ϕ'):

This calculation is employed to convert site mean directions to site poles and to convert regional mean directions to regional poles (in Calculations A and B, respectively, in Figure C1). Referring to Figure C2, the latitude, λ', of the paleopole is given by the relation: $\lambda' = 90° - s$

where s = colatitude of paleopole = $\cos^{-1}$ ($\cos n \cos p + \sin n \sin p \cos D'$),

and n = colatitude of site with respect to paleopole = $\tan^{-1}(2/\tan I)$

p = colatitude of site = $90° - \lambda$

D' = $360° - D$

The longitude of the paleopole is given by: $\phi' = \phi + \phi''$

where ϕ = longitude of site,

and ϕ'' = $\sin^{-1}(\sin D' \sin n) / \sin s$

b) Mapping a paleopole (λ', ϕ') to a direction (D, I):

The declination of the expected paleodirection at the site is:

$$D = 360 - D'$$

where $D' = \sin^{-1}(\sin \phi'' \sin s / \sin n)$

and $n = 90° - \lambda_p$

$\cos(90° - \lambda_p) = \cos s \cos p + \sin s \sin p \cos \phi''$

$\cos(90° - \lambda_p) = \cos(90° - \lambda') \cos(90° - \lambda) + \sin(90° - \lambda') \sin(90° - \lambda) \cos \phi''$

$$\lambda_p = \sin^{-1}(\sin \lambda' \sin \lambda + \cos \lambda' \cos \lambda \cos \phi'')$$

The inclination, I, expected at the site, S, is derived from the paleolatitude, λ_p, of the site by the relation: $I = \tan^{-1}(2 \tan \lambda_p)$

2. ERRORS FOR MEAN APPARENT TILT BY REGIONS (TABLE 5.3)

The 95% confidence interval for the magnitude of apparent tilt, T, is estimated by the root mean square of the half-angles of the circles of confidence, α_{95}, about the reference mean direction (*ref*) and the observed mean (*obs*) for the sampling region:

$$T \pm {}^{\sigma}T = T \pm \left[{}^{\alpha}95^{2}_{ref} + {}^{\alpha}95^{2}_{obs} \right]^{1/2}$$

The method employed to calculate the 95% confidence interval for the direction of apparent tilt, $T_d \pm {}^{\sigma}T_d$, is detailed in Figure C3.

Table C1: Site directions used in calculation of the Eocene reference direction.

SITE	*D* (°)	*I* (°)	SITE	*D* (°)	*I* (°)	SITE	*D* (°)	*I* (°)
Bearpaw Mountains, Ma. (50-54 Ma)						**Diehl and others (1989)**		
BP1	143.6	-71.4	BP13	178.9	-66.1	BP33	165.5	-70.6
BP2	186.7	-43.7	BP14	163.3	-78.8	BP34	008.1	66.0
BP3	071.1	77.5	BP15	003.3	45.7	BP36	199.1	-67.8
BP4	355.8	66.1	BP17	308.4	79.5	BP37	163.6	-76.9
BP5	010.5	36.1	BP18	147.2	-50.7	BP38	147.2	-67.7
BP6	351.8	77.5	BP20	168.6	-54.4	BP41	160.6	-70.5
BP7	350.8	76.9	BP21	151.5	-67.2	BP42	159.4	-60.9
BP9	342.8	73.6	BP23	349.6	68.6	BP44	351.8	74.6
BP11	025.6	78.6	BP30	046.6	69.3	BP45	335.4	66.1
BP12	335.3	62.7	BP32	132.7	-69.1	BP46	152.6	-44.1
Highwood Mountains, Ma. (49-53 Ma)						**Diehl and others (1989)**		
HW1	013.2	55.6	HW17	048.2	74.7	HW30	333.0	70.3
HW2	336.5	37.8	HW18	015.1	44.9	HW31	315.4	57.2
HW7	000.4	54.6	HW19	356.1	67.4	HW32	326.4	63.7
HW8	320.9	55.8	HW21	003.7	72.6	HW33	008.2	40.1
HW9	315.2	75.2	HW22	003.3	36.6	HW34	023.2	64.4
HW10	341.5	72.5	HW23	036.3	66.0	HW36	312.9	59.0
HW11	340.4	78.3	HW24-25	330.0	72.0	HW38	339.2	65.9
HW12	357.4	59.6	HW26-27	315.1	69.1	HW39	308.4	59.5
HW13	348.2	73.6	HW28	351.0	56.2	HW40	353.3	63.6
HW16	350.8	47.8	HW29	346.1	69.2	HW41	354.6	71.0
Absaroka Volcanics, Wyoming (48 Ma)						**Shive and Pruss (1977)**		
1	034.3	70.3	10	017.1	80.1	39	008.8	57.2
3	183.0	-73.3	11	013.6	52.1	40	319.5	36.8
4	164.4	-69.2	12	024.1	62.7	44	161.5	-69.0
5	152.7	-17.1	14	349.4	61.1	48	311.4	45.5
6	343.4	64.3	16	171.1	-38.1	51	333.1	77.3
8	121.8	-73.1	31	034.6	60.1			
9	316.1	74.1	32	010.2	39.4			

Table C1: Site directions used in calculation of the Eocene reference direction, continued.

SITE	*D* (°)	*I* (°)	SITE	*D* (°)	*I* (°)	SITE	*D* (°)	*I* (°)
Kamloops Volcanics, B.C. (49±2 Ma)						**Symons and Wellings (1989)**		
1	152.7	-74.0	9	066.0	71.4	17	151.5	-46.5
2	190.2	-74.7	10	068.5	74.6	18	040.0	54.9
3	188.2	-76.6	11	099.8	75.2	19	313.2	75.5
4	159.7	-72.4	12	049.2	72.7	23	011.2	73.8
5	146.3	-65.4	13	311.5	72.5	24	318.0	58.0
6	162.0	-69.7	14	302.3	58.3	25	027.8	63.2
7	117.0	82.0	15	306.3	68.7	26	308.1	54.0
8	060.9	73.8	16	028.7	45.6	27	352.4	65.3
Kelowna Volcanics, B.C. (52±2 Ma)						**Bardoux and Irving (1989)**		
M1	037	39	M17	347	66	M35	043	84
M4	020	61	M18	034	62	M37	306	66
M5	014	61	M19	017	60	M40	034	69
M8	331	71	M20	038	63	M41	013	66
M10	321	62	M31	311	61	M42	328	54
M11	322	59	M32	276	52	M43	290	59
M12	045	70	M33	043	73	M47	348	60
M16	358	66	M34	016	77	M50	013	68

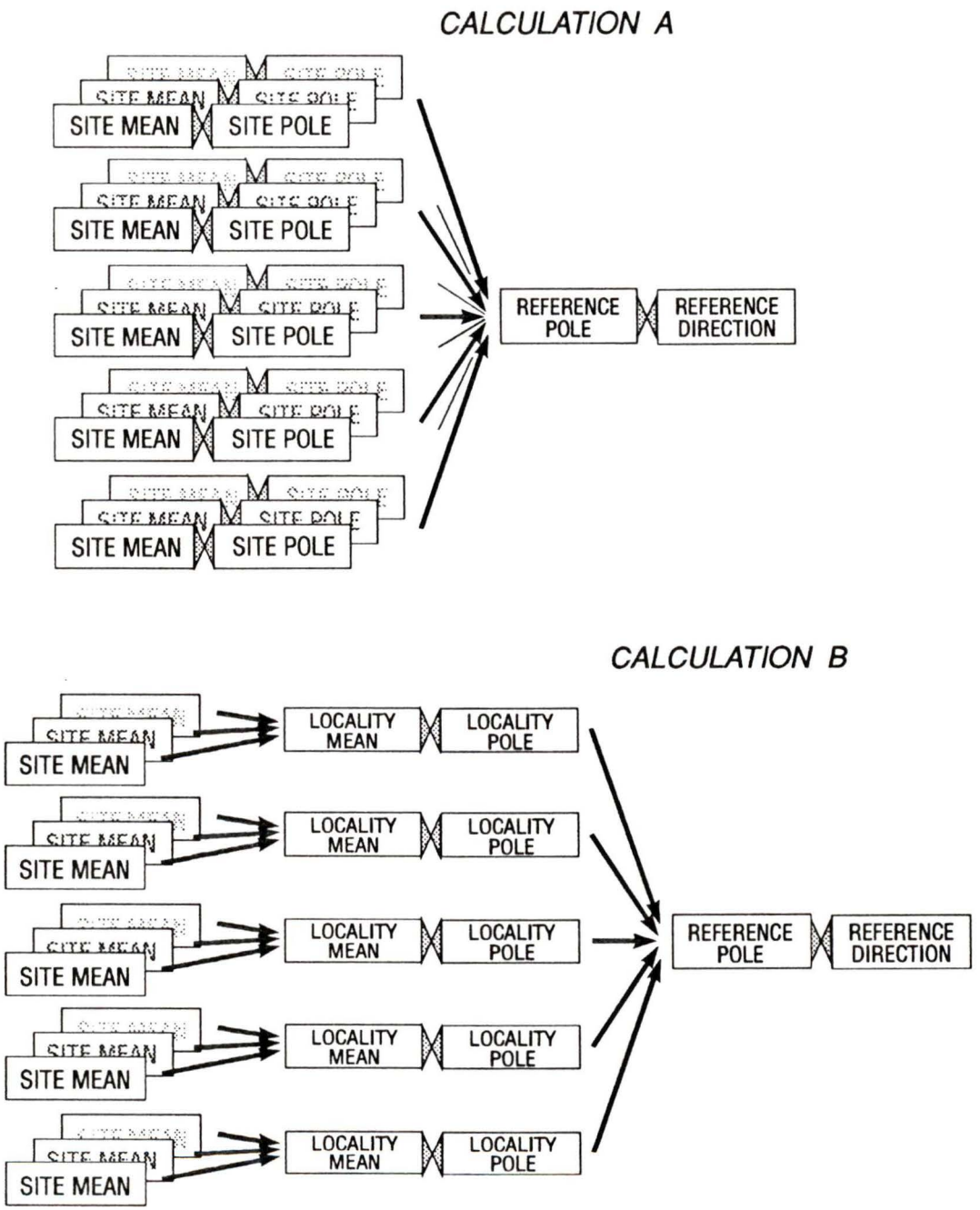

Figure C1: Methods employed in calculating the reference direction. Using Calculation A, the 127 site mean directions are each given unit weight (top). In Calculation B (bottom), each locality mean direction is given unit weight. Refer to section 5.3 and Table 5.3 for explanation.

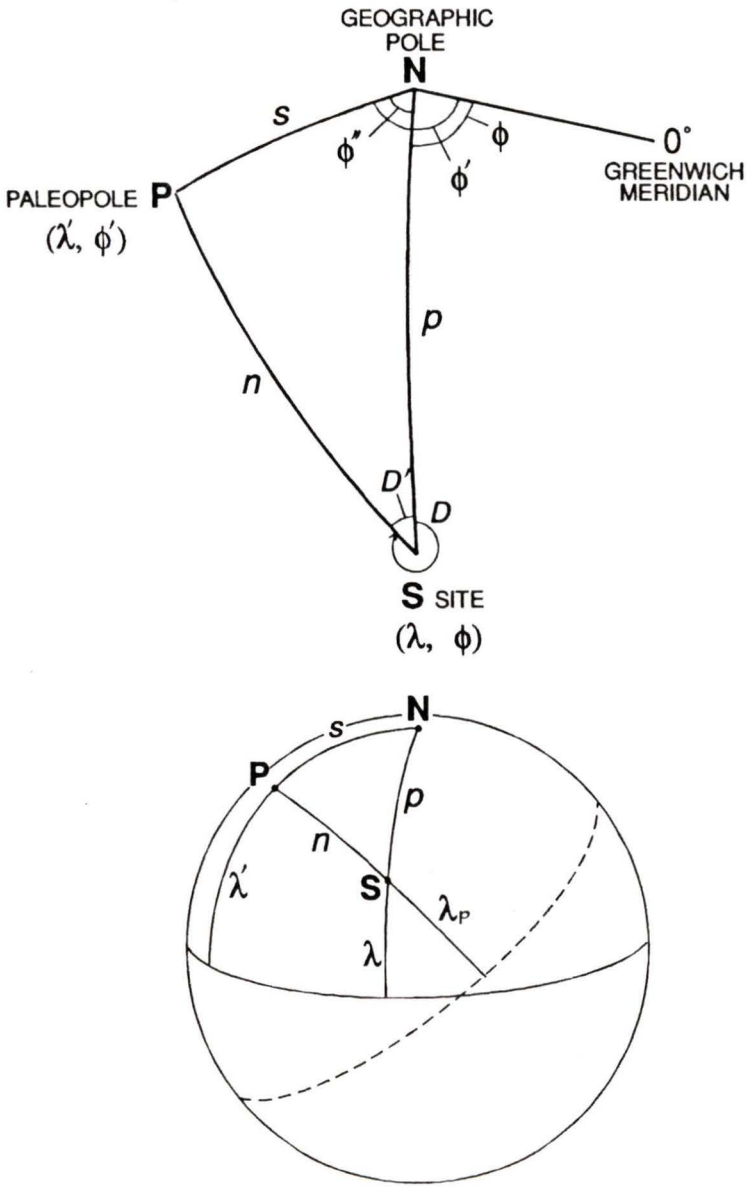

Figure C2: Diagrams illustrating the geometric relations between geographic north, **N**, and a paleopole, **P**, which corresponds to the paleodirection observed at a sampling site, **S**.

a)

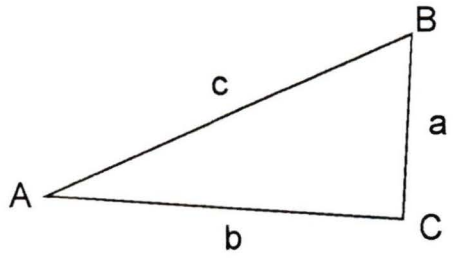

$$\sin A / \sin a = \sin B / \sin b = \sin C / \sin c \qquad (1)$$

b)

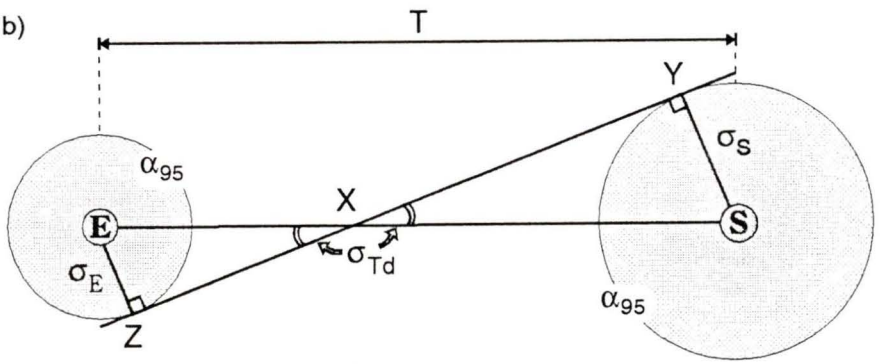

c)

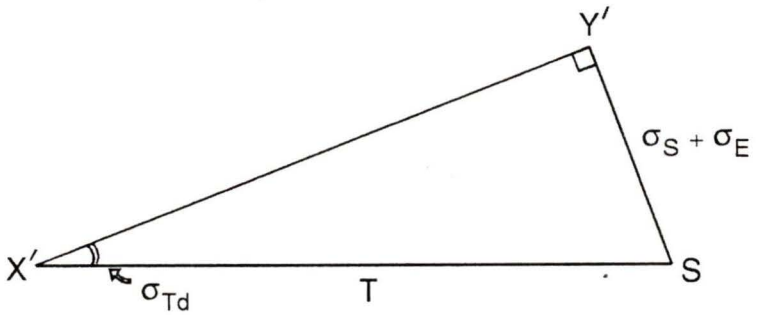

$$\sin Y' / \sin T = \sin {}^{\sigma}T_d / \sin ({}^{\sigma}S + {}^{\sigma}E) \qquad (2)$$

$$\sin {}^{\sigma}T_d = \sin ({}^{\sigma}S + {}^{\sigma}E) / \sin T \qquad (3)$$

Figure C3: Derivation of the 95% confidence interval for the direction of apparent tilt. a) A fundamental theorem of spherical trigonometry states that *the sines of the angles of a spherical triangle are proportional to the sines of the opposite sides* (equation 1). b) the error in the tilt direction is given by the size of the angle, σT_d, subtended by line T, the magnitude of tilt, and line YZ, which is tangential to the α_{95} circles of confidence about the observed, S, and reference, E, directions. c) from triangle XYS is b), a similar triangle X'Y'S is derived by translating line YZ along the radii σS and σE until Z meets E. Substitution of values into equation 1 leads to a solution for the error, σT_d, in the tilt direction (equations 2, 3). Note that the value of σT_d increases as the magnitude of tilt decreases.

VITA

Surname: Wingate **Given Names:** Michael Thomas David

Place of Birth: Glasgow, Scotland

Educational Institutions Attended:

Carleton University	1986 to 1990
University of Victoria	1990 to 1993

Degrees awarded:

B.Sc. (Highest Honours)	Carleton University	1990

Honours and Awards:

NSERC Post-graduate Scholarship, PGSB	1992
President's Research Scholarship, University of Victoria	1991,92
NSERC Post-graduate Scholarship, PGS2	1991-92
University of Victoria Fellowship	1990-91
Carleton University Senate Medal for Academic Excellence	1990
Dean's Honour List, Carleton University	1987,88,89,90
F.K. North Book Award	1990
Geological Association of Canada Student Prize	1989
Bickle Foundation Scholarship	1987,88,89
Morley Wilson Scholarship	1988,89
George Fierheller Scholarship	1988,89
Mineralogical Association of Canada Student Award	1988
Jacob Freedman Scholarship	1987

Publications:

Wingate, M.T.D., and Irving, E. 1993. Extension in high-grade terranes of the southern Omineca Belt, British Columbia: evidence from paleomagnetism, in preparation.

Wingate, M.T.D. 1992. Paleomagnetically observed tilts in the southern Omineca Belt (abstract), LITHOPROBE Southern Cordillera Transect Workshop and Cordilleran Tectonics Workshop, Report No. 24, Edmonton, Alberta, p. 132.

Wingate, M.T.D. 1992. The kinematics of extension in high-grade terranes: paleomagnetically-observed tilts in the southern Omineca Belt (abstract), 1992 Spring Meeting abstract volume, *supplement to* Eos, Transactions, American Geophysical Union, p. 87.

Wynne, P.J., Irving, E., Hamilton, T.S., Souther, J.G., Baker, J., Wingate, M.T.D., and Wheadon, P. 1992. Paleomagnetic evidence for tilting and northerly extension of the Queen Charlotte Islands: the tilt hypothesis tested on Ramsay Island (abstract), 1992 Spring Meeting abstract volume, *supplement to* Eos, Transactions, American Geophysical Union, p. 87.

King, J.E., Van Nostrand, T., Bethune, K., Wingate, M.T.D., and Relf, C. 1991. Final field report on the Contwoyto - Nose Lakes map area, central Slave Province, District of MacKenzie, N.W.T., *in:* Current Research, Part C, Geological Survey of Canada, Paper 91-1C, p. 99-108.

PARTIAL COPYRIGHT LICENSE

I hereby grant the right to lend my thesis to users of the University of Victoria Library, and to make single copies only for such users or in response to a request from the Library of any other university, or similar institution, on its behalf or for one of its users. I further agree that permission for extensive copying of this thesis for scholarly purposes may be granted by me or a member of the University designated by me. It is understood that copying or publication of this thesis for financial gain shall not be allowed without my written permission.

Title of thesis:

"Extension in High-grade Terranes of the Southern Omineca Belt: Evidence from Paleomagnetism"

Author: 

MICHAEL T.D. WINGATE

November 23, 1992.

FIGURE 5.6: SIMPLIFIED TECTONIC MAP OF THE STUDY AREA, SHOWING MAGNITUDE AND DIRECTION OF APPARENT TILT

0 2 4 6 8 10 km

CORYELL INTRUSIVE SUITE
Middle Eocene syenite, monzonite

MARRON AND KETTLE RIVER FM.s
Middle Eocene volcanic and sedimentary rocks

PRE-EOCENE ROCKS
Intruded by Mesozoic to Lower Eocene Plutons

SAMPLE SITES
No prefix: present study; M: Marquis (1988); B: Bardoux and Irving (1989).

GEOLOGICAL CONTACT
Defined; approximate or assumed

EOCENE FAULT, NORMAL FAULT, VALKYR SHEAR ZONE (VSZ) Defined; approximate or assumed; ornamentation on upper plate

APPARENT TILT (of pre-tilt paleohorizontal plane). Arrows indicate magnitude (degrees below horizontal) and direction (azimuth); those with dashed outline have less than 95% probability of being significantly different from Eocene reference direction. Crosses indicate untilted rocks. Larger bold arrows give mean apparent tilt of sampling region.

ISOTOPIC AGES (Ma) K-Ar (b = biotite, h = hornblende, m = muscovite, w = whole rock); U-Pb

3 PROVINCIAL HIGHWAY

ROSSLAND DEVELOPED AREA

Sources of information: Little, 1957, 1982; Preto, 1970; Corbett and Simony, 1984; Fyles, 1984, 1990; Carr and others, 1987; Hunt and Roddick, 1987-1990; Marquis, 1988; Parrish and others, 1988; Carr and Parkinson, 1988; Marquis and Irving, 1990; Irving and Archibald, 1990; Andrew and others, 1991; P. Simony, personal communication, 1991.

Apparent tilt of post-mid-Cretaceous age, inferred from paleomagnetic data and from batholocrial mineral assemblages (shaded arrow) by Irving and Archibald (1990)